General Disclaimer

One or more of the Following Statements may affect this Document

- This document has been reproduced from the best copy furnished by the organizational source. It is being released in the interest of making available as much information as possible.

- This document may contain data, which exceeds the sheet parameters. It was furnished in this condition by the organizational source and is the best copy available.

- This document may contain tone-on-tone or color graphs, charts and/or pictures, which have been reproduced in black and white.

- This document is paginated as submitted by the original source.

- Portions of this document are not fully legible due to the historical nature of some of the material. However, it is the best reproduction available from the original submission.

Produced by the NASA Center for Aerospace Information (CASI)

NASA CR-137652

BBN Report No. 3022

STUDY OF A POROUS SURFACE MICROPHONE SENSOR IN AN AEROFOIL

D.U. Noiseux

N.B. Noiseux

Y. Kadman

March 1975

(NASA-CR-137652) STUDY OF A POROUS SURFACE MICROPHONE SENSOR IN AN AEROFOIL (Bolt, Beranek, and Newman, Inc.) 95 p HC $4.75 CSCL 09A

N75-23932

Unclas

G3/35 22391

Submitted to:

NASA
Ames Research Center
Moffett Field, California 94035

Attn: Mr. Paul Soderman

NASA CR-137652

BBN Report No. 3022

STUDY OF A POROUS SURFACE MICROPHONE SENSOR IN AN AEROFOIL

D.U. Noiseux
N.B. Noiseux
Y. Kadman

March 1975

Submitted to:
NASA
Ames Research Center
Moffett Field, California 94035
Attn: Mr. Paul Soderman

TABLE OF CONTENTS

1. INTRODUCTION

The Porous Microphone in an Aerofoil is a directional sensor which rejects flow noise. The aerofoil allows the sensor to be rotated in the airflow over a wide range of yaw angles, 0° to 90°, avoiding flow separation over the surface of the sensor and its associated additional flow noise.

The directivity and the rejection of flow noise are inherent to the basic design of porous surface sensors[1]. The design consists of a thin porous surface which couples the external pressure field to a long, thin cavity inside the sensor. For a porous strip sensor, the cavity has a constant width, and its depth decreases linearly towards the tip of the sensor, when the specific acoustic impedance z of the porous surface is constant, real and equal to

$$z = r = \rho_0 c_0 \frac{L}{d} \qquad (1)$$

where L is the length of the cavity and d is its maximum depth; then the cavity becomes anechoic in the direction towards the tip of the sensor. Under this condition, the response R of the sensor can be taken as the product

$$R = s(\omega)\ H(\underset{\sim}{k}) \qquad (2)$$

where $s(\omega)$ is the frequency response which would be constant under the condition in Eq. (1), and $H(\underset{\sim}{k})$ is the directivity function:

---

[1]Noiseux, D.U. and Horwath, T., "Design of a Porous Surface Microphone for the rejection of flow Noise," submitted to the Journal of Acoustical Society of America.

$$H(\underset{\sim}{k}) = \frac{\sin[(k_1-k_i)L/2]}{(k_1-k_i)L/2} \tag{3a}$$

where, k_i is the wavenumber of the gas inside the cavity, k_1 is the wavenumber component of the external pressure field along the axis of the porous strips.

For sonic signals (propagating with the speed of sound) we have

$$k_1 = k_0 \cos\theta \tag{3b}$$

where k_o is the wavenumber of the gas outside the sensor, and θ is the direction of propagation with respect to the axis of the sensor. The maximum of the directivity function occurs at $\theta = 0$ when

$$k_1 = k_0 = k_i \tag{4}$$

For subsonic signals (propagating at a velocity smaller than the speed of sound), like the pressure fluctuations associated with a turbulent subsonic flow, the range of values of k_1 at one frequency ω is predominantly larger than k_i and, hence, the value of the directivity function is small, thus, providing the attenuation of these signals: the flow noise is rejected.

The Porous Microphone in an Aerofoil uses the porous strip design. Under the ideal condition, Eq. (1), this sensor very nearly maintains the properties given by Eqs. (2) through (4). An earlier design[2] has shown that an airfoil is desirable and

[2]Noiseux, D.U., "Study of Porous Surface Microphones for Acoustic Measurements in Wind Tunnels," NASA CR-114593, BBN Report No. 2539, April 1973.

effective in reducing flow noise when the sensor is rotated over a large range of yaw angles. However, this early design also showed two important limitations. First, the frequency response was not constant but dropped very fast with increasing frequency. Second, the airfoil introduces an additional flow noise, which could be further reduced by a redesign of the airfoil.

The Porous Microphone in an Aerofoil has been redesigned, resulting in considerable improvements of its frequency response, and of its flow noise rejection over a wide range of yaw angles.

The frequency response $s(\omega)$ is affected directly by the specific acoustic impedance of the porous surface. A systematic analysis and measurement of the properties of the porous strips has been undertaken and the results reported[3]. It turns out that the frequency response, normalized to unity at low frequencies, is

$$s(\omega) = \frac{y_{12}(\omega)}{y_{11}(\omega)} \tag{5}$$

where $y_{12}(\omega)$ is the specific transfer admittance of the thin porous strip and y_{11} is its driving point admittance; in terms of the thickness h of the porous strips and of its internal complex wavenumber γ, we get

$$s(\omega) = [\cosh \gamma h]^{-1} \tag{6}$$

[3]Noiseux, D.U., "Development, Fabrication and Calibration of a Porous Surface Microphone in an Aerofoil," NASA CR-132636, BBN Report No. 3014, March 1975.

From Eq. (6) the frequency response can be controlled by the selection of the porous material and its thickness. This important result has been experimentally supported. The new Porous Surface Microphone has a higher frequency response than the earlier design. The acoustic properties of this new design are shown in Appendix I, where we can see the improved frequency response. The directivity function is also shown to follow closely the directivity of an ideal porous strip sensor given by Eq. (3). The mechanical stiffness of the porous strips and the acoustic modes inside the cavity of the sensor, are now the limitations of the high frequency end of the present design, in the frequency range of 15 kHz to 20 kHz. These limitations can be pushed to higher frequencies by using narrower strips and narrower acoustic cavities.

The new airfoil chosen is NACA-64-012, which has a smaller thickness-to-chord ratio than the airfoil used earlier[2]. The flow noise due to flow separation at large yaw angles has been reduced.

The present report is concerned not only with the flow noise of the Porous Surface Microphone in an Aerofoil, but also with its vibration sensitivity and with the effect of the Mach number of the flow on the directivity function. The results of these investigations are presented in the following section. The details of the analysis and experimental results are given in a set of appendices.

2. RESULTS

The results are divided into four topics which are discussed in the following subsections.

2.1 Acoustic Properties

The acoustic properties of the Porous Microphone in an Aerofoil are its frequency response and its directivity pattern. They are shown in Appendix I.

The frequency response $s(\omega)$ follows very closely the response predicted by the acoustic properties of the porous strips, Eq. (6). At high frequencies, between 15 kHz and 20 kHz, the frequency response shows resonances which are attributed to the first bending mode of the porous strips and to the first mode of the acoustic cavity. These two resonances could be shifted to higher frequencies by using narrower strips and acoustic cavity.

The measured directivity patterns follow the patterns given by Eq. (3). The symmetrical design, using two porous strips on opposite faces of the aerofoil, has cancelled to a large extent the diffraction of the body of the aerofoil. The envelope of the minor lobes of the directivity pattern does not decrease as fast as Eq. (3) would predict. This limitation of the minor lobes is attributed to the non-uniformity of the specific impedance of the porous surface. This effect has been analyzed previously[4] and the results are consistent with the patterns shown in Appendix I.

The acoustic properties of the sensor are discussed in more detail in Ref. (3).

---

[4] See Ref. 2, Appendix I.

2.2 Vibration Sensitivity

The thin aerofoil of the sensor will be excited by the time varying component of lift in a turbulent flow. At the flexural modes of the aerofoil, the vibration response of the aerofoil could be relatively large and create an extra component of noise. Fortunately, the symmetrical design of the porous surfaces will, to a first order, cancel out the noise due to the flexural response of the sensor. The resultant vibration sensitivity of the Airfoil Sensor is therefore very low.

The vibration sensitivity of the Airfoil Sensor is examined in Appendix II. An estimate of the vibration sensitivity is first derived and shown to be less than 75 dB SPL per G (SPL being referred to 0.0002 microbar). This is a very low value, which is almost equal to the vibration sensitivity of a B&K half-inch condenser microphone.

The vibration levels of the aerofoil are measured in the wind tunnel over a wide range of flow velocities. Using the estimate of vibration sensitivity and the measured vibration levels, we show in Appendix II, that the contribution of the vibration sensitivity of the Airfoil Sensor to its flow noise is completely negligible.

This result is obtained when the base, on which the sensor is mounted, is tied to a floor having itself a low vibration level.

2.3 Effect of Mach Number on the Directivity Function

The response of the Airfoil Sensor has been expressed as the product of a frequency response $s(\omega)$ and a directivity function $H(\underset{\sim}{k})$, see Eqs. (2) and (3).

The frequency response $s(\omega)$ should not be affected by air flow except if the acoustic resistance of the porous surface is modified by the presence of tangential flow. However, the porous material was selected to have essentially all its acoustic resistance caused by viscous loss *inside* the material and only a negligible part caused by the transition of the inside gas velocity to the surface gas velocity[5].

The directivity function $H(\underset{\sim}{k})$ is sensitive to airflow; the effect of Mach number can be introduced explicitly in Eq. (3). By measuring the actual directivity function of the sensor in air flow and comparing these experimental results with the calculated directivity function including air flow, we can show whether the computed directivity function with Mach number is valid or not. This is the purpose of a series of tests made in the wind tunnel.

The directivity function, including Mach number, is derived in Appendix III for a stationary acoustic sensor and a stationary receiver in a moving gas. The directivity function has the form given by Eq. (3) with k_1 replaced by

$$k_1 = \frac{k_s \cos\alpha}{1+M\cos\theta} \tag{7}$$

where

$$k_s = \frac{\omega_s}{c_o} \tag{8}$$

[5]See Ref. 3, Appendix VI.

is the ratio of the excitation frequency ω_s of the source and c_o is the sound velocity of air, α is the angle between the direction of propagation of the sound in the flow and the axis of the Porous Sensor, and θ is the angle between the direction of flow and the direction of propagation of the sound in the flow.

The acoustic tests in the wind tunnel are planned as follows: an Acoustic source is located in the throat of the nozzle of the wind tunnel. A B&K half-inch condenser microphone with nose cone measures the acoustic output of the Source at different flow velocities and over a wide range of frequencies; let e_1 be the electrical output of the B&K sensor at frequency ω and Mach number M:

$$e_1 = s_1(\omega)\ H_1(\underset{\sim}{k})\ P(\omega) \tag{9}$$

The same acoustic pressures are measured at the same flows with the Airfoil Sensor, giving an electrical output e_2

$$e_2 = s_2(\omega)\ H_2(\underset{\sim}{k})\ P(\omega) \tag{10}$$

The ratio of the directivity functions is

$$\frac{e_2 s_1(\omega)}{e_1 s_2(\omega)} = \frac{H_2(\underset{\sim}{k})}{H_1(\underset{\sim}{k})} \tag{11}$$

If we assume that the B&K sensor is omnidirectional, at least over the frequency range of interest, then

$$H_1(\underset{\sim}{k}) \cong 1 \tag{12}$$

and Eq. (11) gives the directivity function of the Airfoil Sensor including the effect of Mach number. With this plan, the effect of Mach number on the radiation impedance of the Source cancels out.

The acoustic characteristics of the Source are shown in Appendix IV, with and without flow. The test results of the response of the Airfoil Sensor and the B&K Sensor to the Acoustic Source are presented in Appendix V for the case $\alpha = \theta = 0$. The ratio in Eq. (11) is calculated under the assumption in Eq. (12), as a function of frequency, for different Mach numbers, M = 0.075 to 0.2. The directivity function, including Mach number, is also calculated from Eqs. (3) and (7) for $\alpha = \theta = 0$ and compared with the experimental results.

The calculations and the experimental results of directivity function of an Aerofoil Sensor, including Mach number, agree up to approximately 10 kHz, in the range of the tests: M = 0.075 to 0.2. Above 10 kHz, the calculations and the experimental results start to diverge. It is difficult to attribute this divergence to the Airfoil Sensor. Its sensitive surface has a high impedance which is not modified by air flow, as already discussed. In contrast, the sensitive surface of the B&K Sensor, i.e., the fine mesh screen on the side of the nose cone, has a much lower acoustic impedance which could be more easily affected by flow.

It would appear from the experimental results that the response $s_1(\omega)\, H_1(\underset{\sim}{k})$ of the B&K sensor is not independent of Mach number, contrary to the assumption taken in the calculations using Eq. (11). The results suggest that either $H_1(\underset{\sim}{k})$ decreases with airflow or that $s_1(\omega)$ increases with airflow or even that both effects occur simultaneously, in the frequency range above 10 kHz. Since the B&K condenser microphones with nose cones are used extensively in wind tunnels, the effect of Mach number of their response should be investigated further.

The effect of Mach number on the directivity function of the Aerofoil Sensor could be eliminated if the wavenumber of the acoustic signals applied to the Sensor were matched to the wavenumber k_i of the gas inside the acoustic cavity of the Sensor; if this match is achieved,

$$k_i = \frac{k_s \cos\alpha}{1 + M \cos\theta} \quad ,$$

then the directivity $H(\underset{\sim}{k})$ becomes unity. This match of wavenumbers could be realized by using a mixture of gas inside the Sensor so that its sound velocity matches the trace velocity of the acoustic signals to be measured.

2.4 Flow Noise

The flow noise of Airfoil Sensor in the BBN quiet wind tunnel is compared with the flow noise of the B&K half-inch condenser microphone with nose cone in the same wind tunnel, over a range of flow velocities from 26 to 70 m/sec. The B&K sensor is always pointing directly into the flow; the airfoil sensor is oriented over the full range of yaw angles, 0° to 90°, in 15° increments. The flow noise *reduction* of the Airfoil Sensor, is defined as the ratio of the flow noise of the B&K sensor pointing directly into the flow, to the flow noise of the Airfoil Sensor at given yaw angles.

The test conditions and the test results are presented in Appendix VI[6].

---

[6]This appendix is identical to Appendix X of Ref. 3: the experiment has been supported jointly by NASA Ames and NASA Langley.

The flow noise rejection of the Airfoil Sensor will depend on the intensity and the scale of turbulence of the air flow. When the intensity of turbulence of the wind tunnel is very low, as found in the results of Appendix VI, the flow noise rejection of the Airfoil Sensor is not considerable; this is shown in Fig. 1 for different yaw angles at a flow velocity of 62 m/sec. When the intensity of turbulence is larger, as found in the acoustic tests of Appendix V, the flow noise rejection can be quite large; this is shown in Fig. 2.

The flow noise of the Airfoil Sensor for a given flow velocity is minimum at a yaw angle of approximately 30°; this minimum is not yet fully understood.

The results of flow noise have not been analyzed in detail. It would be useful to identify the different causes of flow noise and thereby assess the performance of the Airfoil Sensor in a more independent way than to rely on the B&K sensor for comparison.

ORIGINAL PAGE IS
OF POOR QUALITY

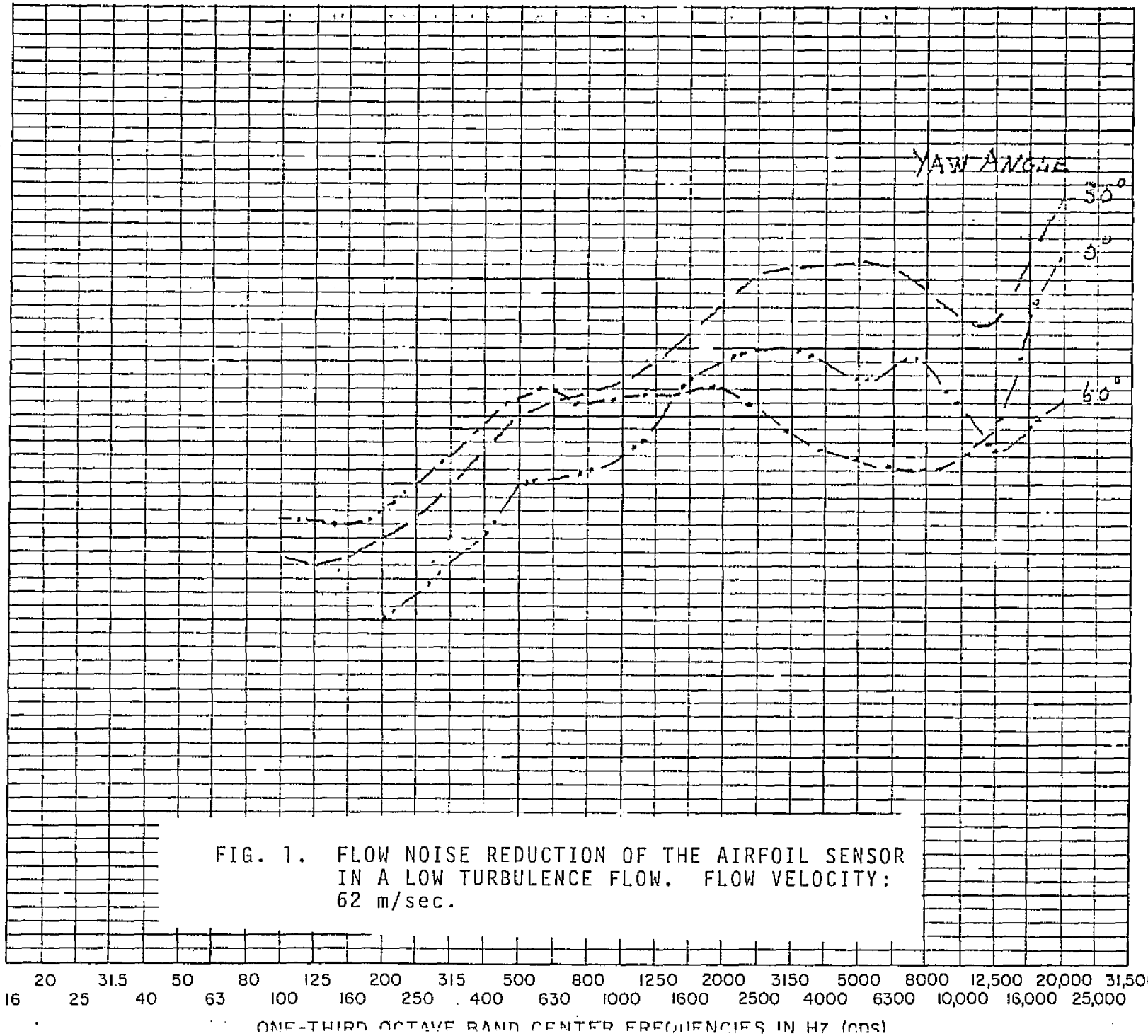

FIG. 1. FLOW NOISE REDUCTION OF THE AIRFOIL SENSOR IN A LOW TURBULENCE FLOW. FLOW VELOCITY: 62 m/sec.

BOLT BERANEK & NEWMAN INC

ORIGINAL PAGE IS
OF POOR QUALITY

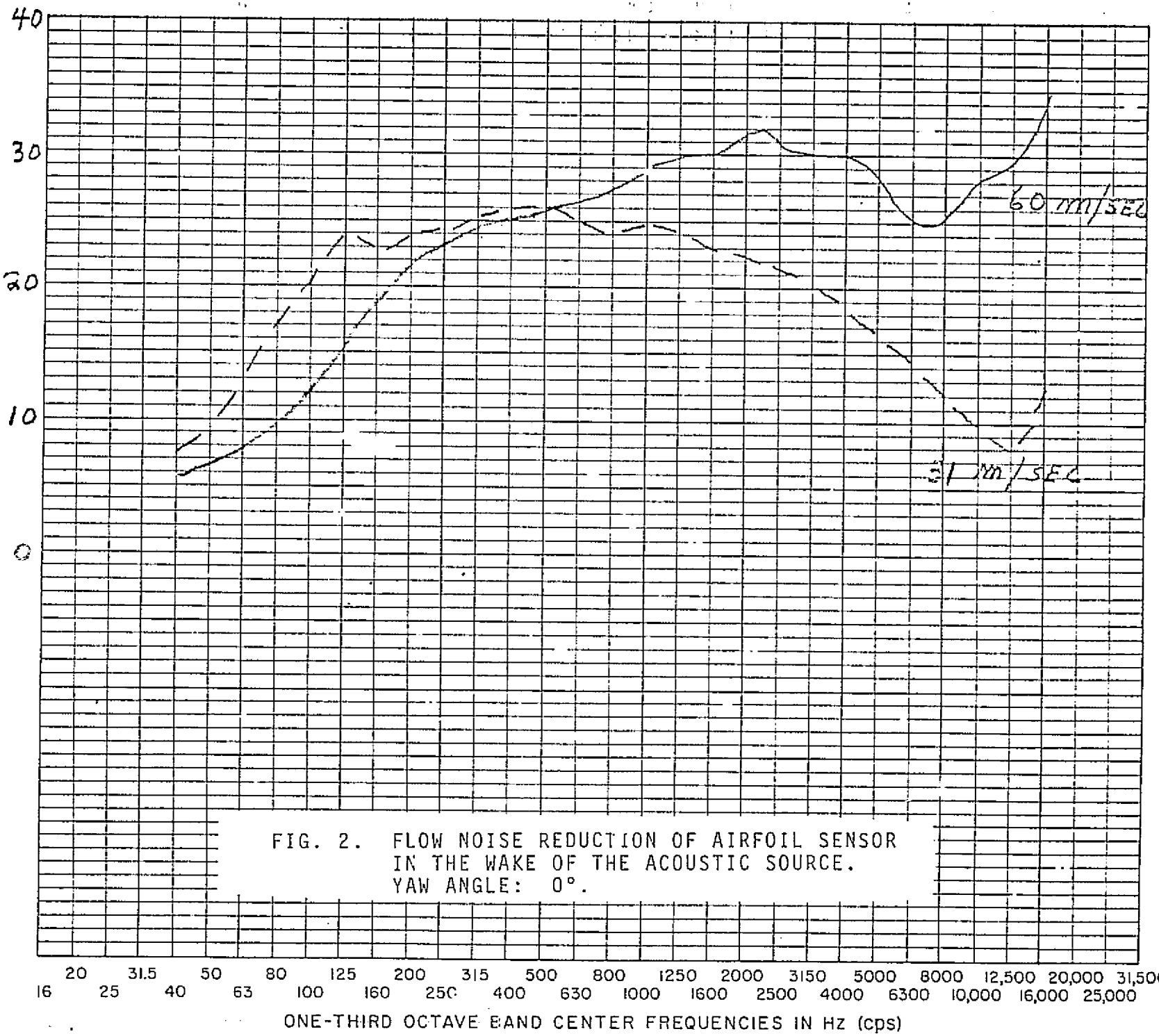

FIG. 2. FLOW NOISE REDUCTION OF AIRFOIL SENSOR IN THE WAKE OF THE ACOUSTIC SOURCE. YAW ANGLE: 0°.

BOLT BERANEK & NEWMAN INC

3. CONCLUSIONS

The new Porous Surface Microphone in an Airfoil, Model 342, has achieved substantial improvements over the earlier design. The frequency response has been extended; the flow noise, especially the component due to flow separation on the airfoil, has been reduced for the full range of yaw angles.

The flow noise rejection of the Airfoil Sensor, referred to the B&K Sensor with nose cone, is significant even at very low intensity of turbulence; it could be very large when the intensity of turbulence is large.

The acceleration sensitivity of the Airfoil Sensor is very low and can be neglected for most of the practical situations.

The effect of Mach number on the directivity function of the Airfoil Sensor is predictable in the subsonic range, at least up to 10 kHz. This effect consists of a sequence of large dips in the sensor response, even when the sensor is pointed directly towards the sound source. The location in frequency of these dips depends on the Mach number and the orientation of the sensor with respect to the sound source. These dips limit the usefullness of the current design; however, they could be eliminated by using, instead of air, a proper gas mixture inside the sensor. This modification merits further consideration.

APPENDIX I

ACOUSTIC CALIBRATION OF THE NEW POROUS SURFACE MICROPHONE IN AN AIRFOIL, MODEL 342, S/N2

A new design of a Porous Surface Microphone in an Airfoil has been developed recently[1]; Model 342. This new design has an improved frequency response and should have a lower flow noise than the earlier design[2].

A second unit of this new design has been fabricated for NASA Ames. This memo presents the acoustic calibration of this second unit.

The photograph of Fig. 1 shows the Porous Surface Microphone on the left, the microphone base and the tail end of the base on the right. All three sections are rigidly bolted together and preserve the shape of the airfoil: this shape is a NACA 64-0012 section. A pipe is cemented to the base and carries the electrical leads of the preamplifier.

The microphone cartridge and preamplifier, without grid cap, screws into the microphone hole at the end of the Porous Surface Microphone. The cartridge must be a B&K-type 4134 which has a flat pressure response up to approximately 20 kHz, and which equalizes its internal pressure to the front of the cartridge.

The porous strips are each 14 inches long. The specific acoustic resistance of the two porous strips is shown in Fig. 2. The mean value is close to $50\ \rho_0 c_0$ where $\rho_0 c_0$ is the characteristic impedance of air; the variations from the mean are approximately ±1 dB.

The frequency response of the Porous Surface Microphone has been measured in the plane wave tube and in the anechoic room. The results, shown in Fig. 3, give also the sensitivitv

---

[1]With Langley Research Center see: D.U. Noiseux

[2]D.U. Noiseux, "Study of Porous Surface Microphones for Acoustic Measurements in Wind Tunnels," NASA CR-114593, April 1973.

with respect to the pressure sensitivity of the microphone cartridge. The frequency response of Units 1 and 2 are very nearly identical.

The directivity patterns measured for Unit No. 1 will also apply to Unit No. 2 because their geometries are identical. Only the details of the high order minor lobes will be different; these details depend on the local variations of the acoustic resistance of the porous strips.

The directivity patterns of Unit No. 1 are reproduced[2] as the original Figs. 6 and 7. The directivity has been measured about two axes of rotation which are indicated in the figures. At 10 kHz, the envelope of the directivity of an ideal line sensor of the same length as the porous strips of the Airfoil Sensor, has been calculated and is shown in Fig. 6e and 7e.

[2]See Ref. 1, Appendix IX.

ORIGINAL PAGE IS
OF POOR QUALITY

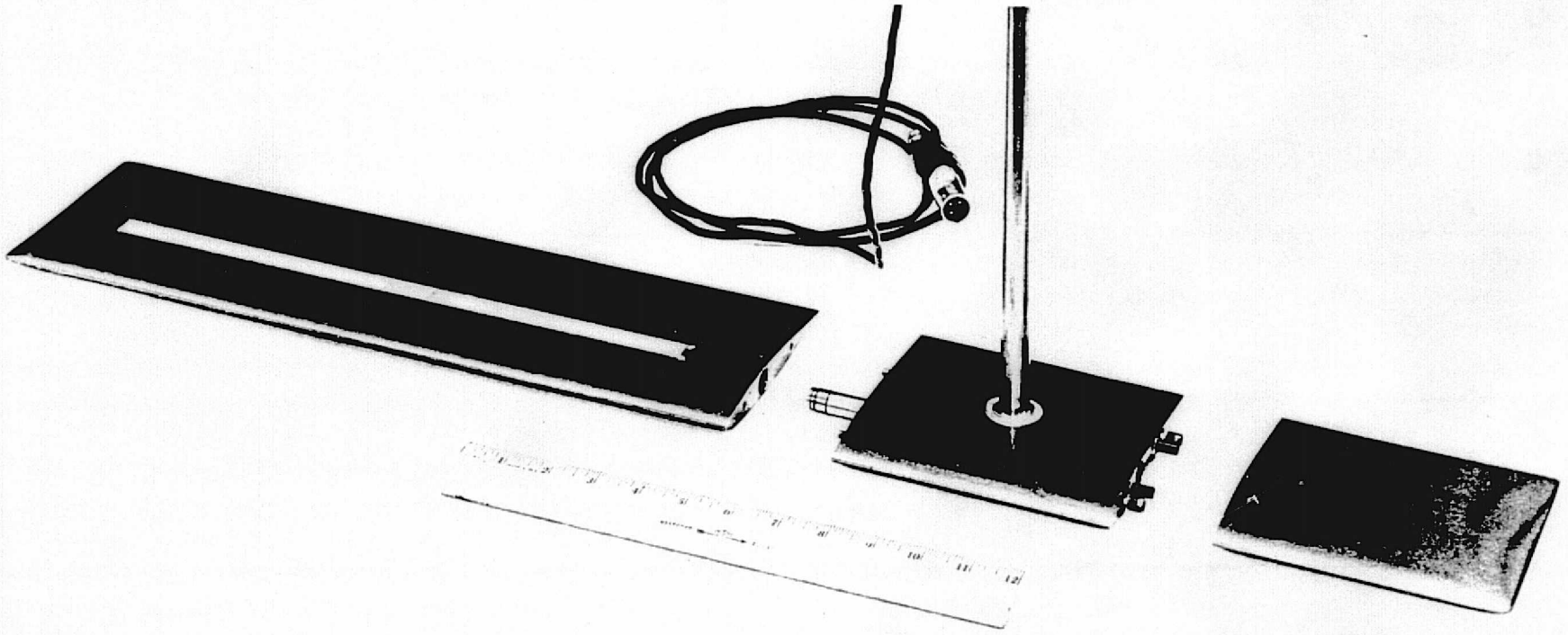

FIG. 1 POROUS SURFACE MICROPHONE IN AN AIRFOIL
MODEL 342, SHOWN WITH BASE

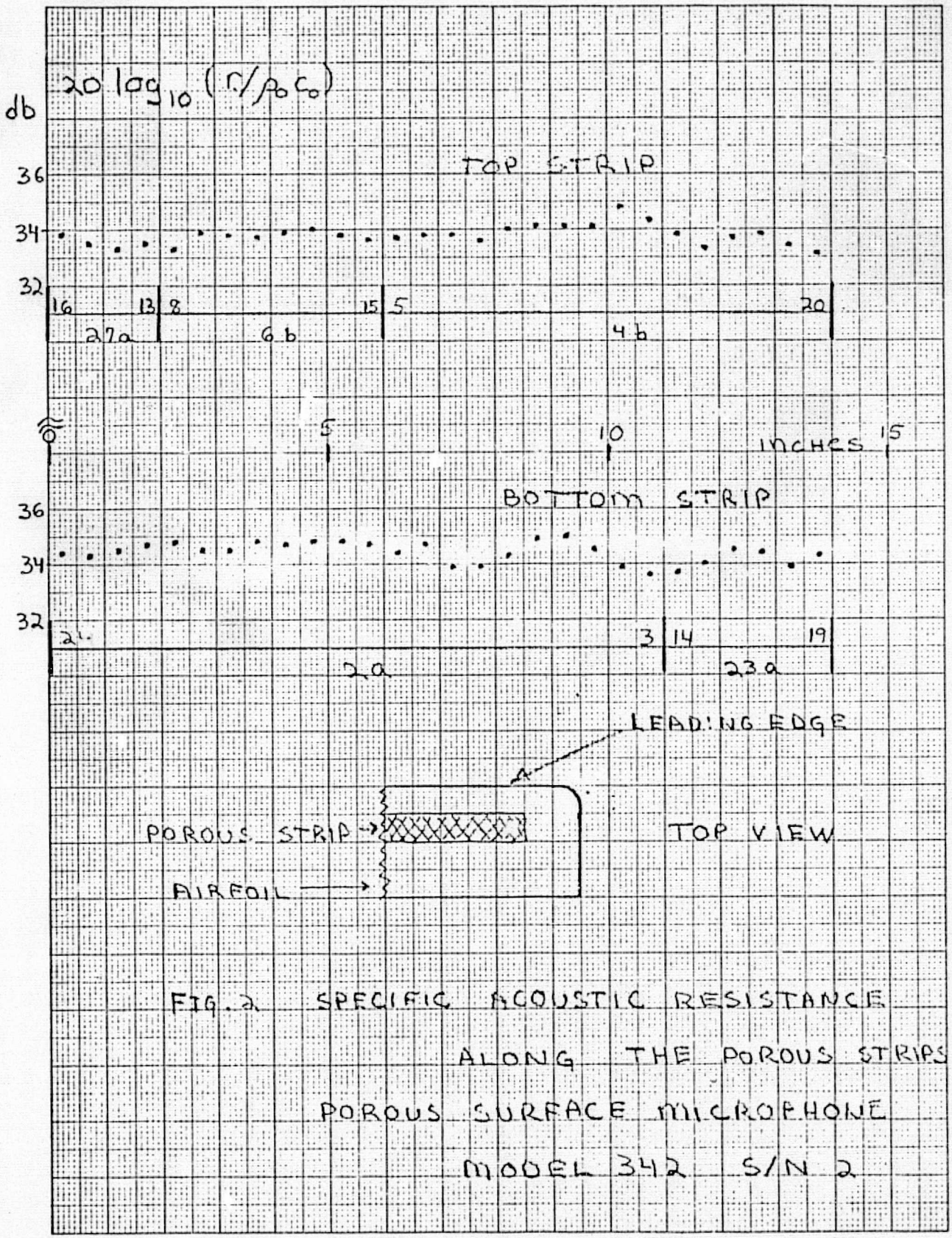

FIG. 2 SPECIFIC ACOUSTIC RESISTANCE ALONG THE POROUS STRIPS

POROUS SURFACE MICROPHONE

MODEL 342 S/N 2

ORIGINAL PAGE IS
OF POOR QUALITY

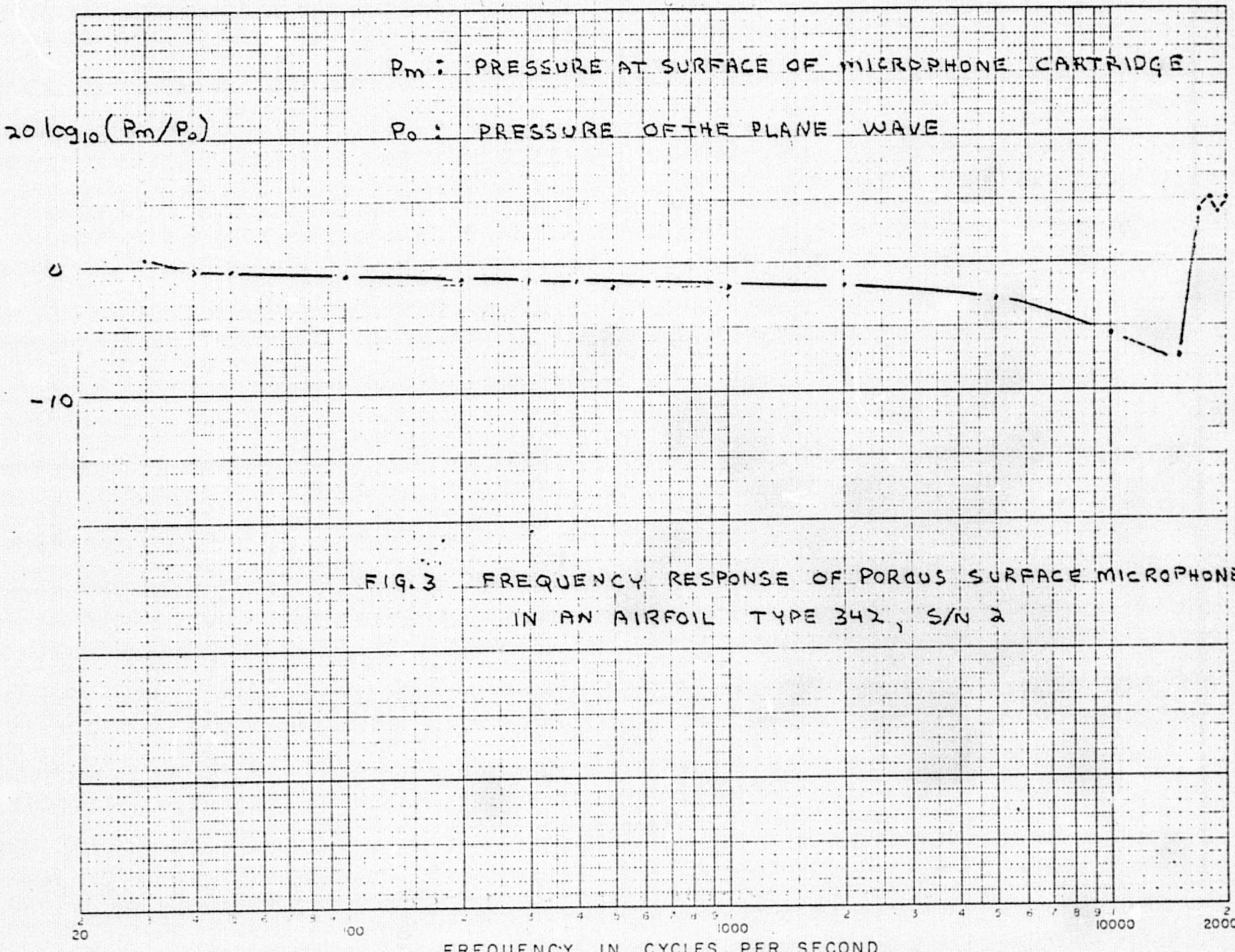

FIG. 3 FREQUENCY RESPONSE OF POROUS SURFACE MICROPHONE IN AN AIRFOIL TYPE 342, S/N 2

5.1

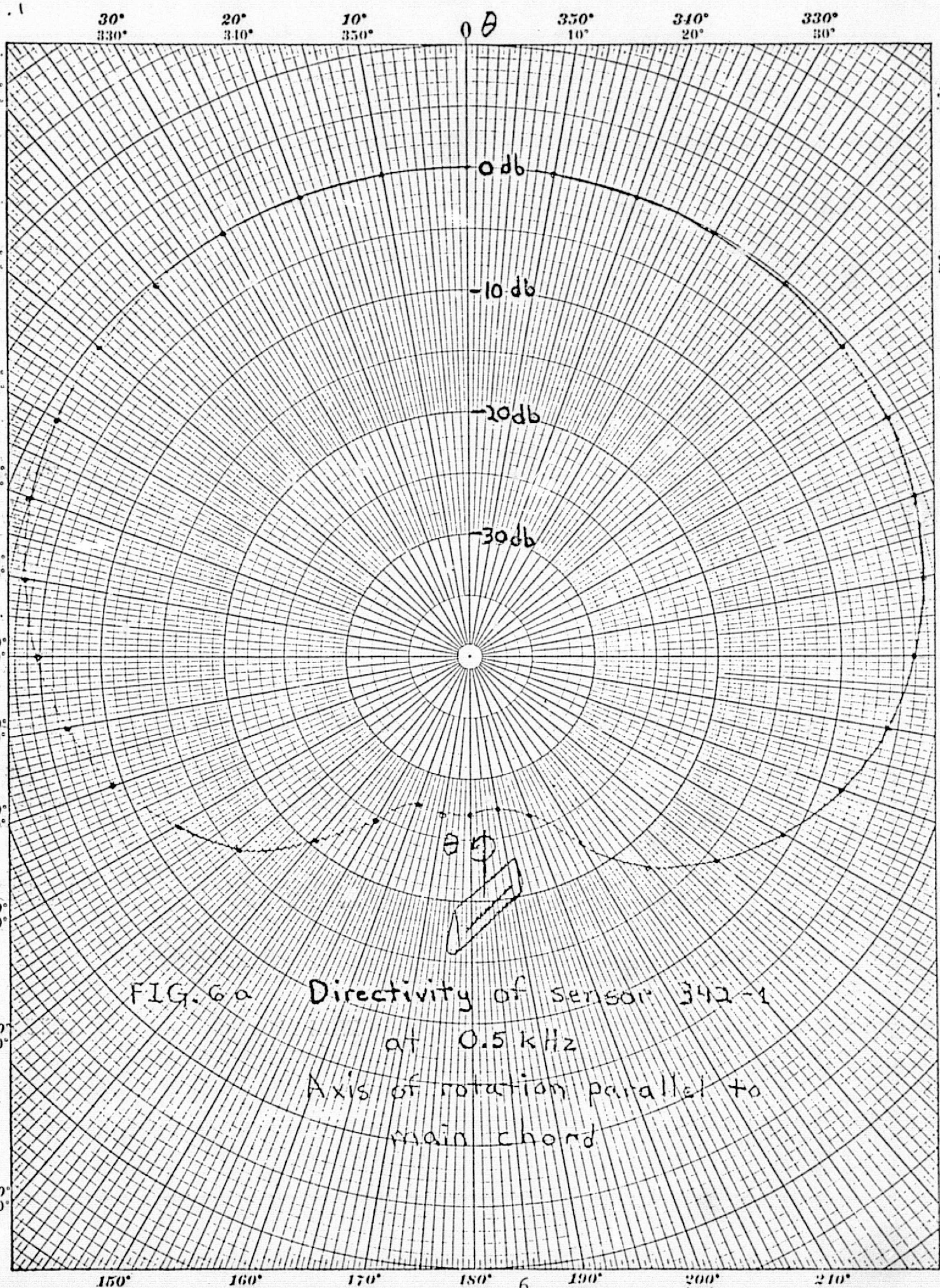

FIG. 6a Directivity of sensor 342-1
at 0.5 kHz
Axis of rotation parallel to
main chord

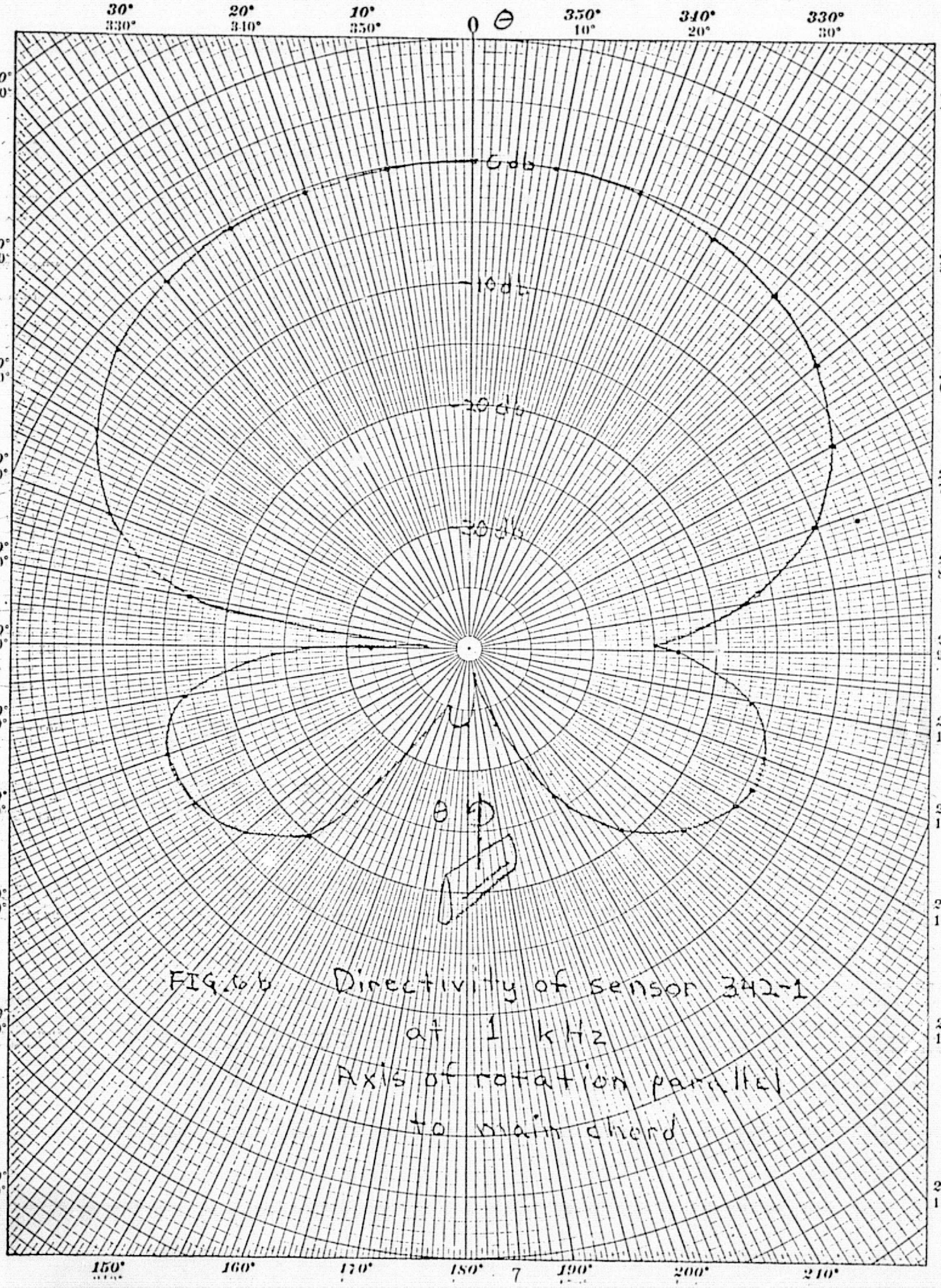

FIG 6b Directivity of sensor 342-1
at 1 kHz
Axis of rotation parallel
to main chord

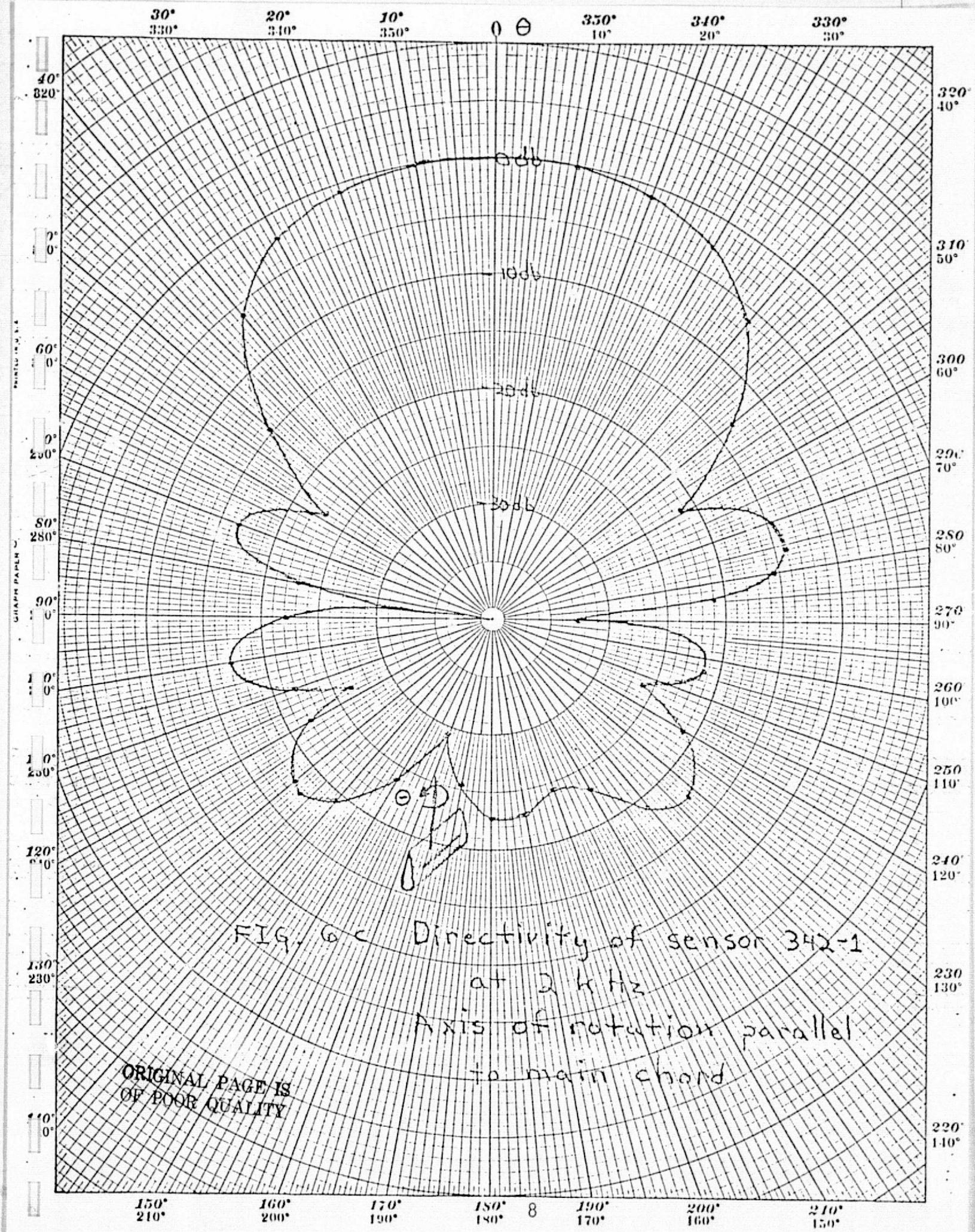

FIG. 6c Directivity of sensor 342-1
at 2 kHz
Axis of rotation parallel
to main chord

ORIGINAL PAGE IS
OF POOR QUALITY

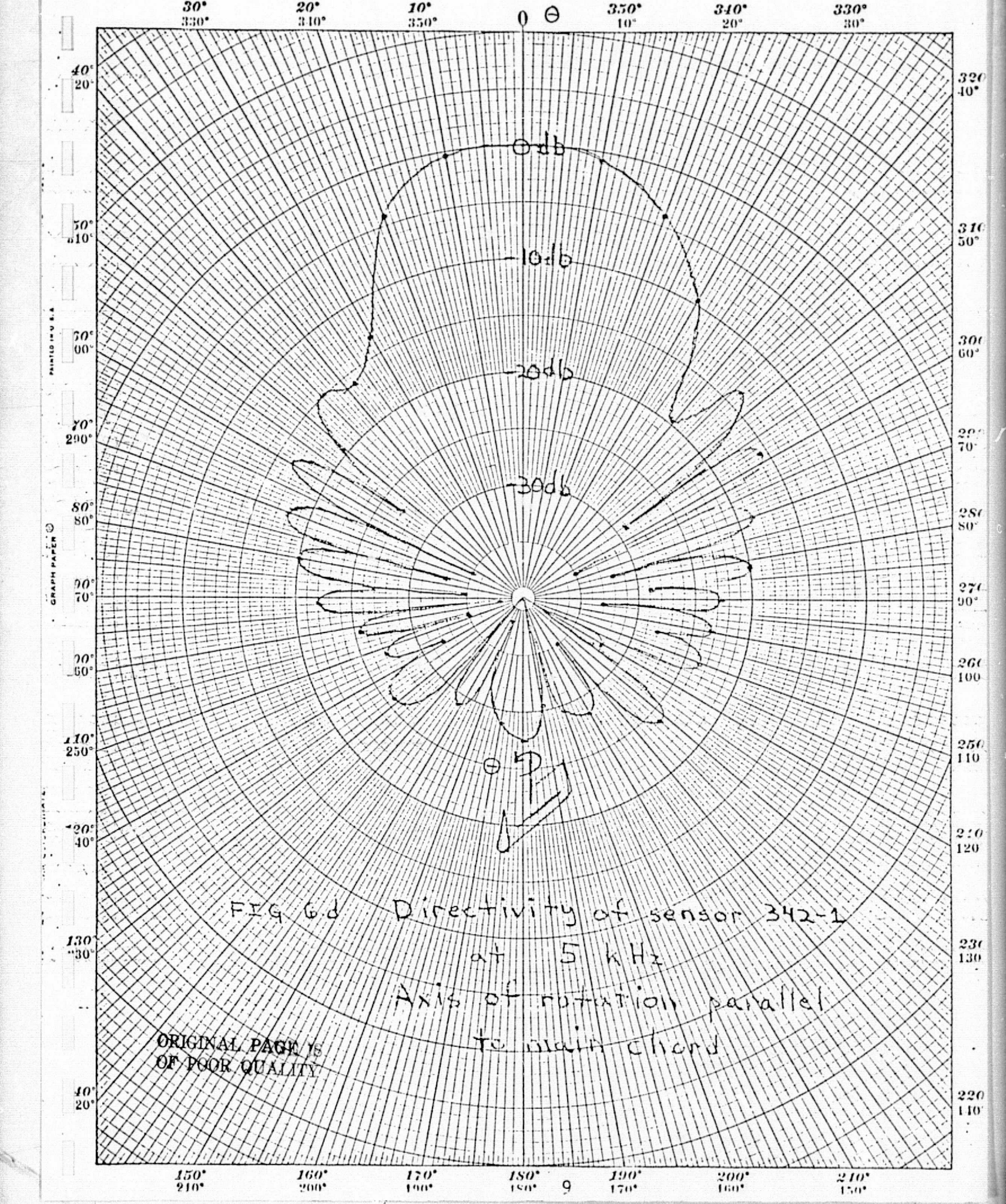

FIG 6d Directivity of sensor 342-1 at 5 kHz Axis of rotation parallel to main chord

ORIGINAL PAGE IS OF POOR QUALITY

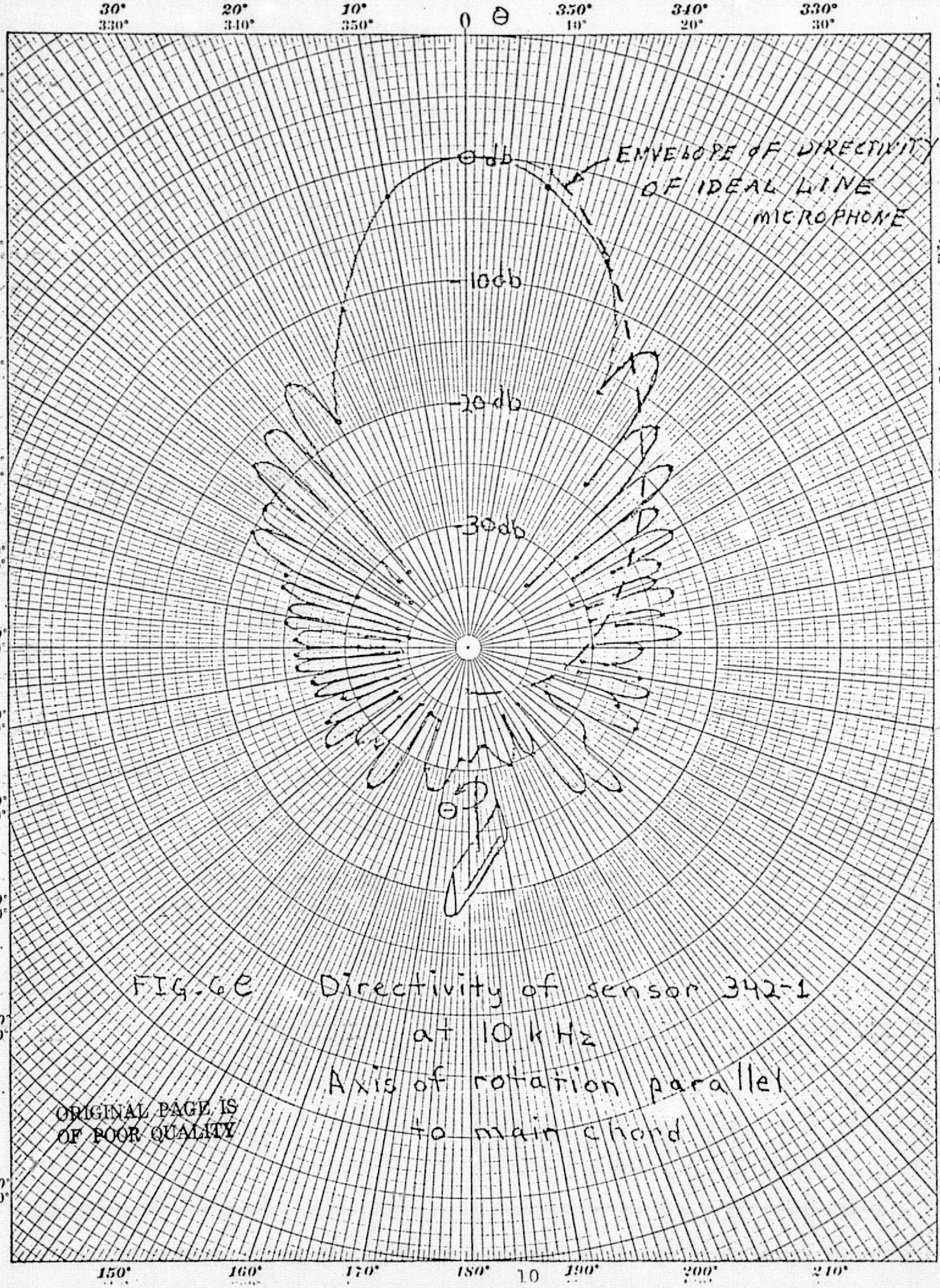

FIG. 6E Directivity of sensor 342-1
at 10 kHz
Axis of rotation parallel
to main chord

ORIGINAL PAGE IS
OF POOR QUALITY

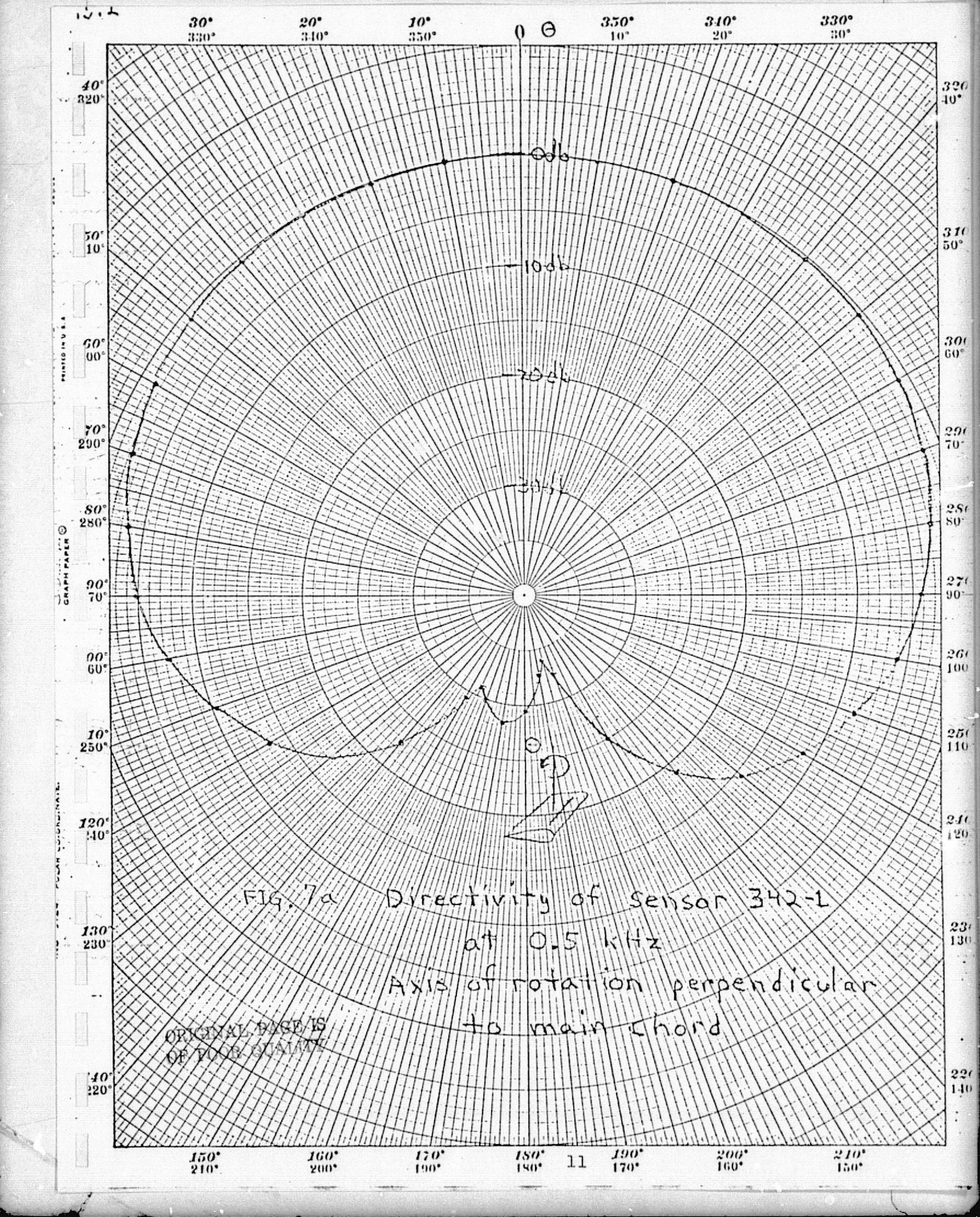

FIG. 7a Directivity of Sensor 342-1
at 0.5 kHz
Axis of rotation perpendicular
to main chord

ORIGINAL PAGE IS
OF POOR QUALITY

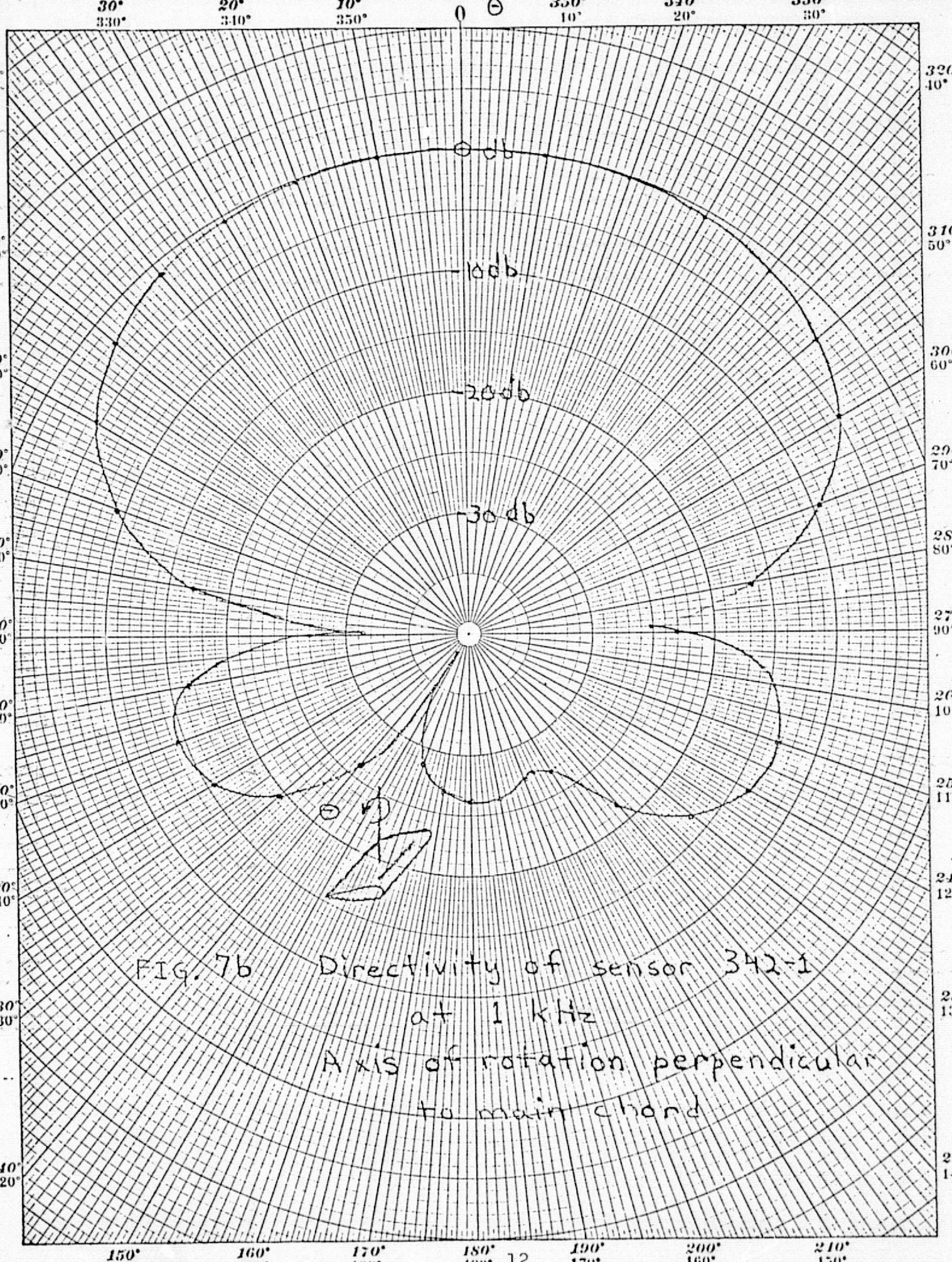

FIG. 7b Directivity of sensor 342-1
at 1 kHz
Axis of rotation perpendicular
to main chord

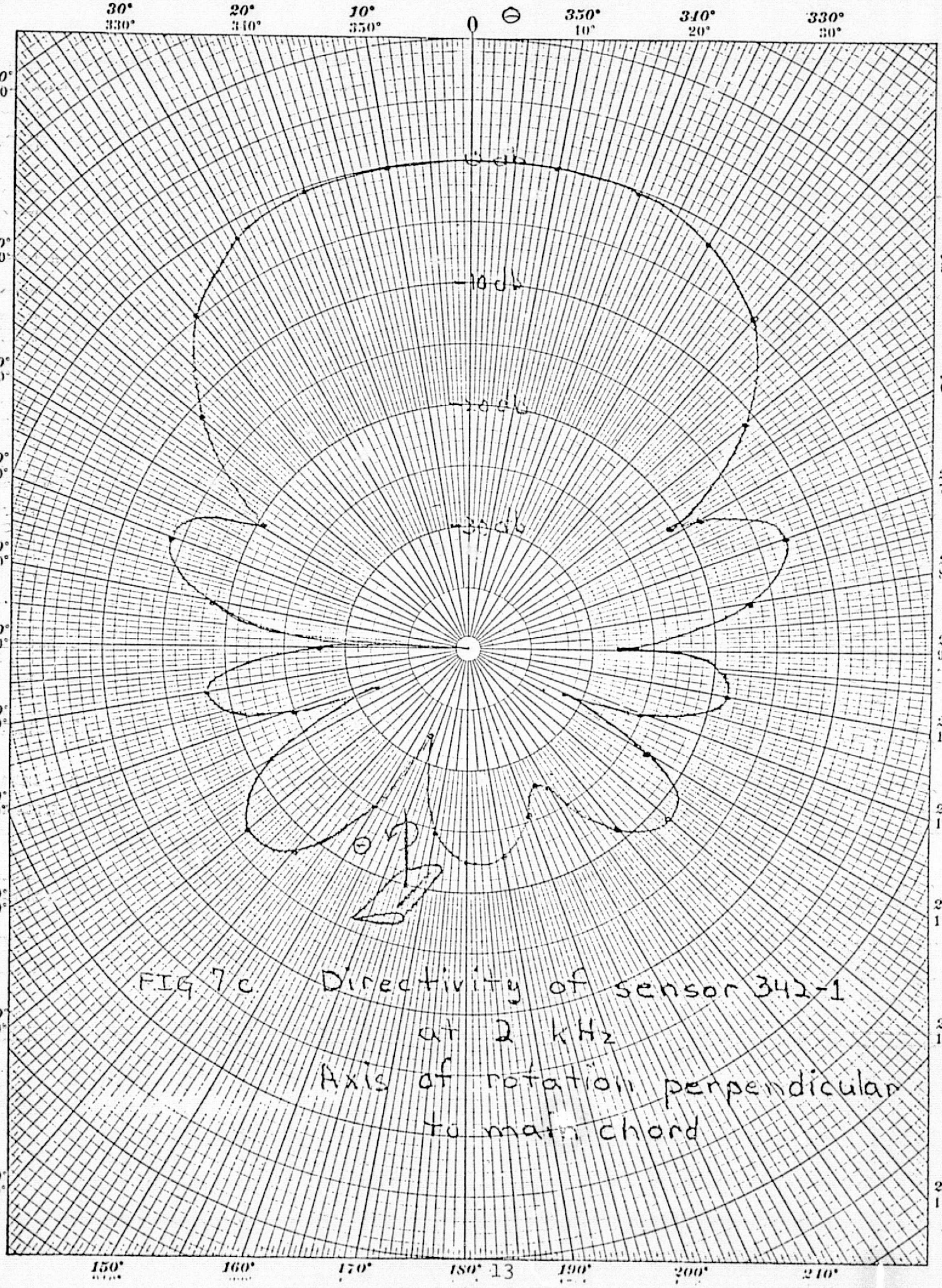

FIG 7c Directivity of sensor 342-1
at 2 kHz
Axis of rotation perpendicular
to main chord

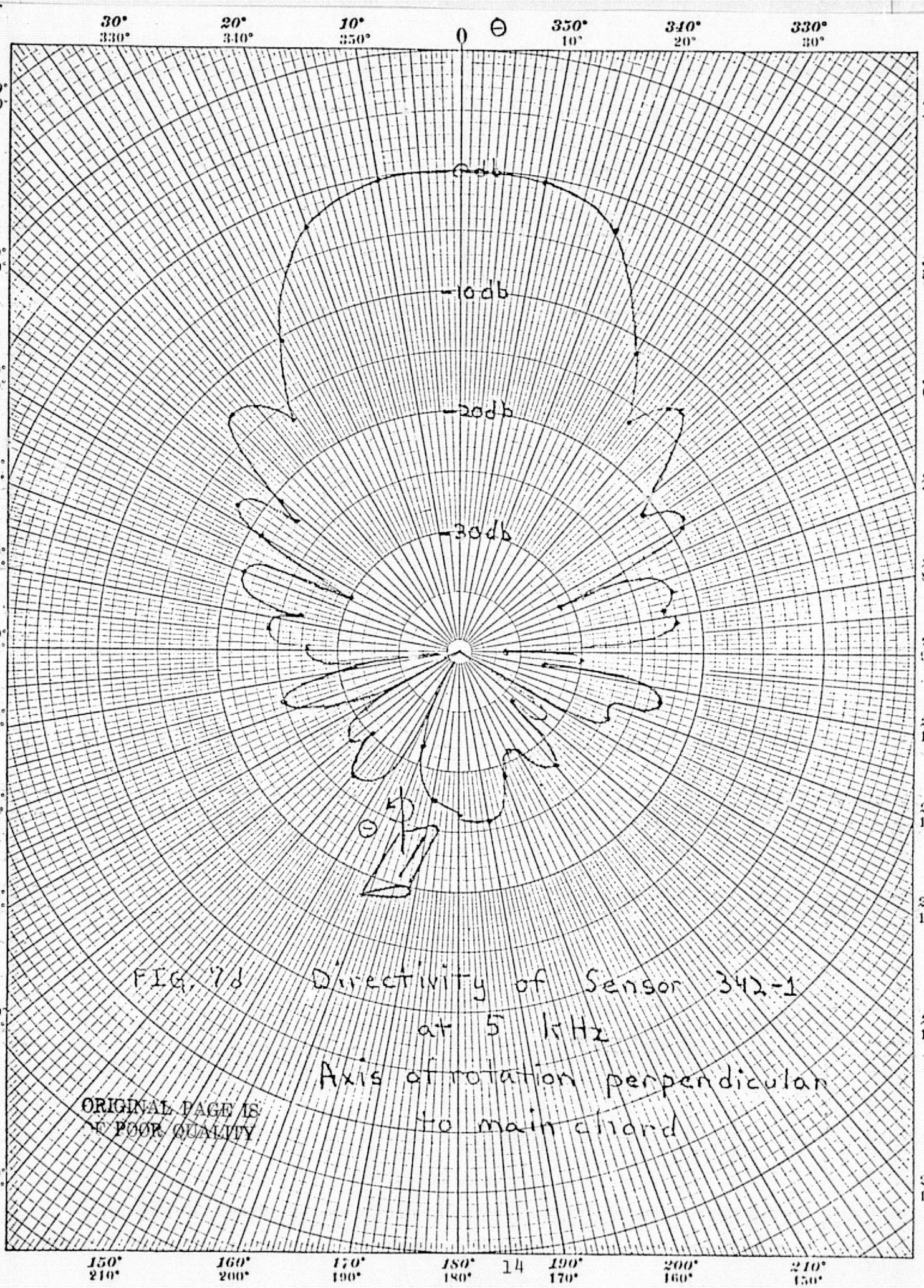

FIG. 7d Directivity of Sensor 342-1
at 5 kHz
Axis of rotation perpendicular
to main chord

ORIGINAL PAGE IS
OF POOR QUALITY

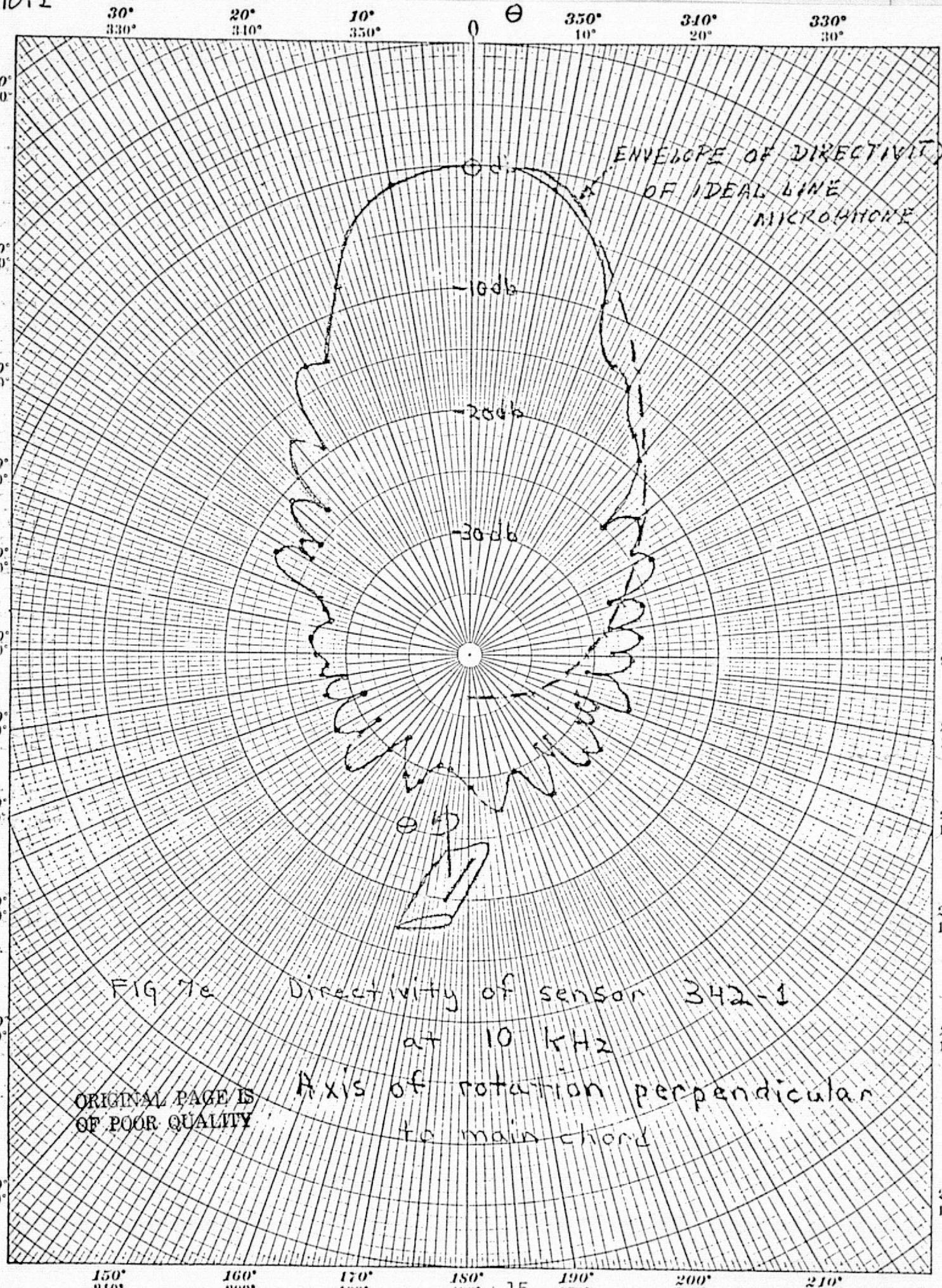

FIG 7a Directivity of sensor 342-1
at 10 kHz
Axis of rotation perpendicular
to main chord

ORIGINAL PAGE IS
OF POOR QUALITY

APPENDIX II

VIBRATION SENSITIVITY OF THE POROUS SURFACE MICROPHONE IN AN AIRFOIL

1. INTRODUCTION

When the Airfoil Porous Surface Sensor is subjected to air flow, the dominant type of vibration of the airfoil will be flexural waves. These vibration waves will create surface pressures on the porous strips of the Airfoil Sensor. However, the symmetrical design of the Airfoil Sensor makes it rather insensitive to flexural vibrations: pressures generated at one face of the sensor are equal to and of opposite polarity from the pressures generated at corresponding points on the opposite face; when these local pressures enter the acoustic cavities of the sensor and reach the common surface of the microphone cartridge, they cancel out. The degree of cancellation depends on the variations of the specific acoustic resistance of the porous strips; with variations maintained to less than 10%, we anticipate a cancellation of more than 20 dB.

An evaluation of the contribution of the vibration of the Airfoil Porous Surface Sensor to the flow was planned; the original plan will be modified because of the difficulty of measuring directly the acceleration sensitivity of the sensor.

The original plan consisted of the following steps:

(1) The flow noise spectrum of the Airfoil Sensor is measured at different flow velocities for one yaw angle $\alpha = 90°$.

(2) The acceleration spectrum of the Airfoil Sensor due to air flow is measured at one point of the surface of the sensor for the same flow velocities and the yaw angle $\alpha = 90°$.

(3) The acceleration sensitivity of the Airfoil Sensor excited by a shaker and monitored by an accelerometer is measured: the ratio of the output of the Sensor in equivalent pressure, to the acceleration level is the acceleration sensitivity.

(4) The acceleration sensitivity obtained in (3) multiplied by the acceleration spectrum measured in (2) yields approximately the contribution of vibration to flow noise. This contribution is then compared with the net flow noise measured in (1).

Measurements (1) and (2) in air flow are readily done. Measurement (3) is much more difficult to realize because of the low vibration sensitivity of the Airfoil Sensor: the pressures sensed by the Sensor during the shaker test are dominated at low frequencies by the ambient noise of the test chamber. (The acceleration levels produced by the small shaker used were very low.) In view of this experimental difficulty, the direct measurement (3) of the acceleration sensitivity was replaced by an estimate of the vibration sensitivity which is developed in Section 2. This estimate may be more useful than the direct measurement because the estimate shows why the acceleration sensitivity of the Airfoil Sensor is so low.

An estimate of the acceleration sensitivity of the Airfoil Sensor is developed in Section 2. The flow noise and acceleration spectra are shown in Section 3. The contribution of acceleration of the Airfoil to the net flow noise is calculated in Section 4.

2. ESTIMATE OF THE ACCELERATION SENSITIVITY OF THE AIRFOIL SENSOR

The estimation proceeds as follows:

(1) An estimate of the point pressure on *one* surface of the airfoil per unit acceleration is calculated as a function of frequency.

(2) To this pressure field is associated a bending wavenumber k_b. The pressure field is filtered by the directivity function of the Airfoil Sensor using $\pm k_b$ instead of the acoustic wavenumber component, $k_o \cos\alpha$, along the axis of the porous strips.

(3) The pressure fields from the surfaces of the two porous strips combine at the surface of the microphone element resulting in a net cancellation which is estimated to be at least one order of magnitude (20 dB).

The sequence of these three calculations yields an estimate of the acceleration sensitivity of the Airfoil Sensor.

In view of the many approximations which will be used to estimate the point pressures on one surface, done in (1), the further calculation of the filtering done in (2) becomes almost irrelevant and will not be carried forth. The net effect of calculating (1) and (3) but not (2) is an overestimation of the acceleration sensitivity.

The point pressure $p(\omega)$ are one surface of the Airfoil, per unit acceleration is estimated in three frequency ranges.

At low frequencies, below the first bending mode frequency of the airfoil, the specific impedance $z(\omega)$ of the fluid loading is similar to the fluid loading of a flat disc of radius r:

$$p(\omega) = U(\omega)\ z(\omega)$$

$$= \frac{a(\omega)}{i\omega}\ z(\omega)$$

where $a(\omega)$ is the acceleration and ω is the angular frequency, and, for a flat disc*

$$z(\omega) \triangleq 0.067\ i\omega\rho_0(2\pi r) \quad ; \quad \text{low frequencies}$$

If the perimeter $2(\ell+w)$ of the airfoil is introduced instead of the circumference $2\pi r$ of the flat disc, we get a slight overestimate of the low frequency acceleration sensitivity of one face of the Airfoil Sensor:

$$\frac{p(\omega)}{a(\omega)} = 0.135\ \rho_0(\ell+w)$$

where ρ_0 is the density of air.

At high frequencies, but below the frequency at which the flexural wave velocity equals the sound velocity in air, (the so-called coincidence frequency), the Airfoil will behave as a plate of the same thickness, and its fluid loading becomes

$$z(\omega) = \frac{i\omega\rho_0}{k_b}$$

$$k_b = 1.86\sqrt{\frac{\omega}{c_\ell h}}$$

---

*L.L. Beranek, *Acoustics*, McGraw Hill Book Co., Article 504, pp. 128.

where k_B is the bending wavenumber, c_ℓ is the longitudinal wave velocity of the material of the airfoil (epoxy) and h is the thickness. Hence, the acceleration sensitivity of one face of the airfoil becomes

$$\frac{p(\omega)}{a(\omega)} \triangleq \frac{\rho_0}{k_b}$$

$$\cong \frac{\rho_0}{1.86}\sqrt{\frac{c_\ell h}{\omega}} \quad ; \text{ medium frequencies.}$$

Above coincidence frequency, the fluid loading impedance is the characteristic impedance $\rho_0 c_0$ of the fluid. Hence,

$$\left| \frac{p(\omega)}{a(\omega)} \right| = \frac{\rho_0 c_0}{\omega} \quad ; \text{ above coincidence frequency.}$$

The estimates for the three frequency regions are sketched in Fig. 1 using the parameters of the Airfoil Sensor: ℓ, w, h and c_ℓ. It is interesting to note that the acceleration sensitivity of one face of the Airfoil Sensor is everywhere lower than the acceleration sensitivity of a one-inch condenser microphone in free air: 93 dB SPL/G.

For two faces of the Airfoil Sensor, a cancellation of 20 dB is introduced in Fig. 1 to yield to net acceleration sensitivity. Again, the asymptotic values shown in Fig. 1 are overestimates of the true acceleration sensitivity. The overestimation is of the order of 6 dB.

ORIGINAL PAGE IS
OF POOR QUALITY

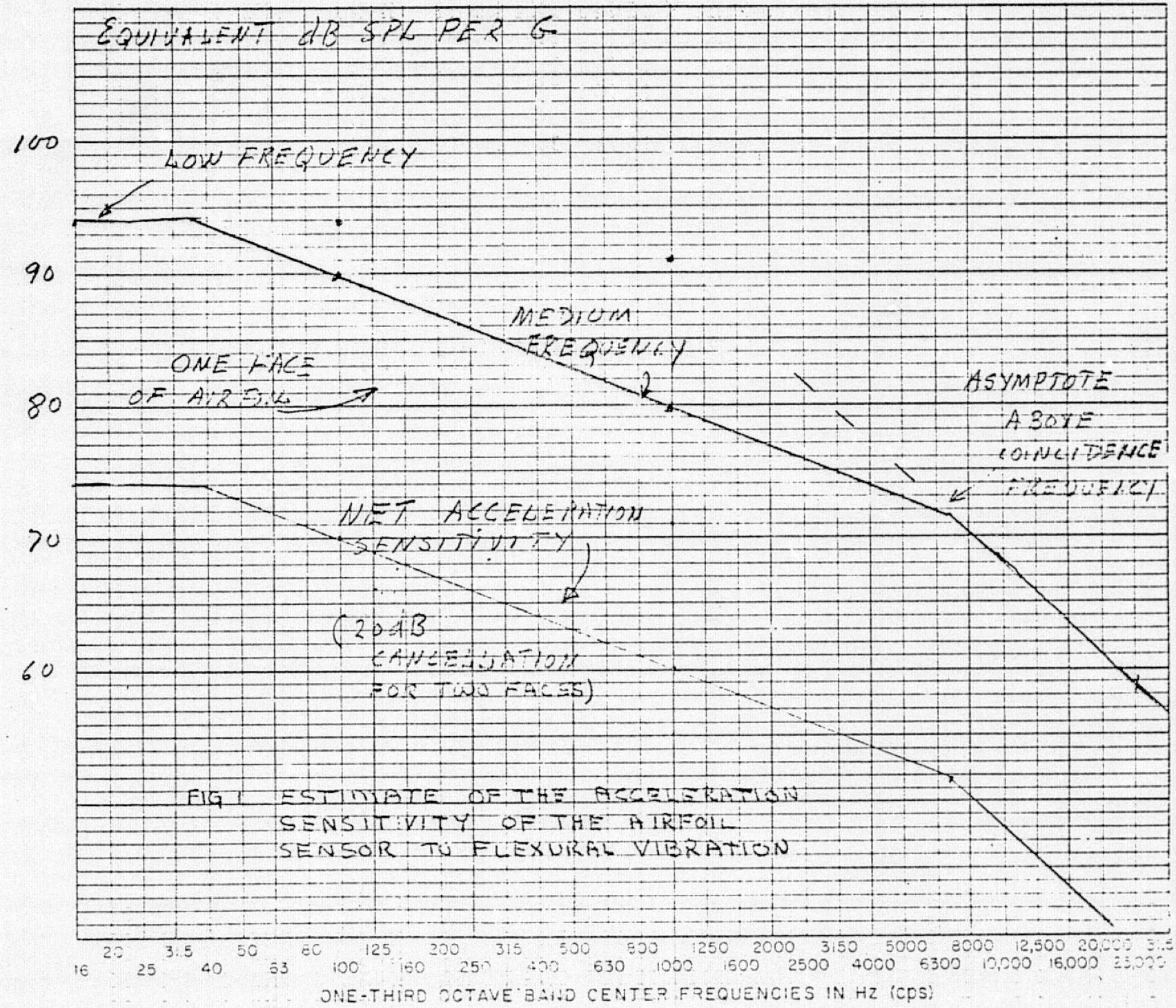

FIG 1 ESTIMATE OF THE ACCELERATION SENSITIVITY OF THE AIRFOIL SENSOR TO FLEXURAL VIBRATION

BOLT BERANEK & NEWMAN INC

3. FLOW NOISE AND ACCELERATION LEVELS OF THE AIRFOIL SENSOR

A small accelerometer is cemented on the Airfoil Sensor, at approximately 2/3 of the distance from the tip of the sensor and the acceleration levels recorded for different flow velocities when the yaw angle α is 90°. The results are shown in third octave bands in Fig. 2.

The flow noise measured by the Airfoil Sensor, without the accelerometer, for the same range of flow velocities and for yaw angle α = 90° is shown in Fig. 3.

The resonances shown in Fig. 2 correspond to the simple bending modes of a cantilever beam of the same thickness and material as the airfoil; the length of the cantilever beam is the length from the tip of the airfoil sensor to the center pipe of the preamplifier base. The resonance frequencies of these modes are calculated (from Tables of resonance frequencies of cantilever beams) to be:

1st mode: 16 Hz
2nd mode: 102 Hz
3rd mode: 290 Hz
4th mode: 565 Hz
5th mode: 940 Hz

They correspond very well with the measured resonances.

ORIGINAL PAGE IS
OF POOR QUALITY

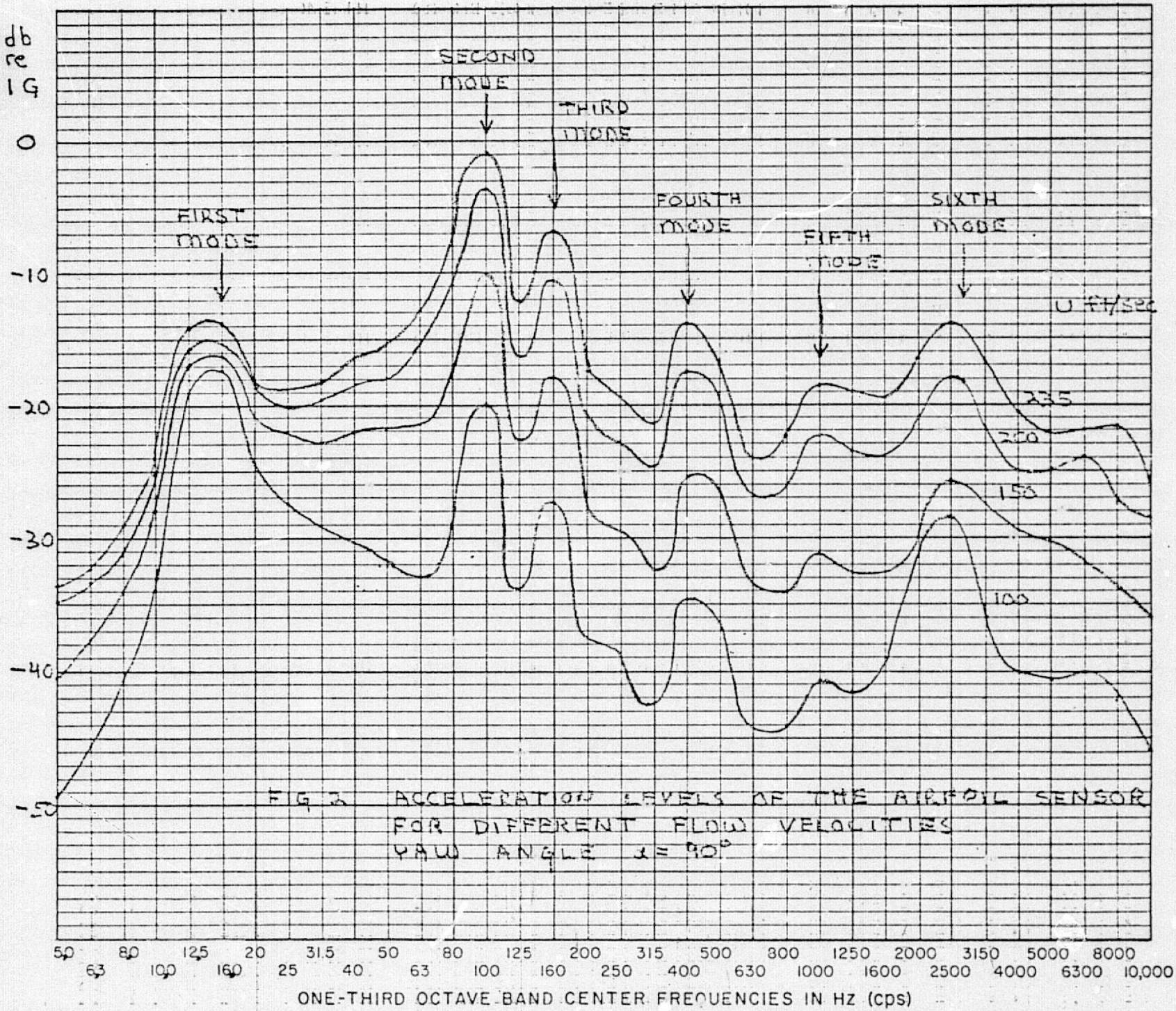

FIG 3 ACCELERATION LEVELS OF THE AIRFOIL SENSOR FOR DIFFERENT FLOW VELOCITIES YAW ANGLE $\chi = 90^{\circ}$

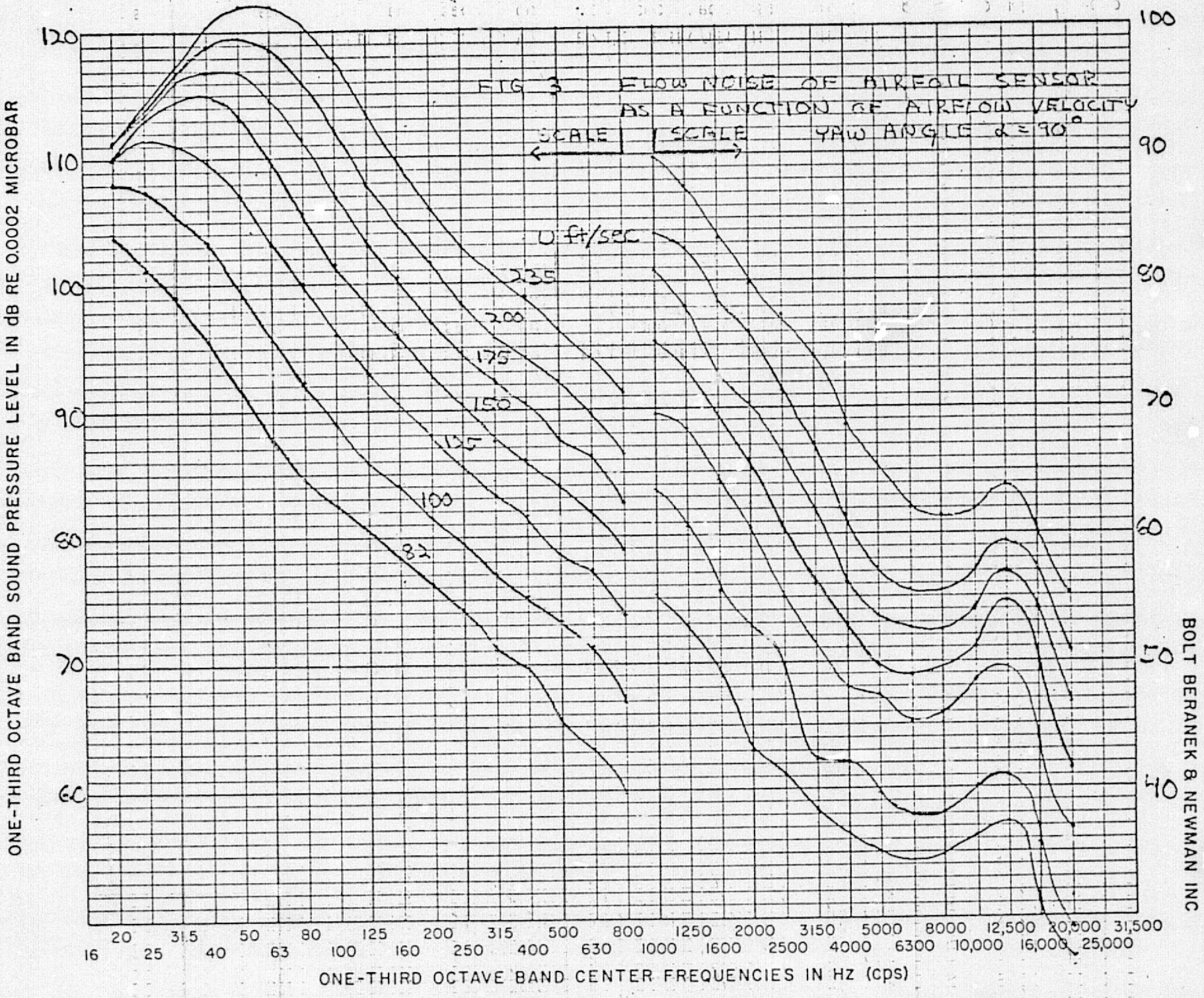
FIG 3 FLOW NOISE OF AIRFOIL SENSOR AS A FUNCTION OF AIRFLOW VELOCITY
YAW ANGLE α = 90°
SCALE
SCALE
U ft/sec
235
200
175
150
125
100
82
ONE-THIRD OCTAVE BAND SOUND PRESSURE LEVEL IN dB RE 0.0002 MICROBAR
120
110
100
90
80
70
60
100
90
80
70
60
50
40
16 20 25 31.5 40 50 63 80 100 125 160 200 250 315 400 500 630 800 1000 1250 1600 2000 2500 3150 4000 5000 6300 8000 10,000 12,500 16,000 20,000 25,000 31,500
ONE-THIRD OCTAVE BAND CENTER FREQUENCIES IN Hz (cps)
BOLT BERANEK & NEWMAN INC

4. CONTRIBUTION OF ACCELERATION TO FLOW NOISE

The acceleration levels of Fig. 2, multiplied by the estimate of the net acceleration sensitivity of the Airfoil Sensor given in the lower curve of Fig. 1, yield the contribution of the acceleration to the flow noise: this contribution is shown in

Comparing Fig. 4 and Fig. 3, we find that the contribution of the acceleration of the Airfoil Sensor is at least 30 dB below the net flow noise of the Sensor; the contribution is effectively negligible. This conclusion is also apparent from the flow noise spectrum of Fig. 3 which does not exhibit any resonances associated with the resonances seen in the acceleration spectrum of Fig. 2.

When the Airfoil Porous Surface Sensor is used in normal wind tunnel conditions where the vibration of the Sensor is caused by the turbulence of the airflow, the contribution of the acceleration of the sensor to the flow noise can be neglected. The normal wind tunnel conditions imply that the stand on which the Airfoil Sensor is mounted is rigid like the stand we have used in the present tests.

ORIGINAL PAGE IS
OF POOR QUALITY

FIG 4 CONTRIBUTION OF ACCELERATION OF AIRFOIL SENSOR TO FLOW NOISE. YAW ANGLE $\alpha = 90°$

BOLT BERANEK & NEWMAN INC

APPENDIX III

STATIONARY SOURCE AND RECEIVER IN A MOVING GAS

1. INTRODUCTION

When air is flowing between a stationary acoustic source and a stationary receiver, the acoustic radiation from the source and the directivity function of the receiver are modified from their original values when the air is stationary. In this appendix, we formulate the modification of the directivity function of the receiver, leaving out the much more difficult problem of the modification of the radiation of the source: we assume that the source is radiating a plane acoustic wave in the region of the receiver.

The modification of the directivity function of the receiver is formulated by two methods. The first method, presented in Section 2, is an *ad hoc* formulation specifically for a plane harmonic wave. A more general method, leading to the same results for a plane wave, is presented in Section 3. The motivation for using the general method is to clarify possible ambiguities in its general results when applied to a plane wave.

2. PLANE WAVE

The positions of the source and receiver are shown in Fig. 1, in the laboratory coordinates $\underset{\sim}{x} = \{x_1, x_2, x_3\}$. The gas between the source and the receiver is moving uniformly with a velocity $\underset{\sim}{U}$ with respect to the laboratory coordinates.

We consider the case where the source is far from the receiver so that the pressure field in the region of the receiver is effectively a plane wave. If we select only one harmonic component of the plane wave and express this wave in the coordinates $\overline{\underset{\sim}{x}}$ moving with the gas, we have

$$\overline{p}\ (\overline{\underset{\sim}{x}},t) = \overline{P}_o \exp\left[-i(\overline{\underset{\sim}{k}}_o \cdot \overline{\underset{\sim}{x}} - \overline{\omega}_o t)\right] \qquad (1)$$

The bar superscript is used to indicate that the quantity is measured in the coordinates, $\overline{\underset{\sim}{x}}$, moving with the gas; $\overline{\underset{\sim}{k}}_o$ is the wavenumber vector and $\overline{\omega}_o$ is the circular frequency of the plane wave measured in the moving coordinates, $\overline{\underset{\sim}{x}}$.

The point pressure $p(\underset{\sim}{x},t)$ in the laboratory coordinates is the same as the point pressure $\overline{p}(\overline{\underset{\sim}{x}},t)$ in the moving coordinates provided

$$\underset{\sim}{x} = \overline{\underset{\sim}{x}} + \underset{\sim}{U}t \quad ; \qquad (2)$$

with (2) in (1) we get

$$p(\underset{\sim}{x},t) = \overline{P}_o \exp\left\{-i[\overline{\underset{\sim}{k}}_o \cdot \underset{\sim}{x} - (\overline{\omega}_o + \overline{\underset{\sim}{k}}_o \cdot \underset{\sim}{U})t]\right\} \qquad (3)$$

From (3) we have the following conclusions: the *level* of pressure measured by a fixed receiver is the same that would be measured by a moving receiver; the wavenumber k_o of the plane wave is unchanged

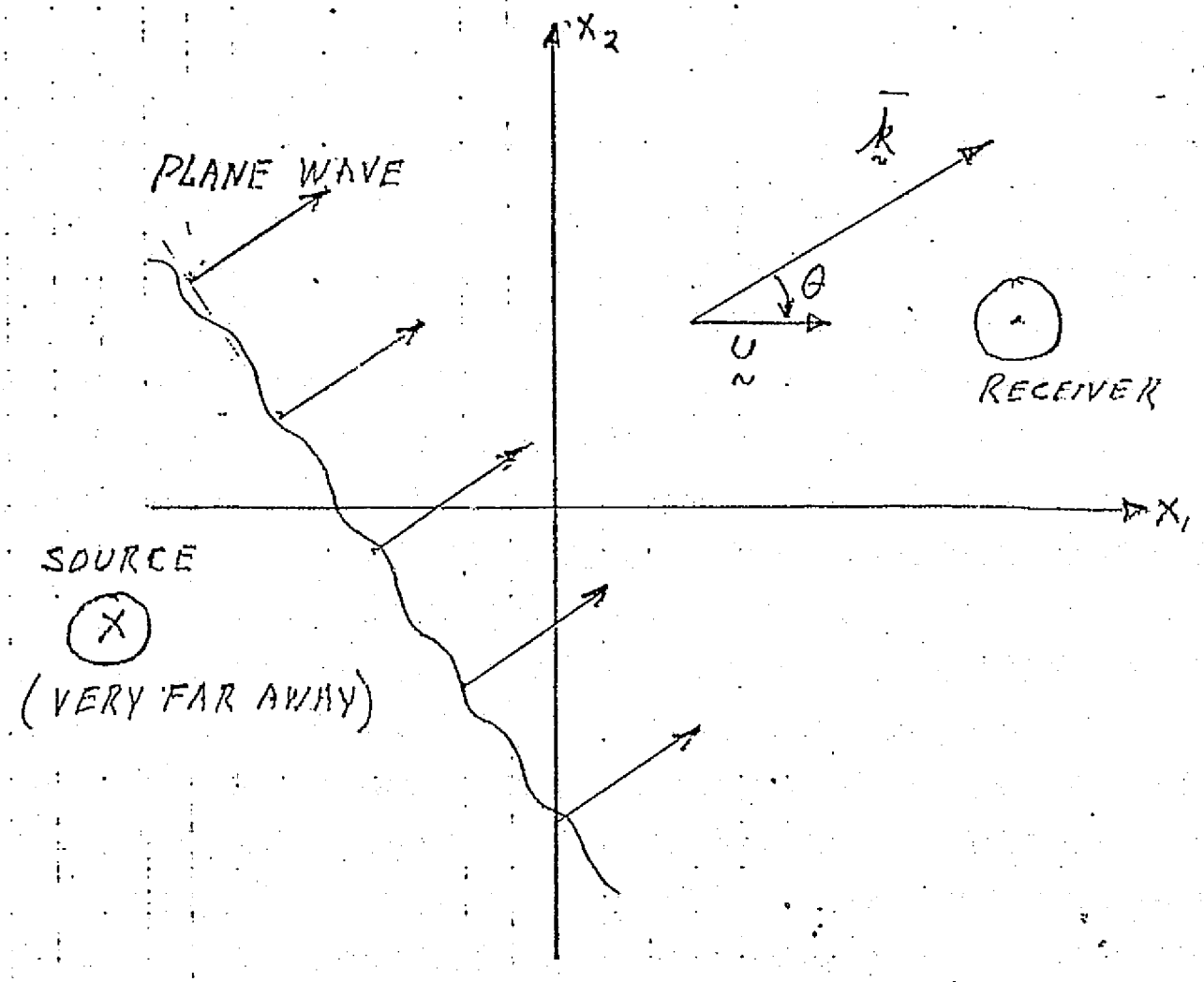

FIG 1 STATIONARY SOURCE AND RECEIVER IN A GAS MOVIN WITH VELOCITY U

ORIGINAL PAGE IS
OF POOR QUALITY

$$k_o = \bar{k}_o \quad ; \tag{4}$$

the frequency, ω_o, measured by a stationary receiver, which is also the frequency, ω_s, of the excitation of the stationary source, is shifted by the usual Doppler shift from the frequency $\bar{\omega}_o$ in the moving fluid:

$$\omega_o = \omega_s = \bar{\omega}_o + \underset{\sim}{\bar{k}}_o \cdot \underset{\sim}{U} \quad ; \tag{5a}$$

if the angle between $\underset{\sim}{\bar{k}}_o$ and $\underset{\sim}{U}$ is θ, (5a) becomes

$$\omega_o = \omega_s = \bar{\omega}_o + \bar{k}_o U\cos\theta \tag{5b}$$

Next, the wavenumber, $\bar{k}_o$ is expressed in terms of ω_s as follows:

The wavenumber $\bar{k}_o$ is defined in the gas:

$$\bar{k}_o = \bar{\omega}_o / c_o \tag{6}$$

where c_o is the sound velocity of the gas. Introducing (5) in (6) and using (4) we find

$$k_o = \bar{k}_o = \frac{\omega_s - \underset{\sim}{\bar{k}}_o \cdot \underset{\sim}{U}}{c_o} \tag{7}$$

$$= k_s - k_o M\cos\theta$$

and solving for k_o

$$k_o = \frac{k_s}{1+M\cos\theta} \tag{8}$$

where M is the Mach number of the moving gas,

$$M = U/c_o \quad , \tag{9}$$

and k_s is the wavenumber of the gas at the frequency ω_s of the excitation of the source:

$$k_s = \omega_s/c_o \tag{10}$$

Finally, the wavenumber vector $\underset{\sim}{\bar{k}}_o$ has a direction which is different from the direction of the wavenumber vector $\underset{\sim}{k}_s$ of the plane wave emitted by the source when the gas is stationary. This is shown in Fig. 2: $\underset{\sim}{\bar{k}}_o$ makes an angle ϕ with respect to k_s which can be readily calculated.

The preceeding results do not consider specifically the effects of fluid flow on the radiation from a *finite* source. This type of problem can be solved only for the simplest geometry.* For the infinite flat source implied in Fig. 2, we have the simple result of a change of direction of $\underset{\sim}{k}_s$ to $\underset{\sim}{\bar{k}}_o$.

The preceeding results are now applied to a stationary porous surface sensor.

The response $E(\omega)$ of the Porous Surface Sensor to a plane wave of amplitude P_o is

$$E(\omega) = s(\omega)\ H(\underset{\sim}{k})\ P_o \tag{11}$$

where $s(\omega)$ is the frequency response and $H(\underset{\sim}{k})$ is the directivity function which is very nearly that of an end-fired line sensor:

---

*Ingard, U. and Singhal, V.K., "Upstream and Downstream Sound Radiation into a Moving Fluid," *JASA*, Vol. 54, No. 5, 1973, pp 1343-6.

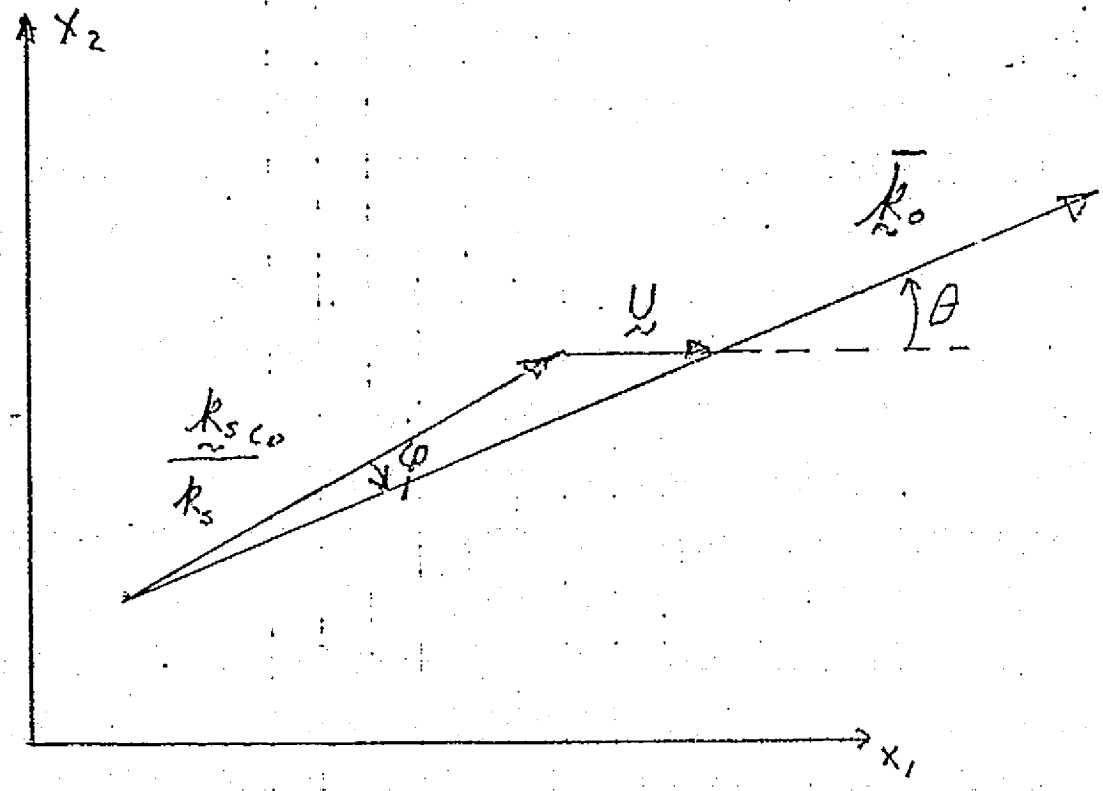

FIG 2 ANGLE φ BETWEEN $\underset{\sim}{k}_s$ AND $\bar{k}_0$

ORIGINAL PAGE IS
OF POOR QUALITY

$$H(\underset{\sim}{k}) = \frac{\sin\left[(k_1 - k_i)L/2\right]}{(k_1 - k_i)L/2} \tag{12}$$

$$k_1 = |\underset{\sim}{k}|\cos\alpha \; ; \tag{13}$$

α is the angle between the vector $\underset{\sim}{k}$ of the plane wave and the axis of the porous strips, L is the active length of the sensor and k_i is the wavenumber of the gas inside the sensor.

In a wind tunnel test where a stationary source is emitting a quasi plane wave at the stationary Porous Surface Sensor receiver, the frequency ω in (11) is the frequency ω_s of the excitation of the source,

$$\omega = \omega_s \tag{14}$$

and $|\underset{\sim}{k}|$ is given by (8)

$$|\underset{\sim}{k}| = \frac{k_s}{1+M\cos\theta} \tag{15}$$

Hence, the ratio

$$\frac{E_o(\omega_s)}{P_{o\,s}(\omega_s)} = \frac{\sin\left[\left(\frac{k_s\cos\alpha}{1+M\cos\theta} - k_i\right)L/2\right]}{\left(\frac{k_s\cos\alpha}{1+M\cos\theta} - k_i\right)L/2} \tag{16}$$

is the directivity function modified by the airflow.

In the wind tunnel tests described in Appendices IV and V the angle θ between the direction of propagation of the quasi plane wave emitted by the source and the velocity $\underset{\sim}{U}$, in the vicinity of the Porous Surface Sensor is zero. Furthermore,

since the gas inside and outside the sensor is the same, air, we have

$$k_i = k_s \tag{17}$$

and (16) reduces to

$$H(\underset{\sim}{k})\Big|_{\theta=0} = \frac{\sin\left[k_s\left(\frac{\cos\alpha}{1+M} - 1\right) L/2\right]}{k_s\left(\frac{\cos\alpha}{1+M} - 1\right) L/2} \tag{18}$$

For the case where the Porous Surface Sensor is pointed directly towards the source, then $\alpha=0$, and (18) further reduces to

$$H(\underset{\sim}{k})\Big|_{\substack{\theta=0\\ \alpha=0}} = \frac{\sin\left[k_s\left(\frac{M}{1+M}\right) L/2\right]}{\left[k_s \frac{M}{1+M} L/2\right]} \tag{19}$$

When $\theta=0$ and the sensor is pointing 90° away from the source ($\alpha = 90°$) the directivity function is unaffected by Mach number; at any other angle α it is affected.

Equation (19) will be used in Appendix VI to calculate the directivity function of the Sensor when it is pointing directly towards the source ($\alpha=0$) and it is aligned with the direction of flow ($\theta=0$).

3. FORMAL DERIVATION

A formal derivation of the effect of Mach number on a stationary receiver in a gas flow is done through frequency and wavenumber transforms. The general result could be confusing when applied to a plane harmonic wave: indeed the results of Eichler* obtained for a moving receiver in a stationary gas is an example of possible misinterpretation.

In the following paragraphs the formalism of Eichler is applied to a pressure field in a *moving gas*, received by a *stationary* microphone.

Let $\underset{\sim}{\bar{x}}$ be coordinates moving with the gas medium at a velocity $\underset{\sim}{U}$; the bar superscript is used to indicate quantities which are referred to the moving coordinates; the stationary coordinates are $\underset{\sim}{x}$:

$$\underset{\sim}{x} = \underset{\sim}{\bar{x}} + \underset{\sim}{U}t \tag{1}$$

A pressure field $\bar{p}(\underset{\sim}{\bar{x}},t)$ in the moving coordinates is the same pressure field $p(\underset{\sim}{x},t)$ in the stationary coordinates,

$$\bar{p}(\underset{\sim}{\bar{x}},t) = p(\underset{\sim}{x},t) \tag{2}$$

provided $\underset{\sim}{\bar{x}}$ and $\underset{\sim}{x}$ are related by (1).

In the coordinates of the moving fluid the frequency transform $\bar{P}(\underset{\sim}{\bar{x}},\omega)$ of $\bar{p}(\underset{\sim}{\bar{x}},t)$, assuming p is deterministic, is defined as

---

*Eichler, E., "Kinematics of Wide-Band Field Sensing by Extended Sensors in Motion," *JASA*, Vol. 50, No. 5 (Part 2), 1971, pp. 1357-1371.

$$\overline{P}(\underset{\sim}{\overline{x}},\overline{\omega}) = \int_{-\infty}^{+\infty} \overline{p}(\underset{\sim}{\overline{x}},t)\ \exp\ (-i\overline{\omega}t)dt \qquad (3)$$

The wavenumber transform $\overline{P}_w(\underset{\sim}{k},t)$ is defined:

$$\overline{P}_w(\underset{\sim}{k},t) = \int_{-\infty}^{+\infty} \overline{p}(\underset{\sim}{\overline{x}},t)\ \exp\ (i\underset{\sim}{k}\cdot\underset{\sim}{\overline{x}})d\underset{\sim}{\overline{x}} \qquad (4)$$

and the frequency wavenumber transform $\overline{P}_{wh}(\underset{\sim}{k},\overline{\omega})$ is defined

$$\overline{P}_{wh}(k,\overline{\omega}) = \int_{-\infty}^{+\infty} \overline{p}(\underset{\sim}{\overline{x}},t)\ \exp[i(\underset{\sim}{k}\cdot\overline{x}-\overline{\omega}t)]d\underset{\sim}{\overline{x}}dt$$

$$= \int_{-\infty}^{+\infty} \overline{P}_w(\underset{\sim}{k},t)\exp(-i\overline{\omega}t)dt$$

$$= \int_{-\infty}^{+\infty} \overline{P}(\underset{\sim}{\overline{x}},\overline{\omega})\ \exp(i\underset{\sim}{k}\cdot\underset{\sim}{\overline{x}})d\underset{\sim}{\overline{x}} \qquad (5)$$

The definitions above follow the more usual conventions; they differ from Eichler's definitions is that $+\underset{\sim}{k}$ is used instead of $-\underset{\sim}{k}$. The wavenumber $\underset{\sim}{k}$ and time t are unaffected by transformation of coordinates.

The same pressure field, in stationary coordinates $\underset{\sim}{x}$, also has its own transforms:

$$P(\underset{\sim}{x},\omega) = \int_{-\infty}^{+\infty} p(\underset{\sim}{x},t)\ \exp(-i\omega t)dt \qquad (6)$$

etc., ... The transforms in the moving and in the stationary coordinates for the same pressure field are related as follows:

$$P(\underset{\sim}{x},\omega) = \int_{-\infty}^{+\infty} \overline{p}(\underset{\sim}{x}-\underset{\sim}{U}t,t)\ \exp(-i\omega t)dt \qquad (7)$$

which cannot be further reduced until p(x,t) is known specifically.

$$P_w(\underset{\sim}{x},t) = \int_{-\infty}^{+\infty} p(\underset{\sim}{x},t)\ \exp(i\underset{\sim}{k}\cdot\underset{\sim}{x})d\underset{\sim}{x}$$

$$= \int_{-\infty}^{+\infty} \overline{p}(\overline{\underset{\sim}{x}},t)\ \exp[\,i\underset{\sim}{k}\cdot(\overline{\underset{\sim}{x}}+\underset{\sim}{U}t)\,]d\overline{\underset{\sim}{x}}$$

$$= \exp\ (i\underset{\sim}{k}\cdot\underset{\sim}{U}t)\ \overline{P}_w(\underset{\sim}{k},t) \qquad (8)$$

$$P_{wh}(\underset{\sim}{k},\omega) = \int_{-\infty}^{+\infty} p(\underset{\sim}{x},t)\ \exp[\,i(\underset{\sim}{k}\cdot\underset{\sim}{x}-\omega t)\,]d\underset{\sim}{x}dt$$

$$= \int_{-\infty}^{+\infty} \overline{p}(\overline{\underset{\sim}{x}},t)\ \exp[\,i(\underset{\sim}{k}\cdot\overline{\underset{\sim}{x}}-(\omega-\underset{\sim}{k}\cdot\underset{\sim}{U})t)\,]d\overline{\underset{\sim}{x}}dt$$

$$= \overline{P}_{wh}(\underset{\sim}{k},\omega-\underset{\sim}{k}\cdot\underset{\sim}{U}) \qquad (9)$$

Equations 2 through 9 are the equivalent of Eichler's Eqs. 1 through 3 and 8 through 12 for a deterministic pressure field in a *moving* gas. The differences are that the sign of $\underset{\sim}{U}$ has been changed because the gas and not the sensor is moving, and the sign of $\underset{\sim}{k}$ in the definitions of transforms has been changed to the more usual notation. Hence, the product $\underset{\sim}{k}\cdot\underset{\sim}{U}$ in Eichler's notation for a moving sensor retains the same sign in our notation for a stationary sensor in a moving gas. Of course, the roles of p and $\overline{p}$ are interchanged in our notation from Eichler's notation.

For a plane wave, moving in the direction of the unit vector $\underset{\sim}{a}$

$$\bar{p}_p(\bar{\underset{\sim}{x}},t) = \bar{p}(\underset{\sim}{a}\cdot\bar{\underset{\sim}{x}}-c_o t) = p(\underset{\sim}{a}\cdot\underset{\sim}{x}-c_o t) \tag{10}$$

where c_o is the sound velocity in the moving gas. For this plane wave, also assumed to be deterministic, we get

$$\bar{P}^p(\bar{\underset{\sim}{x}},\bar{\omega}) = \int_{-\infty}^{+\infty} \bar{p}_p(\underset{\sim}{a}\cdot\bar{\underset{\sim}{x}}-c_o t)\, \exp(i\bar{\omega}t)dt \tag{11}$$

$$P^p(\underset{\sim}{x},\omega) = \int_{-\infty}^{+\infty} p_p(\underset{\sim}{a}\cdot\underset{\sim}{x}-c_o t)\, \exp(i\omega t)dt$$

$$= \int_{-\infty}^{+\infty} \bar{p}_p[\,\underset{\sim}{a}\cdot(\underset{\sim}{x}-\underset{\sim}{U}t)-c_o t]\, \exp(i\omega t)dt$$

$$= \int_{-\infty}^{+\infty} \bar{p}_p[\,\underset{\sim}{a}\cdot\underset{\sim}{x}-c_o(1+\underset{\sim}{a}\cdot\underset{\sim}{M})t]\, \exp(i\omega t)dt$$

$$= \frac{1}{1+\underset{\sim}{a}\cdot\underset{\sim}{M}} \int_{-\infty}^{+\infty} \bar{p}_p(\underset{\sim}{a}\cdot\underset{\sim}{x}-c_o t')\, \exp\left(\frac{i\omega t'}{1+\underset{\sim}{a}\cdot\underset{\sim}{M}}\right) dt'$$

$$= \frac{1}{1+\underset{\sim}{a}\cdot\underset{\sim}{M}}\, \bar{P}\left(\underset{\sim}{x},\, \frac{\omega}{1+\underset{\sim}{a}\cdot\underset{\sim}{M}}\right) \tag{12}$$

This result implies two changes when the frequency spectrum of a plane wave field in a moving gas, $\bar{P}^p(\bar{\underset{\sim}{x}},\bar{\omega})$, is measured by a stationary sensor to become $P^p(\underset{\sim}{x},\omega)$: the amplitude of the spectrum is reduced by the factor $(1+\underset{\sim}{a}\cdot\underset{\sim}{M})^{-1}$, and the frequency $\bar{\omega}$ in the moving gas is reduced by the same factor $(1+\underset{\sim}{a}\cdot\underset{\sim}{M})^{-1}$. Since point sensors have a response which is directly proportional to the pressure field, they appear to acquire a directivity when

either the sensor is moving in the gas (Eichler's analysis) or the sensor is stationary in a moving gas (our analysis). The directivity is the factor $(1+\underset{\sim}{a}\cdot\underset{\sim}{M})^{-1}$ which changes with Mach number vector $\underset{\sim}{M}$, and the unit direction vector $\underset{\sim}{a}$ of the plane wave.

We will show later, in the case of a narrow band plane wave, like a harmonic plane wave, that the apparent directivity factor $(1+\underset{\sim}{a}\cdot\underset{\sim}{M})^{-1}$ cancels out with the factor $(1+\underset{\sim}{a}\cdot\underset{\sim}{M})$ which will appear in $\overline{P}(\underset{\sim}{x},\omega/1+\underset{\sim}{a}\cdot\underset{\sim}{M})$.

The other relations (8) and (9) of course, remain valid for a plane wave.

When the plane wave pressure field is also a harmonic one at a frequency $\overline{\omega}_o$ in the moving gas,

$$\overline{p}(\underset{\sim}{\overline{x}},t) = P_o \exp[-i(\underset{\sim}{k}_o\cdot\underset{\sim}{\overline{x}}-\overline{\omega}_o t)] \tag{13}$$

its frequency transform in the moving gas becomes

$$\overline{P}^p(\underset{\sim}{\overline{x}},\overline{\omega}) = P_o \exp(-i\underset{\sim}{k}_o\cdot\underset{\sim}{\overline{x}})\ 2\pi\delta(\overline{\omega}-\overline{\omega}_o) \tag{14}$$

where δ is the Dirac delta function. In the stationary coordinates the frequency transform becomes, from (12)

$$P^p(\underset{\sim}{x},\omega) = \frac{1}{1+\frac{\underset{\sim}{k}_o}{k_o}\cdot\underset{\sim}{M}}\ P_o \exp(-i\underset{\sim}{k}_o\cdot\underset{\sim}{x})\ 2\pi\delta\left(\frac{\omega}{1+\frac{\underset{\sim}{k}_o}{k_o}\cdot\underset{\sim}{M}} - \overline{\omega}_o\right) \tag{15}$$

where the unit vector $\underset{\sim}{a}$ of the direction of propagation is

$$\underset{\sim}{a} = \frac{\underset{\sim}{k}_o}{k_o} \tag{16}$$

Recalling that a delta function $\delta(x)$, under a change of variable, becomes

$$\delta\left(\frac{x}{a}\right) = a\delta(x)$$

we have

$$\delta\left(\frac{\omega}{1 + \frac{\underset{\sim}{k}_o}{k_o} \cdot M} - \omega_o\right) = \left(1 + \frac{\underset{\sim}{k}_o}{k_o} \cdot M\right) \delta\left[\omega - \bar{\omega}_o\left(1 + \frac{\underset{\sim}{k}_o}{k_o} \cdot \underset{\sim}{M}\right)\right] \tag{17}$$

which gives in (15)

$$P^p(\underset{\sim}{x},\omega) = P_o \exp\left(-i\underset{\sim}{k}_o \cdot \underset{\sim}{x}\right) 2\pi\delta\left[\omega - \omega_o\left(1 + \frac{\underset{\sim}{k}_o}{k_o} \cdot \underset{\sim}{M}\right)\right] \tag{18}$$

This result shows 1) that the amplitude of the plane wave measured by a point sensor moving with the moving gas, or stationary in a moving gas (or, moving in a stationary gas) is *not changed* by the Mach number of the motion; 2) that the frequency ω measured by a stationary sensor in a moving gas,

$$\omega = \bar{\omega}_o\left(1 + \frac{\underset{\sim}{k}_o}{k_o} \cdot \underset{\sim}{M}\right) \tag{19}$$

is modified by Doppler shift from the frequency $\bar{\omega}_o$ of the pressure field measured in coordinates moving with the gas.

The apparent contradiction between (18) and (12) is due to the fact that the plane wave is an harmonic one in (18).

Continuing the case of an harmonic plane wave, its frequency-wavenumber spectrum is, in the moving gas,

$$\bar{P}^{p}_{owh}(\underset{\sim}{k},\bar{\omega}) = \int \bar{P}^{p}(\underset{\sim}{\bar{x}},\bar{\omega}) \exp(i\underset{\sim}{k}\cdot\underset{\sim}{\bar{x}})d\underset{\sim}{\bar{x}}$$

$$= (2\pi)^4 \delta(\bar{\omega}-\bar{\omega}_o) \delta(\underset{\sim}{k}-\underset{\sim}{k}_o)P_o \qquad (20)$$

Using (9) and (20) we get, in stationary coordinates,

$$P^{p}_{owh}(\underset{\sim}{k},\omega) = (2\pi)^4 \delta(\omega-\underset{\sim}{k}_o\cdot\underset{\sim}{U}-\bar{\omega}_o) \delta(\underset{\sim}{k}-\underset{\sim}{k}_o)P_o$$

$$= (2\pi)^4 \delta\left[\omega-\bar{\omega}_o\left(1+\frac{\underset{\sim}{k}_o}{k_o}\cdot\underset{\sim}{M}\right)\right] \delta(\underset{\sim}{k}-\underset{\sim}{k}_o)P_o \qquad (21)$$

after using the relation for the wavenumber in the gas

$$k_o = \frac{\bar{\omega}_o}{c_o} \qquad (22)$$

However, the frequency sensed by the stationary sensor is also the frequency of excitation of the plane harmonic wave, ω_s, when the source is also stationary:

$$\bar{\omega}_o\left(1+\frac{\underset{\sim}{k}_o}{k_o}\cdot\underset{\sim}{M}\right) = \omega_s \qquad (23)$$

When the sensor is extensive, like the Porous Surface Sensor, its sensitivity in frequency-wavenumber spectrum, is usually the product of its frequency response, $s(\omega)$ and its directivity function $H(\underset{\sim}{k})$. For the Porous Surface Sensor of active length L, the

directivity function $H(\underset{\sim}{k})$ is, approximately,

$$H(\underset{\sim}{k}) = \frac{\sin(k_1 - k_i)\ L/2}{(k_1 - k_i)\ L/2} \tag{24}$$

where

$$\underset{\sim}{k} = (k_1,\ k_2,\ k_3) \tag{25}$$

and k_1 is along the axis of the porous strips.

The frequency response $E(\omega)$ of the stationary sensor to a deterministic pressure field $P(\underset{\sim}{k},\omega)$ in stationary coordinates is

$$E(\underset{\sim}{x},\omega) = \int_{\infty}^{\infty} s(\omega)\ H(\underset{\sim}{k})\ P(\underset{\sim}{k},\omega)\ \exp(-i\underset{\sim}{k}\cdot\underset{\sim}{x})d\underset{\sim}{k} \tag{26}$$

For a plane harmonic wave given by (21) and a sensor given by (24) we get

$$E(\underset{\sim}{x},\omega) = s(\omega)2\pi\delta(\omega-\omega_s)\ H(\underset{\sim}{k}_o)P_o \tag{27}$$

and the time response $e(\underset{\sim}{x},t)$ of the sensor becomes

$$e(\underset{\sim}{x},t) = P_o s(\omega_s)\ \exp(i\omega_s t)\ H(\underset{\sim}{k}_o) \tag{28}$$

where, from (24)

$$H(\underset{\sim}{k}_o) = \frac{\sin(k_{o1} - k_i)\ L/2}{(k_{o1} - k_i)\ L/2} \tag{29a}$$

$$\underset{\sim}{k}_o = (k_{o1},\ k_{o2},\ k_{o3}) \tag{29b}$$

$$k_{o1} = k_o \cos\alpha \tag{29c}$$

α being the angle between $\underset{\sim}{k}_o$ and the axis of the porous strips. Finally, relating k_o to the excitation frequency ω_s of the stationary sound source, from (22) and (23)

$$k_o = \frac{\bar{\omega}_o}{c_o} = \frac{\omega_s}{c_o\left(1 + \frac{\underset{\sim}{k}_o}{k_o} \cdot \underset{\sim}{M}\right)} = \frac{k_s}{\left(1 + \frac{\underset{\sim}{k}_o}{k_o} \cdot \underset{\sim}{M}\right)} \qquad (30)$$

and using the angle θ between $\underset{\sim}{k}_o$ and $\underset{\sim}{U}$ in the moving gas we get

$$H(\underset{\sim}{k}_o) = \frac{\sin\left(\frac{k_s \cos\alpha}{1 + M\cos\theta} - k_i\right) L/2}{\left(\frac{k_s \cos\alpha}{1 + M\cos\theta} - k_i\right) L/2} \qquad (31)$$

This is the result obtained previously, and much more simply.

APPENDIX IV

ACOUSTIC TESTS IN AIR FLOW, PART I: CHARACTERISTICS OF THE ACOUSTIC SOURCE

1. INTRODUCTION

The directivity function of the Airfoil Porous Surface Sensor is changed by the presence of air flow; the change has been calculated in Appendix III. It assumes that all the local properties of this sensor, like its local surface sensitivity, are not changed by air flow and that the directivity function of this sensor behaves like the directivity of an end-fired line receiver.

The first assumption could be questioned: the airflow over the porous surface may affect the acoustic resistance of the porous strips. The acoustic resistance of the porous strips can be decomposed into two components*, one being associated with the viscous loss in the pores and the other with the flow transition at the surface. The latter component, which makes the acoustic resistance non-linear, is the only one which could be affected by the air flow. However, the non-linear part of the acoustic resistance of the type of porous strips used in the Airfoil Sensor is negligible even at high acoustic intensities, (surface pressures in the order of 160 dB SPL re 0.0002 microbar). Therefore, we do not expect that the airflow will affect the acoustic resistance of the strips.

The second assumption has been found by the directivity patterns measured in the anechoic room, to be satisfied by the Airfoil Porous Surface Sensor, especially for the main lobe of the directivity.

---

*F.W. Cole, "Graphic Models for Acoustic Flow Resistance," American Society for Metals, 1969 Southern Metals Conference; Materials for Jet Engine Noise Abatement, Technical Note MDD 503, April 1969.

The purpose of the present acoustic tests in airflow is to verify the change in directivity function of the Airfoil Sensor caused by airflow.

An acoustic source is inserted inside the nozzle of the wind tunnel. The acoustic pressure field emitted by the source is measured in the potential core of the jet by a small microphone which is assumed to be omnidirectional and to have a frequency response which is unaffected by airflow. This pressure measurement becomes the reference pressure and will be assumed to belong to a plane wave. The Airfoil Porous Surface Sensor is substituted for the small microphone and its response measured; it is compared with the reference pressure from the small microphone, the ratio being the directivity function of the Airfoil Sensor modified by the flow. The test is repeated for different flow velocities and for different yaw angles of the Airfoil Sensor.

The present appendix describes the conditions of the tests: the acoustic source, the measurement technique and the effects of air flow on the pressure radiated by the acoustic source.

Appendix V will present the acoustic data of the Airfoil Sensor.

2. TEST CONDITIONS

The test conditions include a description of the Acoustic Source, its location in the nozzle of the wind tunnel, and its frequency response with and without flow.

2.1 Acoustic Source

The Acoustic Source consists of a horn driver coupled to a short acoustic horn, both inserted into an aerodynamic cylindrical body; a cross-section of the source is shown in Fig. 1a and a photograph in Fig. 1b.

The trailing cone of the source is a screen which is almost acoustically transparent but present a significant resistance to free air flow. The screen is a non-woven cloth cemented to a rigid wire-mesh which forms the shape of the trailing cone.

The trailing cone will create unavoidable vortices in its wake; the porous surface of this cone should help to inhibit these vortices. The axial response of the source, at constant excitation voltage, in the anechoic room is shown in Fig. 2. The directivity pattern of the source at 10 kHz is shown in Fig. 3; it is compared in Fig. 4 with the calculated directivity of a rigid piston in a baffle, the piston diameter being equal to the diameter of the mouth of the horn. This calculation is used later to estimate the reflections of the source against the sides of the nozzle of the wind tunnel.

The pressure level of the source at 5 kHz is approximately 97 dB re 0.0002 microbar at one meter and for one volt excitation. For the 6 volt excitation used in the wind tunnel tests, the pressure level at 2 meters and 5 kHz will be approximately 106 dB re 0.0002 microbar.

ORIGINAL PAGE IS
OF POOR QUALITY

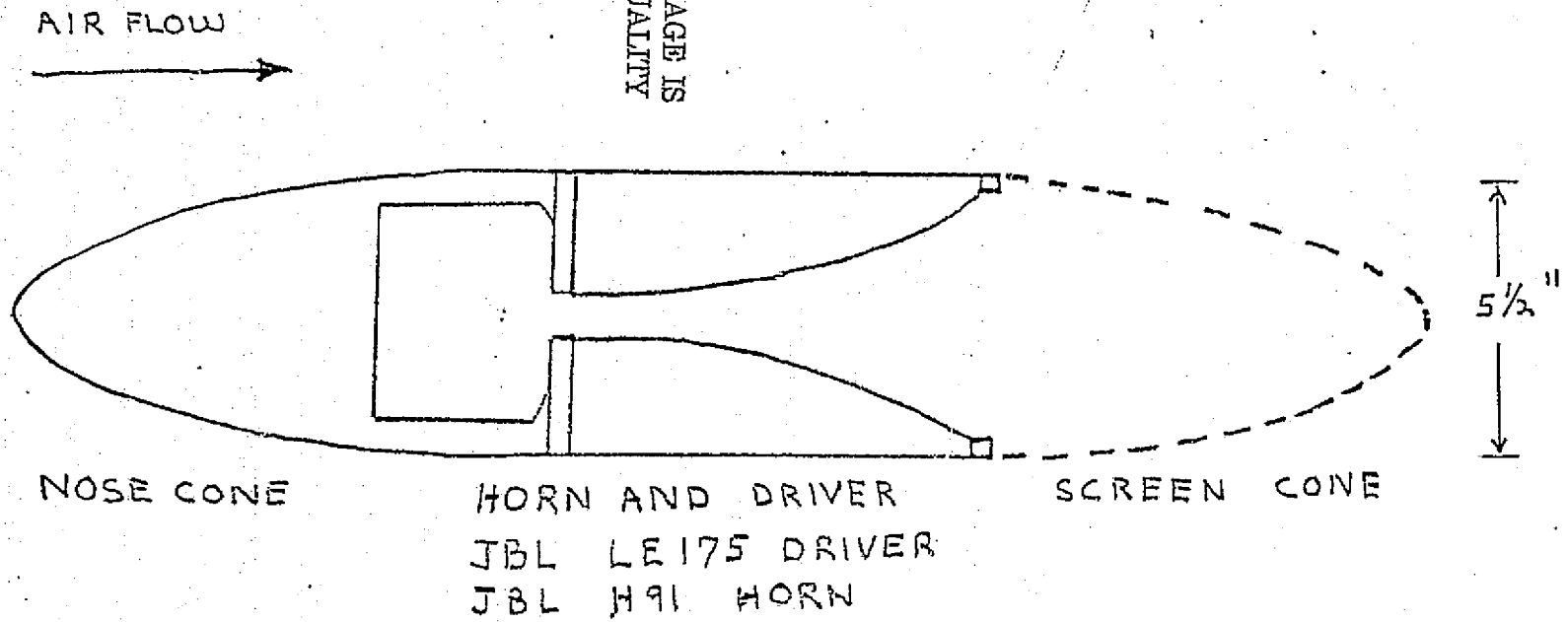

FIG. 1a ACOUSTIC SOURCE

ORIGINAL PAGE IS
OF POOR QUALITY

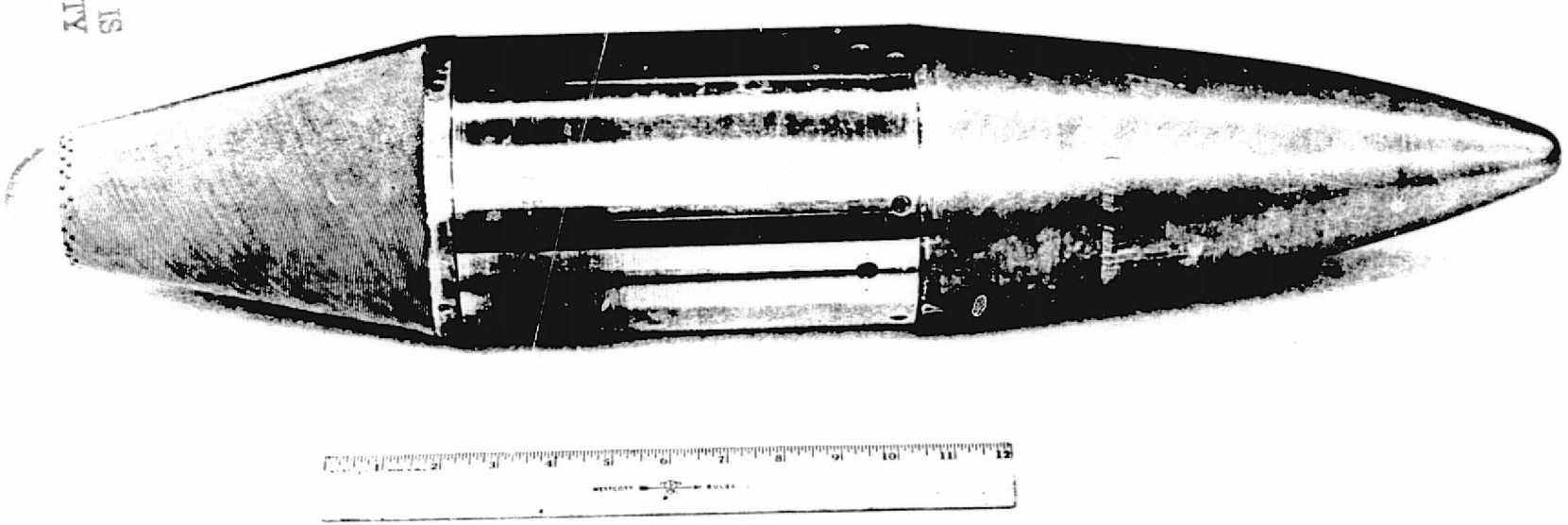

FIG. 1b ACOUSTIC SOURCE

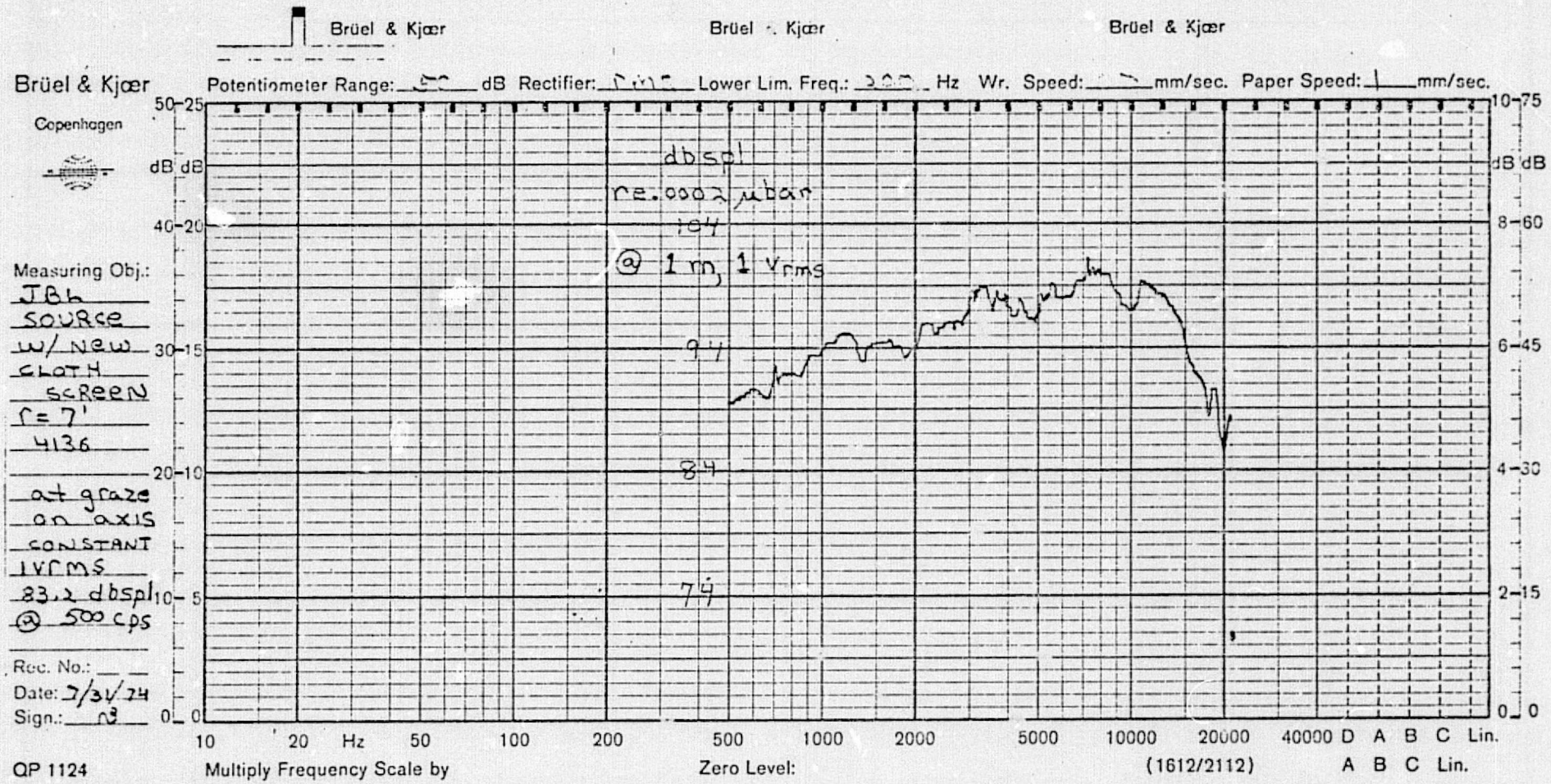

FIG. 2 SOURCE LEVEL OF THE ACOUSTIC SOURCE ON AXIS

ORIGINAL PAGE IS
OF POOR QUALITY

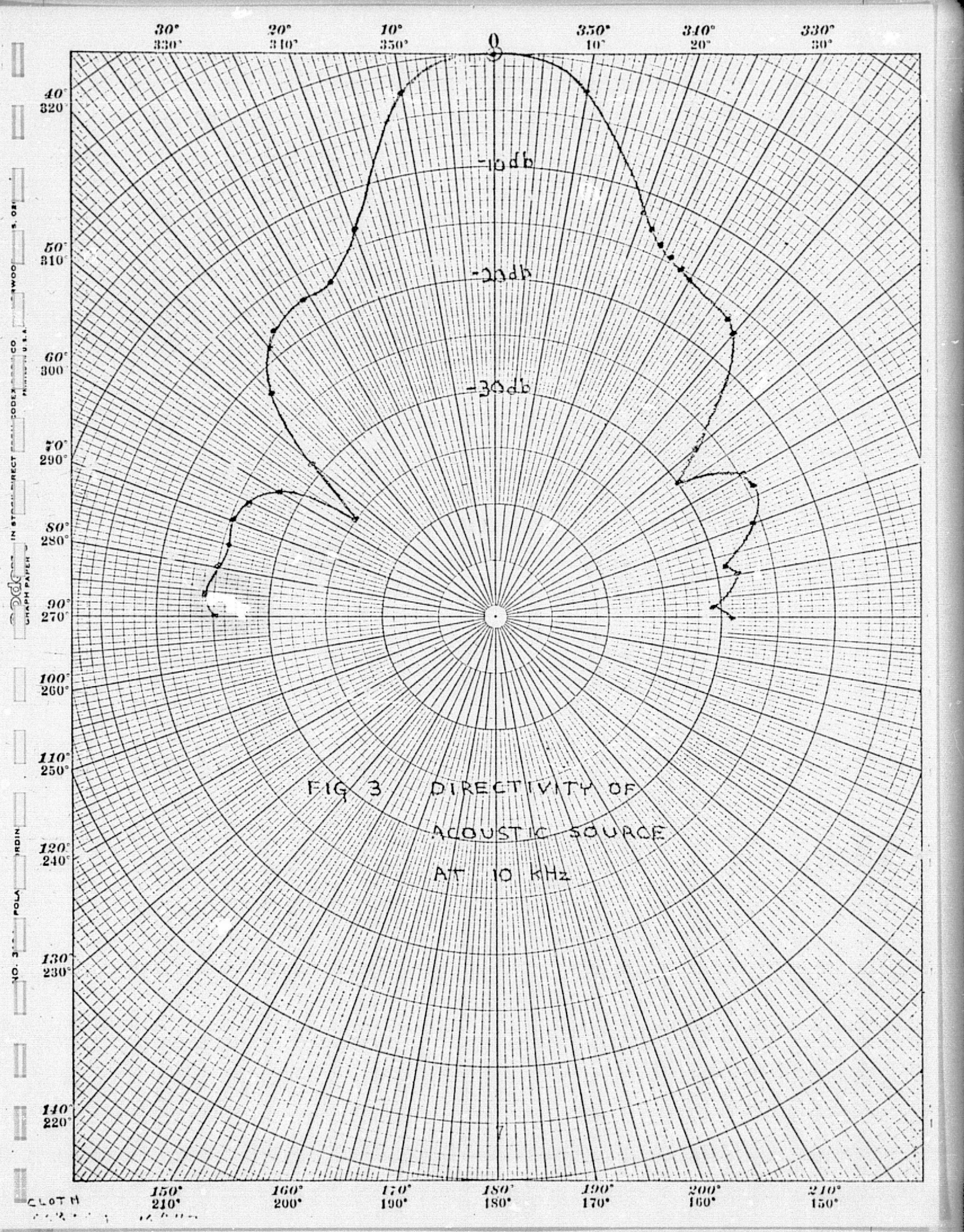

FIG 3 DIRECTIVITY OF ACOUSTIC SOURCE AT 10 KHz

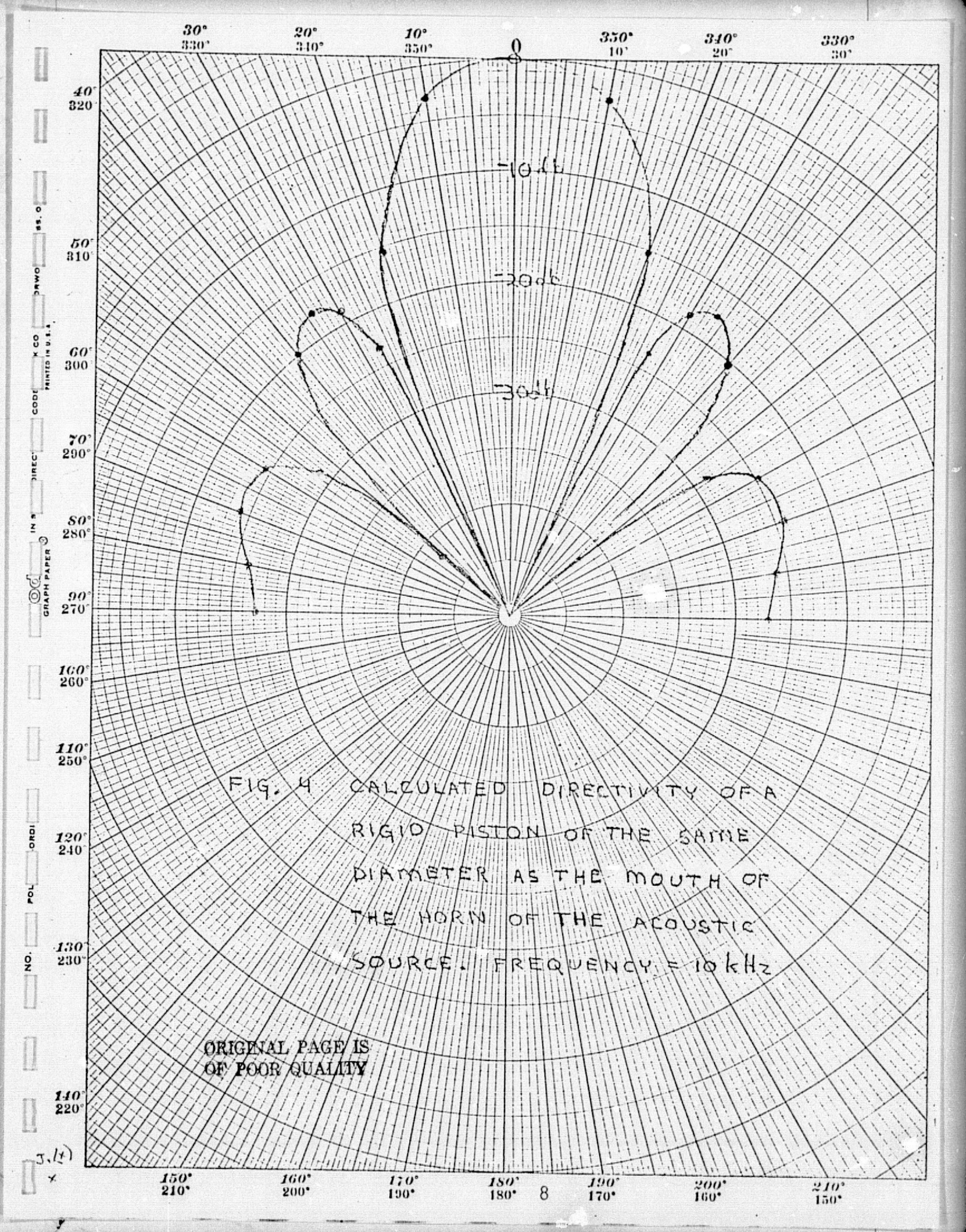

FIG. 4 CALCULATED DIRECTIVITY OF A RIGID PISTON OF THE SAME DIAMETER AS THE MOUTH OF THE HORN OF THE ACOUSTIC SOURCE. FREQUENCY = 10 kHz

ORIGINAL PAGE IS
OF POOR QUALITY

The microphones measuring the sound emitted by the source in the presence of flow will be in the turbulent wake of the source: the flow noise will be substantially higher than what was measured earlier in the free stream. In order to enhance the signal-to-noise ratio of the microphones, the source is excited by pure tones in the form of a frequency sweep and the output of the microphones are filtered by a narrowband tracking filter. The functions of frequency sweep and narrowband filtering and tracking are available simultaneously in some types of Wave Analyzers. A block diagram of the instrumentation setup is shown in Fig. 5; the bandwidth of the filter is 7 Hz. The rate of the frequency sweep is chosen to allow full response of the narrowband filter to the frequency change.

2.2 Location of the Source Inside the Nozzle

The location of the source inside the nozzle is a compromise amongst conflicting requirements: the source should be close to the mouth of the nozzle to minimize reflections from the sides of the nozzle; the source should be deep inside the nozzle to inhibit the turbulence of its wake.

The source is suspended by piano wires inside the nozzle as shown in Fig. 6. The source axis is oriented carefully along the direction of flow. Over the whole range of flow velocities of the tests the source remained stable; only very small vibration of its body could be detected. The trailing cone of the source is in the contraction region of the nozzle so that the turbulence in the wake of the cone will be inhibited to some degree.

The acoustic reflections from the sides of the nozzle will affect the accuracy of the acoustic measurements which depend on the assumption that the pressure field at the microphones is a plane wave. At 10 kHz the main lobe of the directivity of the source is

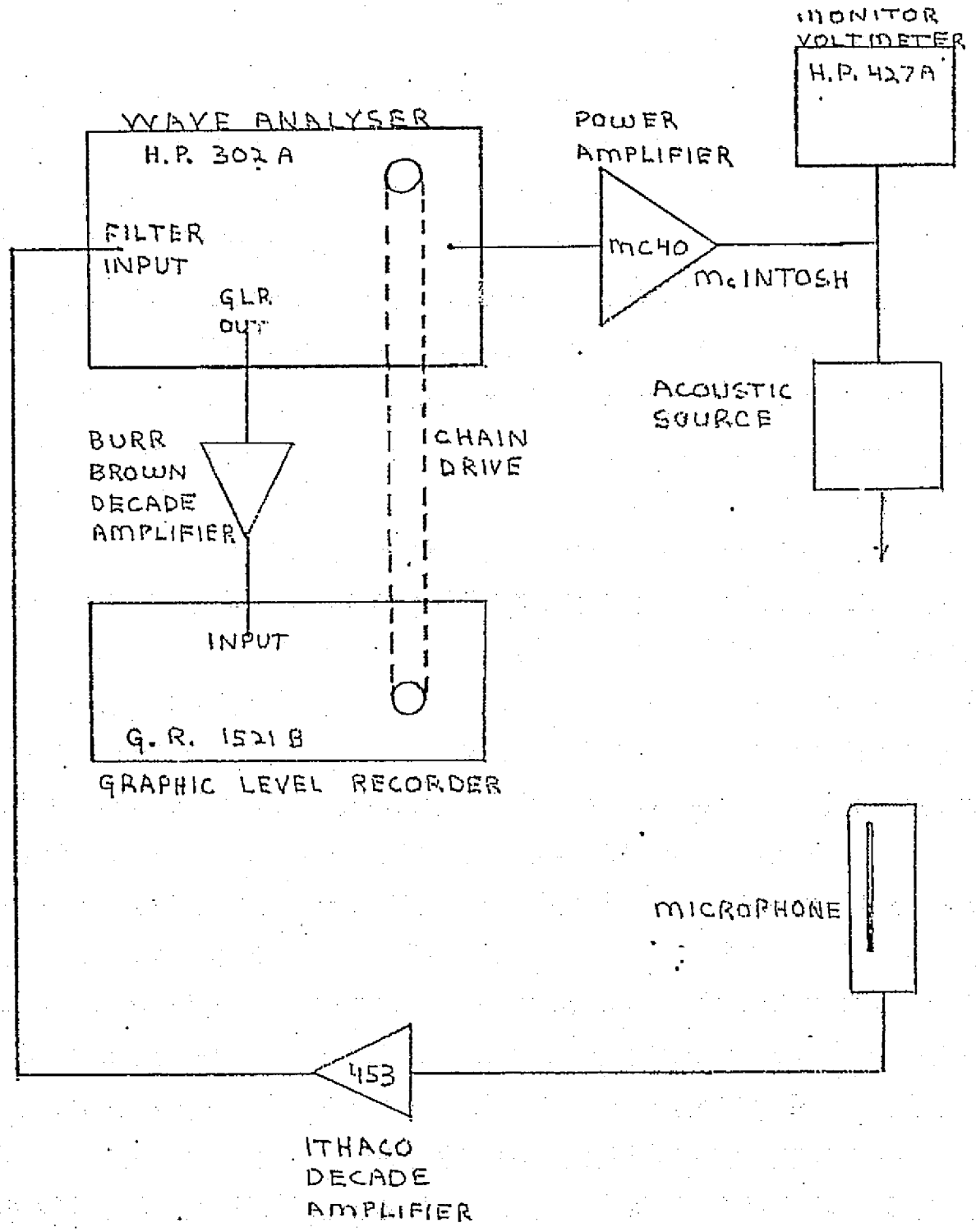

FIG. 5 INSTRUMENTATION OF THE ACOUSTIC TESTS IN THE WIND TUNNEL

ORIGINAL PAGE IS
OF POOR QUALITY

ORIGINAL PAGE IS
OF POOR QUALITY

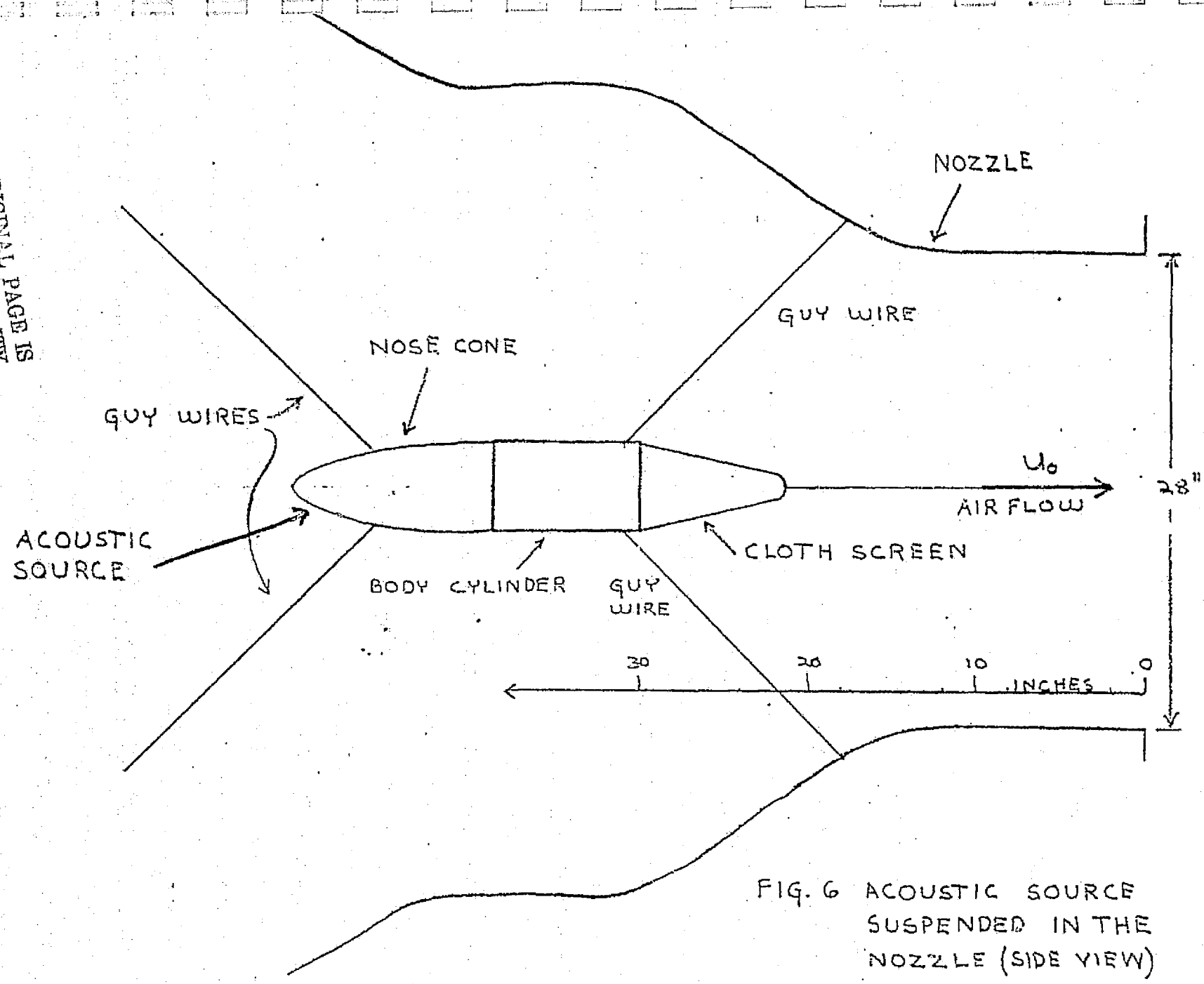

FIG. 6 ACOUSTIC SOURCE SUSPENDED IN THE NOZZLE (SIDE VIEW)

not intercepted by the sides of the nozzle; only the minor lobes are intercepted and their levels are at least 15 dB below the level of the main lobe. At 5 kHz a small fraction of the main lobe is intercepted. At frequencies below 5 kHz the reflections from the sides of the nozzle become more important.

With airflow we will see that the directivity of the source is increased: its main lobe becomes narrower at a given frequency, so that the reflections from the sides of the nozzle are relatively less important. In the tests, we found that at frequencies below 2 kHz the reflections from the sides of the nozzle became excessive, producing strong interferences with the main beam. Hence, all acoustic tests were limited to frequencies above 2 kHz. Fortunately, this is also the frequency region where the change of directivity function due to Mach number is significant.

The location of the sensors in the free jet is limited to not more than approximately one meter from the face of the nozzle: this limitation insures that the Airfoil Sensor, at yaw angle of 90°, is fully within the potential core of the jet. The net distance between the acoustic center of the source and the center of the B&K and Airfoil sensors is approximately 2 meters, which is just barely acceptable to simulate a plane wave in the region of the sensors.

2.3 Frequency Response of the Source in the Nozzle

The frequency response of the source is measured, at different flow velocities, by a B&K half-inch condenser microphone with nose cone. The same test stand used for flow noise[1] tests is also used for these acoustic tests. The narrowband filtering system of Fig. 5 is used.

[1]See Appendix VI.

At zero flow velocity, the frequency response of the source measured in the wind tunnel is compared with the frequency response measured in the anechoic room in Fig. 7. It is clear that at low frequencies there is considerable interference between the main beam of the source and the pressures reflected from the sides of the nozzle. The frequency difference Δf between the nulls (or maxima) of interference is 2.2 kHz; it corresponds to a path difference Δx of one wavelength,

$$\Delta x = c_o/\Delta f$$

which is found to be approximately 15 cm (6 inches). This is, in fact, the difference in path length between the main beam and a wave reflected from the upper or lower sides of the nozzle. This interference pattern decreases with increasing frequency because the directivity of the source increases with frequency.

(All the measurements done in the acoustic tests with the wind tunnel were restricted to an upper frequency of 15 kHz. This restriction will be explained later.)

The interference of the direct and reflected waves will make the acoustic measurements more difficult to interpret and certainly less accurate. The response of the Source, at constant voltage and different flow velocities is shown in Fig. 8a, b.

The interference pattern is seen to decrease progressively as the flow velocity is increased. This result indicates that the directivity of the Source is sharpened by the presence of the flow. A qualitative explanation is shown in Fig. 9: the net velocity of sound viewed from stationary coordinates is increased by the velocity U of the flow; the original acoustic velocity vectors, $(k_o/k)c_o$, which would exist if the flow velocity

ORIGINAL PAGE IS
OF POOR QUALITY

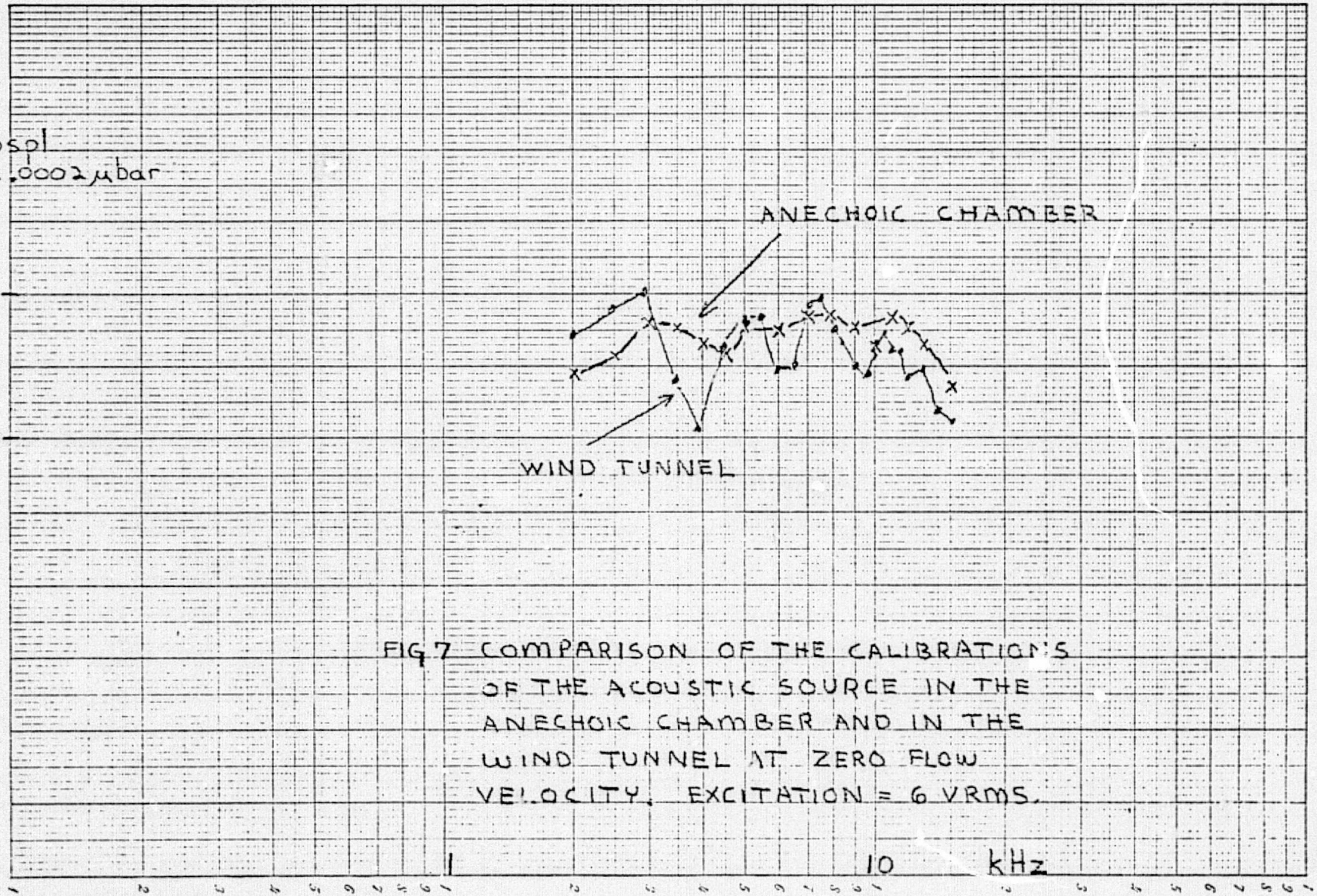

FIG 7 COMPARISON OF THE CALIBRATIONS OF THE ACOUSTIC SOURCE IN THE ANECHOIC CHAMBER AND IN THE WIND TUNNEL AT ZERO FLOW VELOCITY. EXCITATION = 6 VRMS.

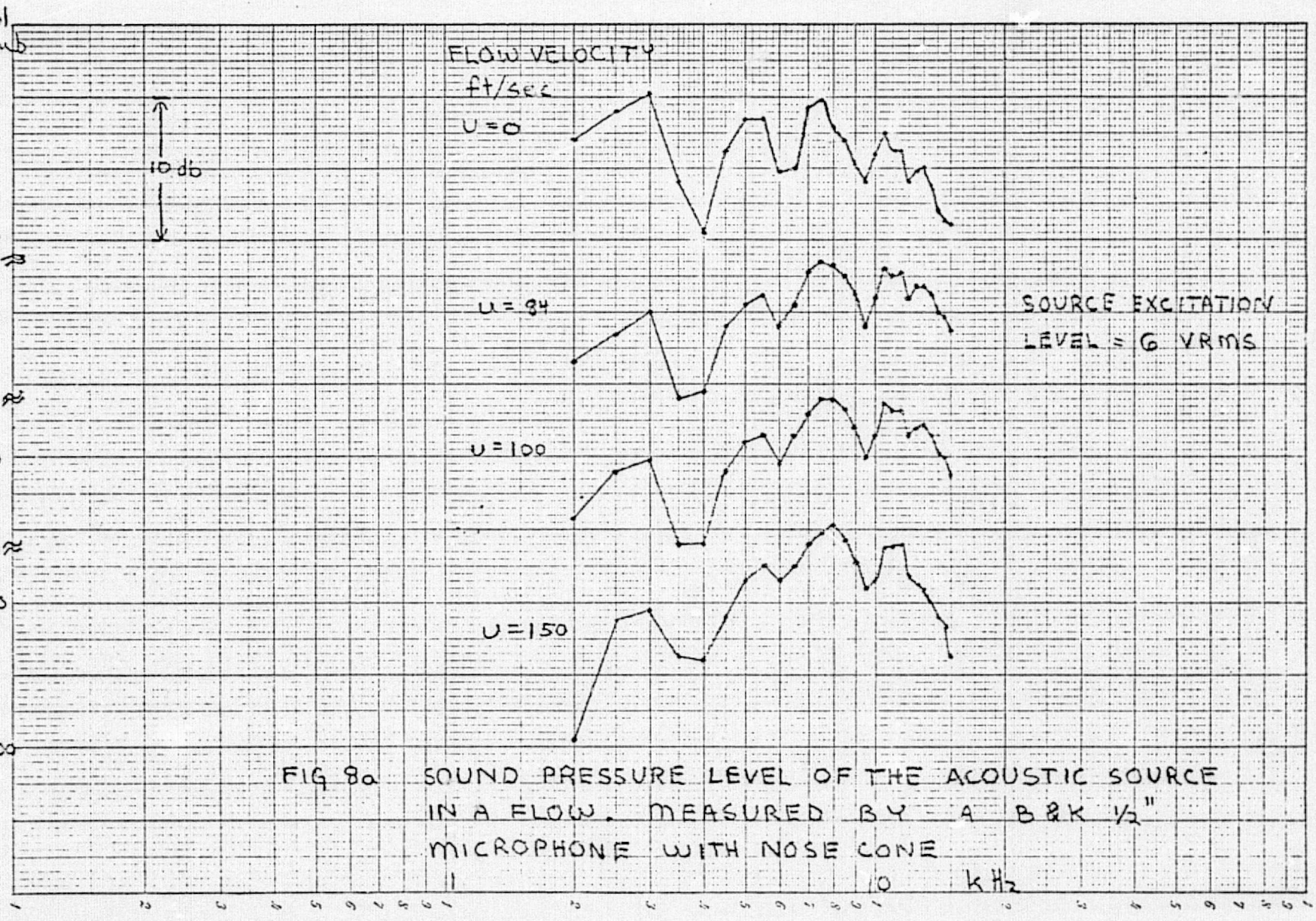

FIG 8a SOUND PRESSURE LEVEL OF THE ACOUSTIC SOURCE IN A FLOW. MEASURED BY A B&K ½" MICROPHONE WITH NOSE CONE

ORIGINAL PAGE IS
OF POOR QUALITY

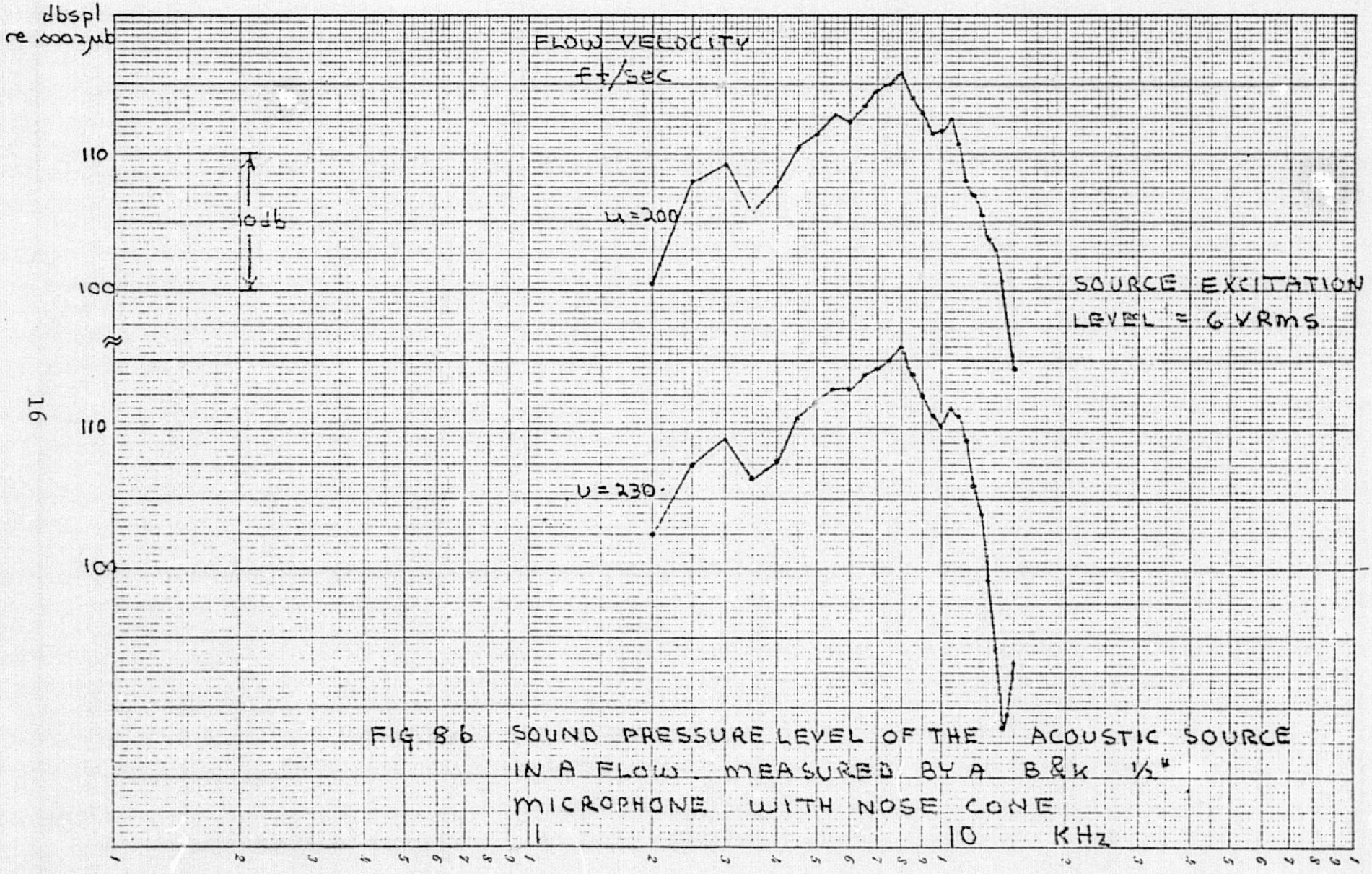

FIG 8 6 SOUND PRESSURE LEVEL OF THE ACOUSTIC SOURCE IN A FLOW. MEASURED BY A B&K ½" MICROPHONE WITH NOSE CONE

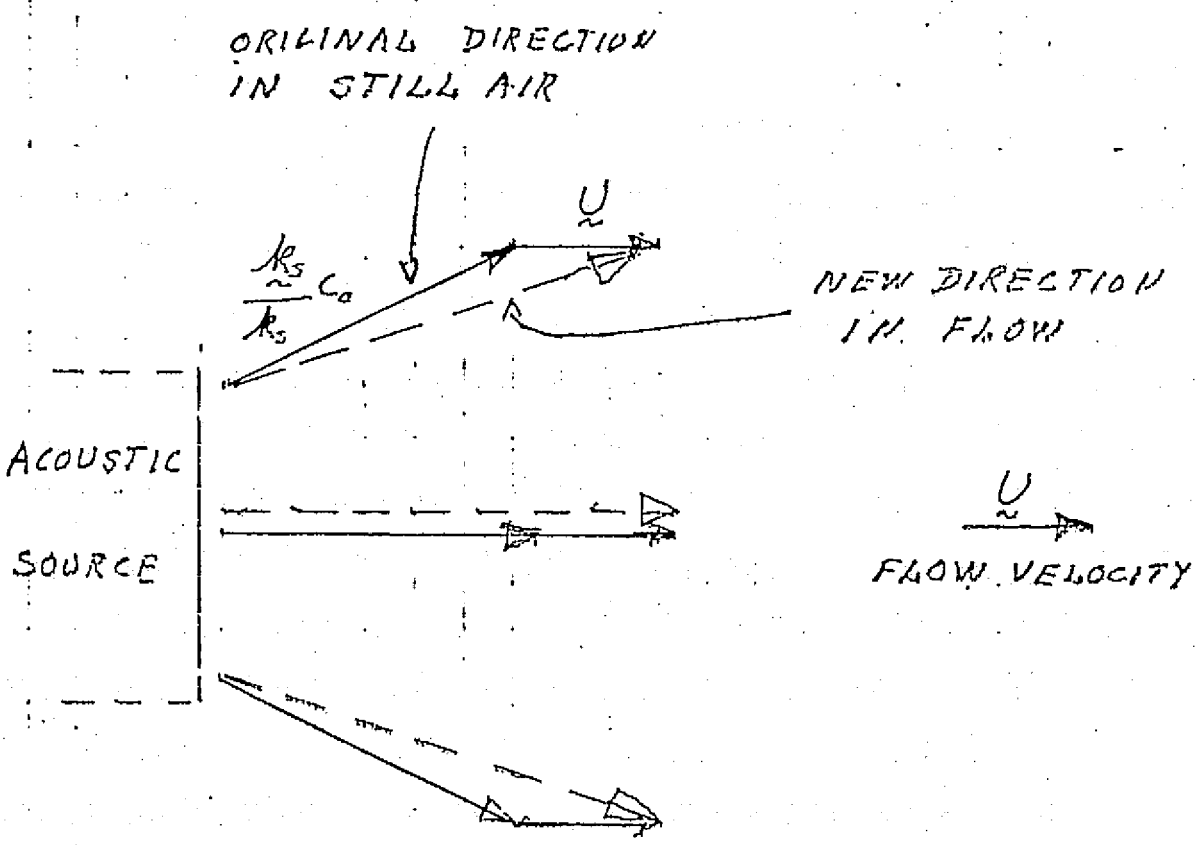

FIG. 9 THE DIRECTIVITY OF THE ACOUSTIC SOURCE IS INCREASED BY AIR FLOW

ORIGINAL PAGE IS
OF POOR QUALITY

were zero are bent symmetrically by the velocity U. The net affect is a sharper beam. This argument assumes that the original radiation of the Source at zero flow is not affected by the flow in the immediate vicinity of the Source.

We could also deduce, from this last assumption, that the pressure level in the main beam would increase as the beam width is decreased, in order to preserve the power emitted by the Source. Letting ϕ be the half angle of the main beam, and using primes to indicate the effect of flow velocity, we get the pressure ratio p'/p on the axis of the main beam and at the same distance from the Source.

$$p'/p = \frac{\sin\phi}{\sin\phi'}$$

$$\tan\phi' = \frac{\tan\phi}{1 + M/\cos\phi}$$

where M is the Mach number of the flow. The pressure ratio p'/p increases gradually with frequency until it reaches a maximum value of 1 + M; at the maximum value of M = 0.2 used in our tests this increase in p'/p is only 2 dB; this is not in accordance with the experimental results which show a much larger increase of the ratio p'/p.

The increase of the pressure ratio p'/p, for different flow velocities is shown in Fig. 10: at low flow velocities (84, 100, 150 ft/sec) the pressure increase as a function of frequency is a gradual one, (disregarding the minor differences in interference patterns), reaching 8 to 10 dB at 15 kHz. This result appears to

ORIGINAL PAGE IS
OF POOR QUALITY

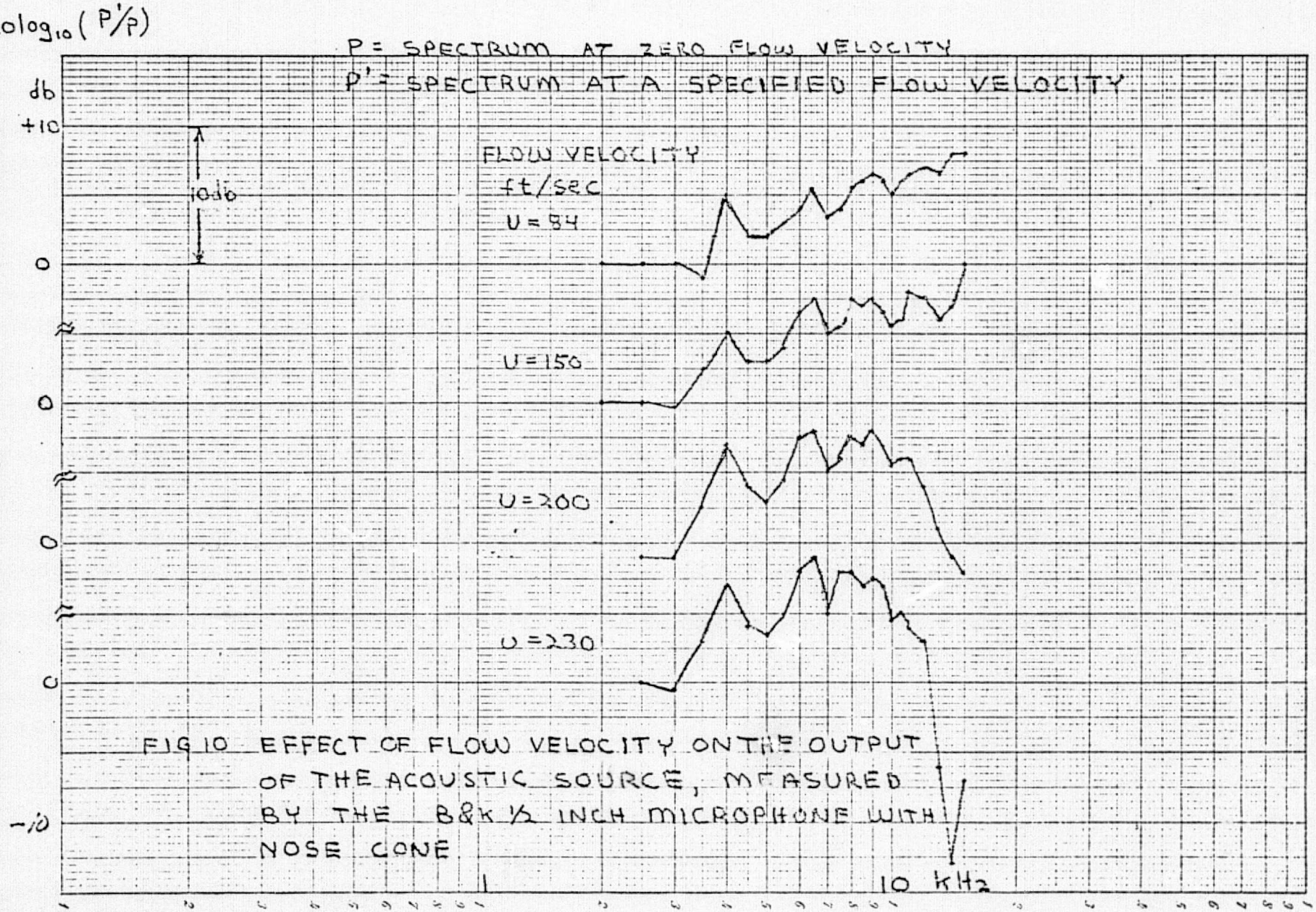

FIG 10 EFFECT OF FLOW VELOCITY ON THE OUTPUT OF THE ACOUSTIC SOURCE, MEASURED BY THE B&K ½ INCH MICROPHONE WITH NOSE CONE

contradict the experimental results of Ingard*, who obtained the opposite effect: he found that the downstream pressure is *decreased* by the presence of flow. However, the experimental conditions of Ingard's and our tests are quite different: in Ingard's tests, the radiation surface of the Source is fully exposed to a cross flow, so that the radiation impedance of the source is directly modified by the flow; in our tests the radiating surface of the Source, (the mouth of the acoustic horn), is not fully exposed to the flow and, further, the flow is perpendicular to radiating surface.

At large flow velocities (U > 150 ft/sec) the high frequency part of the spectrum, in Fig. 10, drops rapidly. This drop could be attributed either (1) to the source, (2) to the B&K microphone with a nose cone, or (3) to the turbulence of the flow dispersing the line spectrum beyond the bandwidth of the filter (7 Hz bandwidth). The drop in spectrum level resulted in a low signal-to-noise ratio at the output of the filter, which lead us to restrict the spectrum to less than 15 kHz.

During the test, the drop in the high frequency part of the spectrum was not sufficiently appreciated to investigate its cause. Nevertheless, we will see from the results of the Airfoil Sensor, that the cause is not the Acoustic Source: the high frequency part of the spectrum measured by the Airfoil Sensor does not drop as drastically as when it is measured by the B&K microphone with a nose cone. We also tend to disregard the third cause: both the B&K microphone and the Airfoil Sensor

---

*U. Ingard and V.K. Singhal, "Upstream and Downstream Sound Radiation in a Moving Fluid," *JASA*, Vol, 54, No. 5, 1973 pp 1343-6.

used the same narrowband filter. We are left to blame the B&K microphone with a nose cone for the drop in the high frequency part. Therefore, it appears that the frequency response of the B&K microphone with nose cone is sensitive to the presence of air flow. This conclusion, which is only an indirect one and has not been specifically investigated, will affect all the calculations based on our earlier assumption that the response of the B&K sensor is not modified by airflow. Although this conclusion applies for frequencies above 10 kHz and for the range of flow velocities of our tests, it will affect seriously the accuracy of the calculations done later, using the B&K sensor as a reference.

If this experiment could be repeated, two major changes would be made: First, the signals from the B&K sensor and the Airfoil Sensor would be analyzed with a broader filter as well as with the narrow band filter, in order to examine if any frequency dispersion is caused by turbulence: Secondly, a quarter inch as well as half inch B&K microphone with nose would be used to measure the signal from the Source, in the hope of finding the frequency response correction.

APPENDIX V

ACOUSTIC TESTS IN AIR FLOW, PART II: MACH NUMBER CORRECTION OF THE DIRECTIVITY OF THE AIRFOIL POROUS SURFACE SENSOR

1. INTRODUCTION

The modification of the directivity function of the Airfoil Porous Surface Sensor by airflow has been developed in Appendix III, under the assumption that the sensor is an ideal end-fired line sensor. This result is now compared with the directivity function of the Airfoil Sensor measured in the presence of air flow.

The procedure to obtain experimentally the effect of Mach number on the directivity function is as follows:

(1) With the Acoustic Source suspended inside the nozzle of the wind tunnel, a B&K half-inch microphone with nose cone is set on the aerodynamic stand inside the potential core of the free jet, at a distance of 1 meter from the face of the nozzle. The pressure measured by this sensor at different flow velocities, after correction for the frequency response of the sensor, is taken as the reference point pressure. The assumption is that the frequency response of the B&K sensor is insensitive to airflow at least within the range of Mach number of our tests: $M \leq 0.2$.

(2) The pressure field at the location of the B&K sensor is assumed to be a plane progressive wave. This assumption is indeed not quite satisfied, except at high frequencies where the directivity of the source minimizes the acoustic reflections from the sides of the nozzle.

(3) Under the assumptions (1) and (2) the ratio of the pressure measured by the Airfoil Sensor to the pressure measured by the B&K sensor is the directivity function of the Airfoil Sensor modified by the Mach number of the flow.

(4) The experimental results (3) is compared with the directivity function $H(k)$ of a line sensor of length L, calculated in Appendix III:

$$H(\underset{\sim}{k}) = \frac{\sin\left[k_s\left(\frac{\cos\alpha}{1+M\cos\theta} - 1\right) L/2\right]}{k_s\left(\frac{\cos\alpha}{1+M\cos\theta} - 1\right) L/2}$$

where α is the angle of the axis of the line sensor with the direction of propagation of the plane wave in the flow and θ is the angle of the flow velocity $\underset{\sim}{U}$ and the direction of propagation of the plane wave in the flow.

This procedure is carried out in Section 3 and the results are given and discussed. The tests also provide an opportunity to measure the flow noise in the turbulent wake of the source, with the B&K sensor and the Airfoil Sensor, and to find the noise reduction afforded by the Airfoil Sensor in this condition of relatively high turbulence. This separate result is presented first in Section 2.

2. FLOW NOISE IN THE WAKE OF THE ACOUSTIC SOURCE

The wake of the Acoustic Source is turbulent. The flow noise of the sensors due to this turbulence will reduce the signal-to-noise ratio of the acoustic tests; see Section 3. This turbulence also presents an opportunity to evaluate the flow noise reduction of the Airfoil Sensor, compared to the B&K sensor under the condition of a relatively high turbulence level. This situation is not an unrealistic one in some practical wind tunnel tests.

The turbulence of the wake at microphone locations was not measured directly; instead the flow noise was measured with the B&K and the Airfoil Sensors.

Figure 1 gives the flow noise of the B&K half inch microphone with nose cone, in the wake of the sound source, 1 meter away from the fact of the nozzle, at different flow velocities. The B&K sensor is pointing towards the flow. Figures 2, 3 and 4 give the flow noise of the Airfoil Sensor at the same position and flow velocities, for yaw angles of 0°, 30° and 90°.

Comparing the flow noise of Fig. 1 with the flow noise measured earlier by the B&K sensor in the free jet (see Fig. 11, Appendix VI) we find that the flow noise in the wake of the Source is approximately 20 dB higher than in the free jet. Since the turbulence of the free jet is very low, it follows that the turbulence of the wake is still not very large. It is doubtfull that the turbulence of the wake of the source could be much reduced.

The flow noise reduction achieved by the Airfoil Sensor, using the flow noise measured by the B&K sensor as a reference, is shown in Figs. 5, 6 and 7 for the yaw angles of 0°, 30° and 90°. The noise reductions are quite large; of course, they depend on the particular turbulent field of the wake of the

ORIGINAL PAGE IS
OF POOR QUALITY

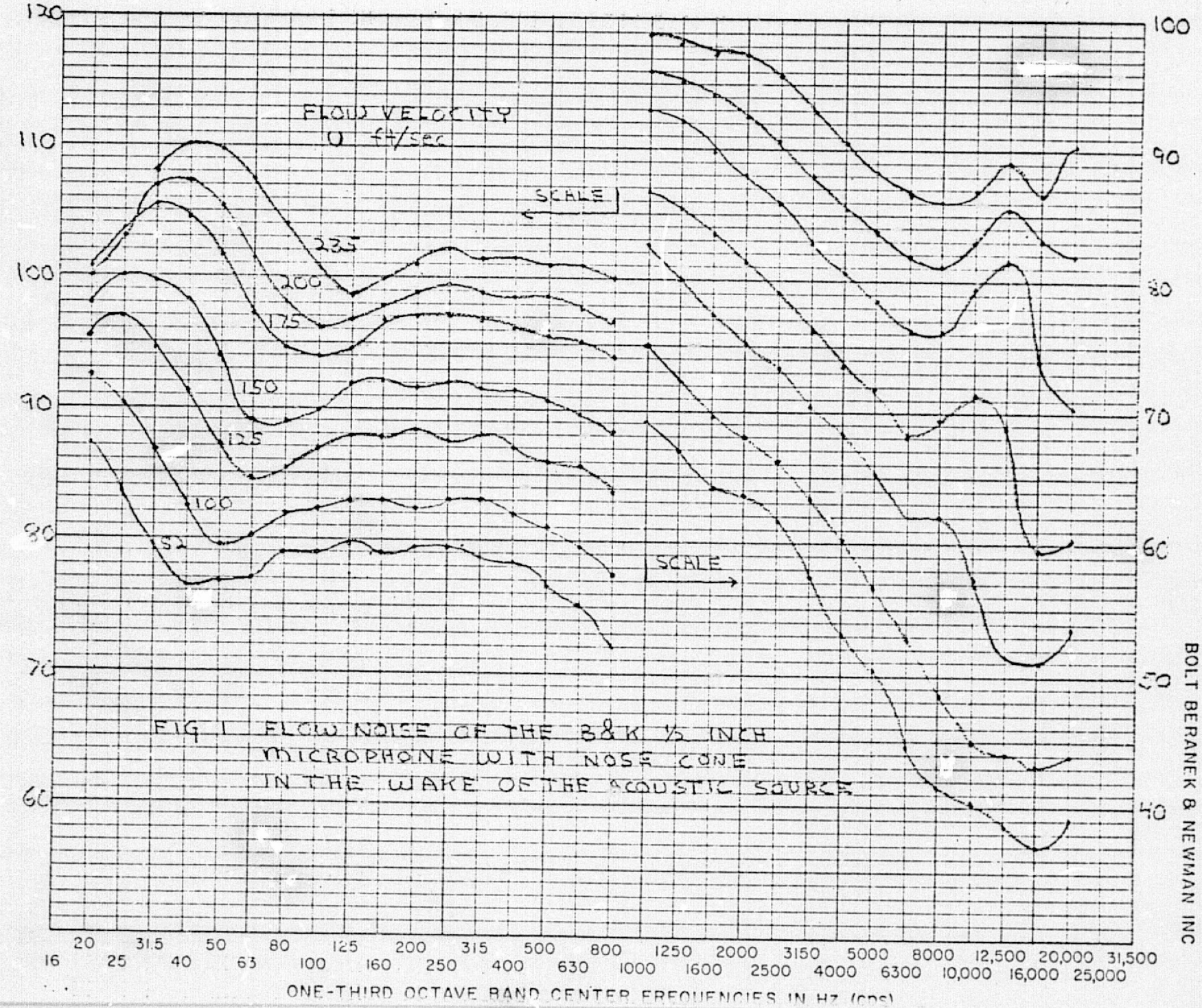

FIG 1 FLOW NOISE OF THE B&K ½ INCH MICROPHONE WITH NOSE CONE IN THE WAKE OF THE ACOUSTIC SOURCE

ORIGINAL PAGE IS
OF POOR QUALITY

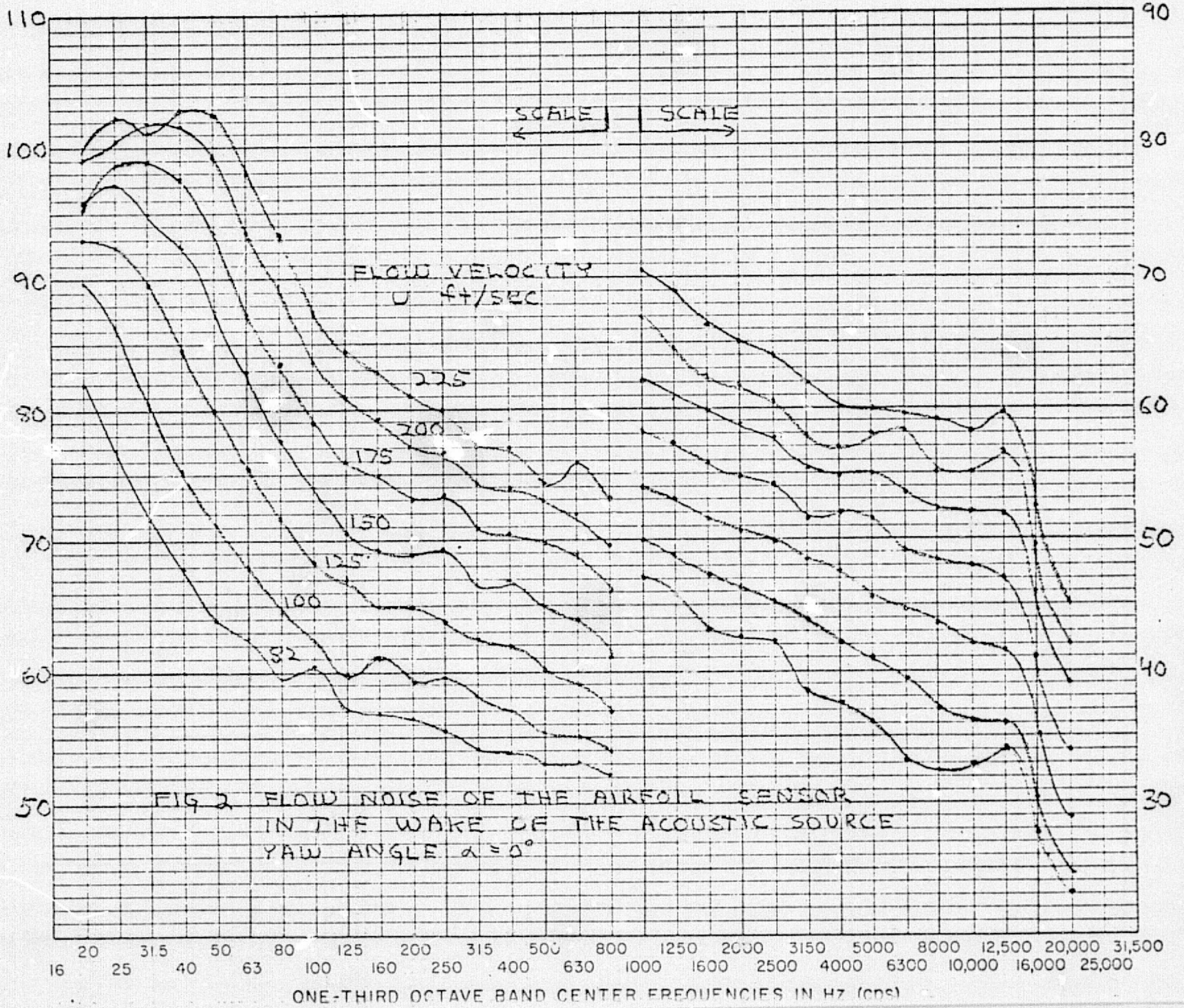

FIG 2 FLOW NOISE OF THE AIRFOIL SENSOR IN THE WAKE OF THE ACOUSTIC SOURCE YAW ANGLE $\alpha = 0°$

BOLT BERANEK & NEWMAN INC

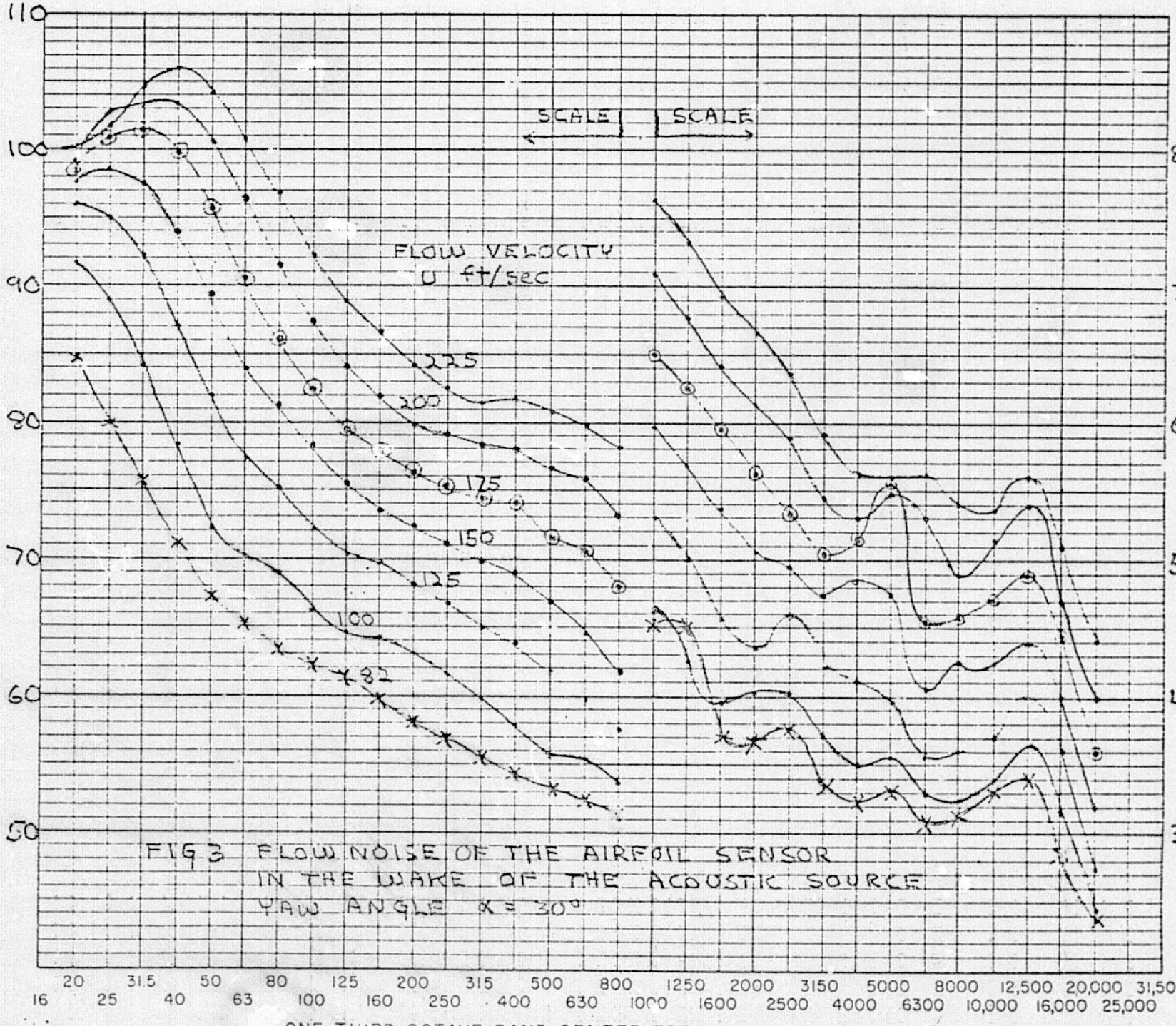

FIG 3 FLOW NOISE OF THE AIRFOIL SENSOR IN THE WAKE OF THE ACOUSTIC SOURCE
YAW ANGLE $\chi = 30°$

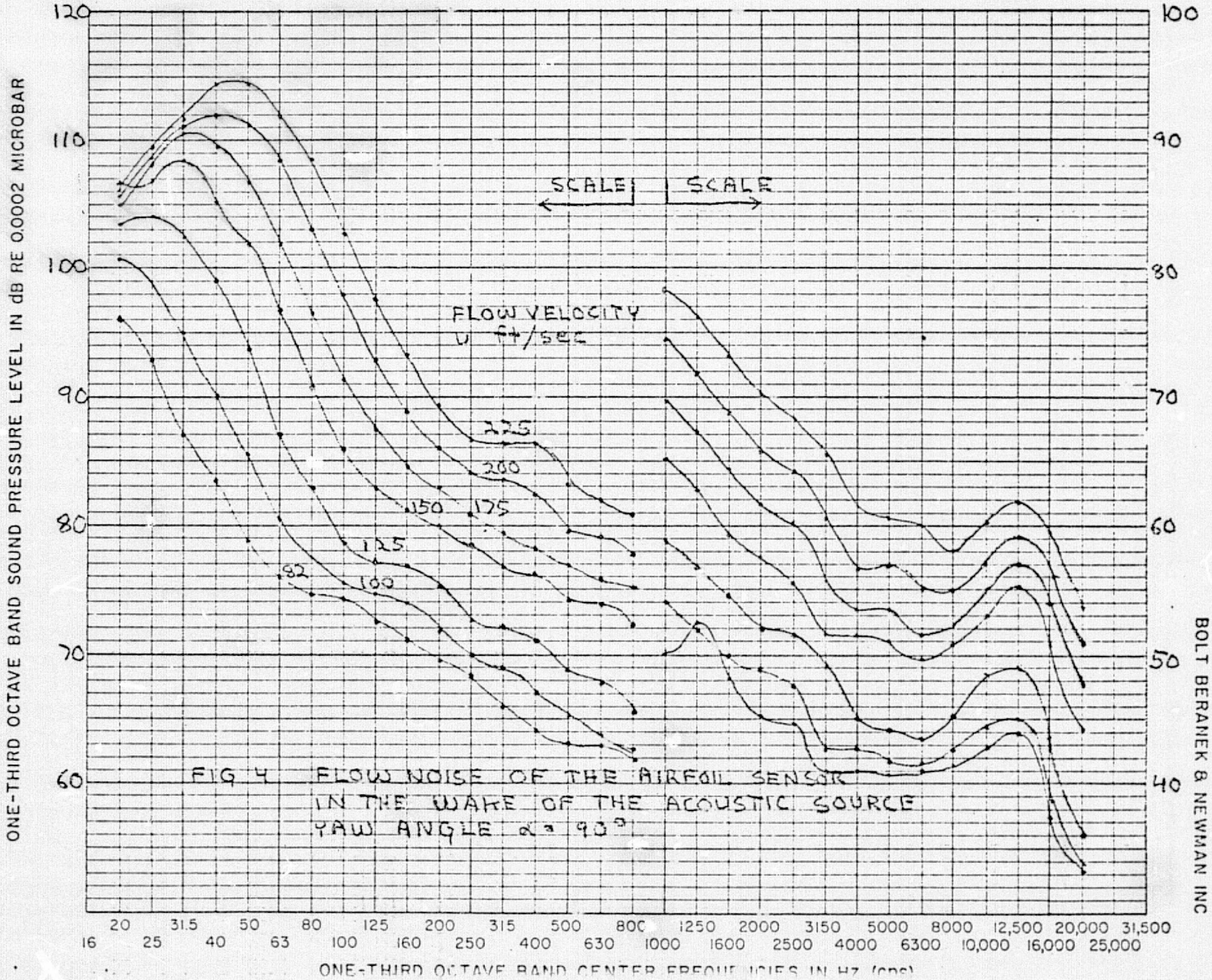

FIG 4 FLOW NOISE OF THE AIRFOIL SENSOR IN THE WAKE OF THE ACOUSTIC SOURCE YAW ANGLE $\alpha = 90°$

ORIGINAL PAGE IS
OF POOR QUALITY

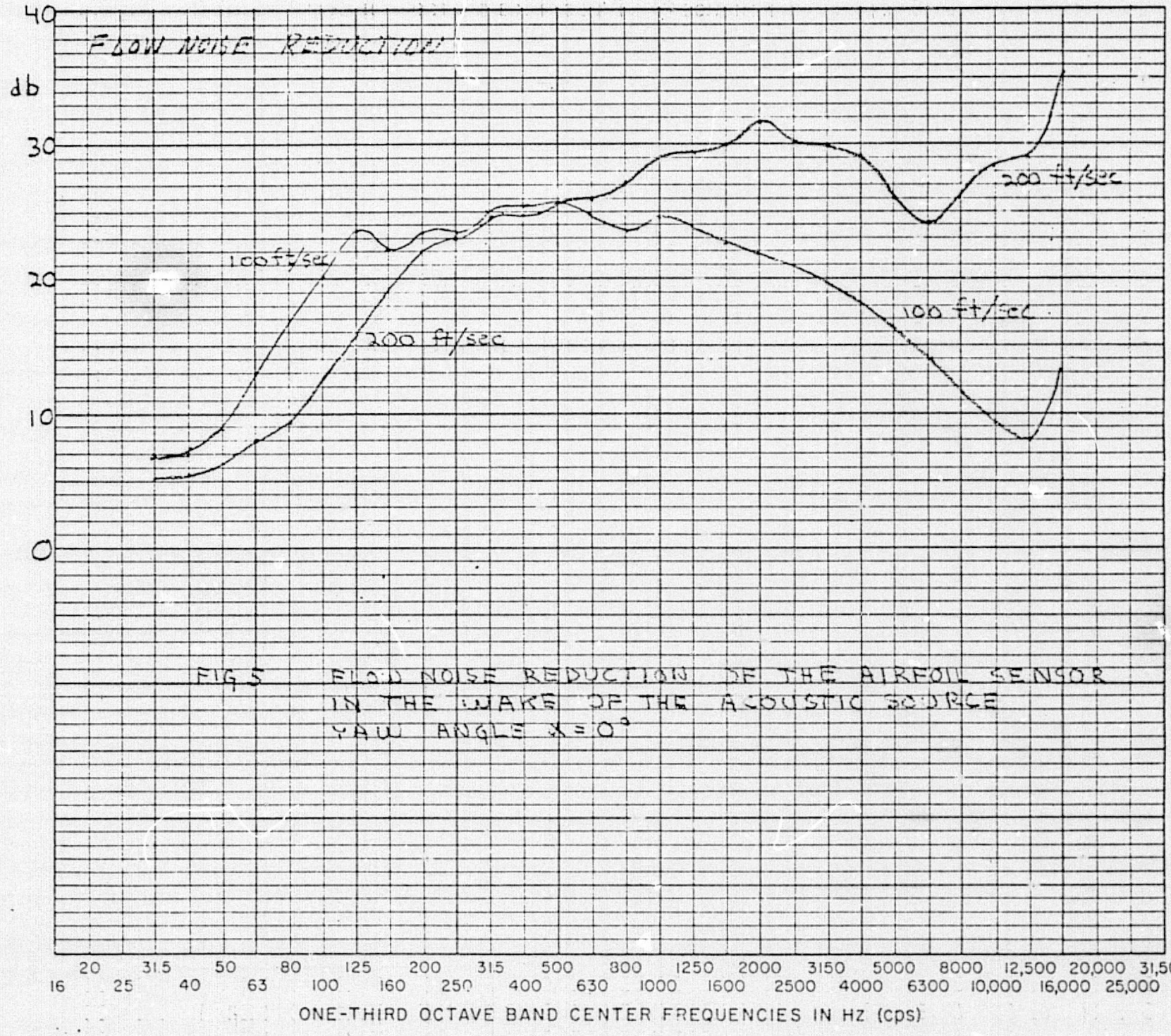

FIG 5 FLOW NOISE REDUCTION OF THE AIRFOIL SENSOR IN THE WAKE OF THE ACOUSTIC SOURCE YAW ANGLE $\chi = 0°$

BOLT BERANEK & NEWMAN INC

ORIGINAL PAGE IS
OF POOR QUALITY

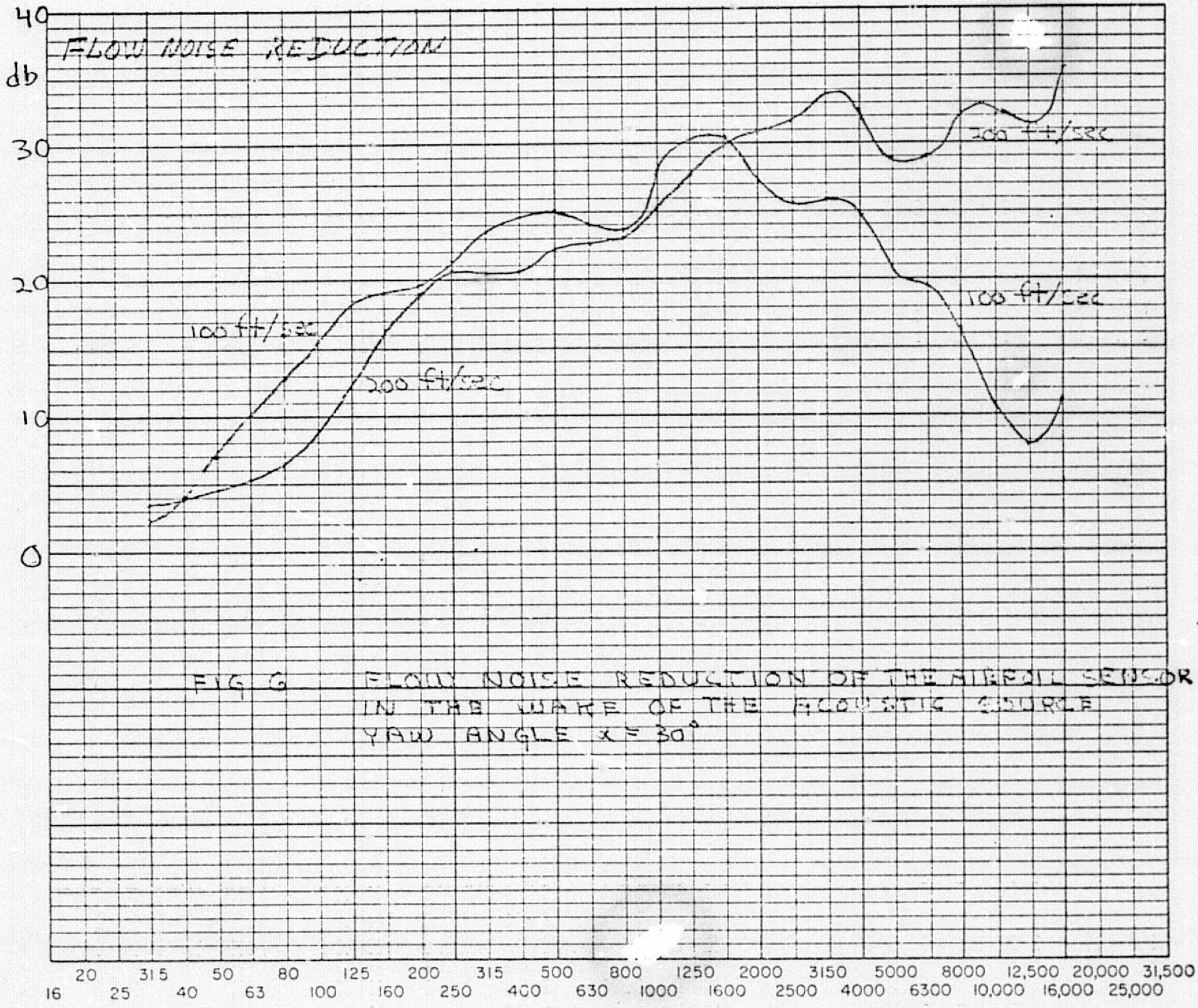

FIG 6 FLOW NOISE REDUCTION OF THE AIRFOIL SENSOR IN THE WAKE OF THE ACOUSTIC SOURCE YAW ANGLE $\chi = 30°$

BOLT BERANEK & NEWMAN INC

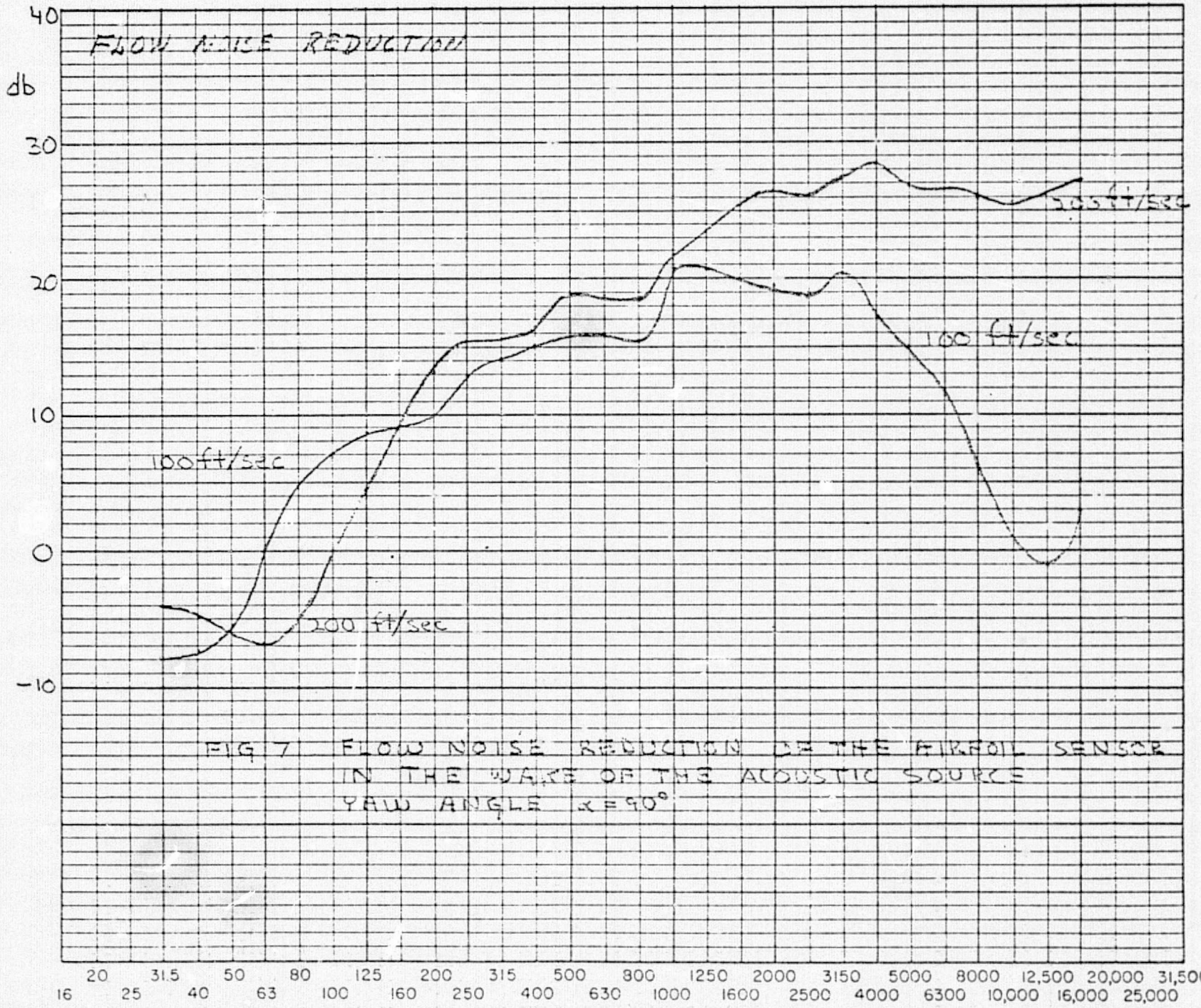

FIG 7 FLOW NOISE REDUCTION OF THE AIRFOIL SENSOR IN THE WAKE OF THE ACOUSTIC SOURCE YAW ANGLE $\chi = 90°$

BOLT BERANEK & NEWMAN INC

Sound Source. However, these noise reductions are typical of what can be achieved in a relatively turbulent flow,* by a porous surface sensor of the same length as the Airfoil Sensor.

At high flow velocities (235 ft/sec) the signal-to-noise ratio of the sound pressure emitted by the source (see Fig. 8b, Appendix IV) to the flow noise of the B&K Sensor, Fig. 1, would become negative in the region of 14 kHz if the analysis were made in third octave bands. In contrast, the signal-to-noise ratio of the Airfoil Sensor would remain positive and large (approximately 20 dB) in the region of 14 kHz, with third octave band analysis. Since the B&K sensor will be used as *the reference* to evaluate the modification of the directivity function of the Airfoil Sensor, narrow band analysis was mandatory.

*See the noise reduction obtained in an artifically spoiled flow: NASA-CR-114593; Appendix VII, Fig. 7.

3. EXPERIMENTAL VALUES OF THE DIRECTIVITY FUNCTION OF THE AIRFOIL SENSOR MODIFIED BY AIRFLOW

The experimental procedure outlined in the Introduction has been followed. The data from the long records produced for each frequency sweep on the Graphic Level Recorder, (see the block diagram of the instrumentation in Fig. 5, Appendix IV), and for each sensor and each flow condition have been reduced to directivity functions. The case of zero degree yaw angle of the Airfoil Sensor is of particular interest.

In all the tests the angle θ between the direction of propagation of the "quasi" plane wave emitted by the Source in the region of the sensors, and the direction of flow is zero. Hence, the ideal directivity function of an end-fired line sensor becomes, from Appendix III,

$$H(\underset{\sim}{k}) = \frac{\sin\left|k_s\left(\frac{\cos\alpha}{1+M} - 1\right) L/2\right|}{k_s\left(\frac{\cos\alpha}{1+M} - 1\right) L/2}.$$

where k_s is the wavenumber in air at the frequency ω_s of the excitation of the source,

$$k_s = \omega_s/c_o$$

c_o is the sound velocity in air and M is the Mach number of the airflow.

3.1 Zero Yaw Angle: $\alpha = 0°$

The Airfoil Sensor is oriented directly into the airflow: $\theta = 0$. Hence, the directivity function of an ideal porous strip sensor, modified by the Mach number becomes

$$H(k) = \frac{\sin\left(k_s \frac{M}{1+M} L/2\right)}{k_s \frac{M}{1+M} L/2}$$

In Figs. 8a through 8e, the measured directivity function of the Airfoil Sensor, at different flow velocities, is compared with the directivity function calculated from the preceeding formula.

The experimental directivity function follows the theoretical one of a line sensor at frequencies up to 10 kHz. Above 10 kHz the experimental and theoretical curves start to diverge. Although the accuracy of the experimental results leave much to be desired, the divergence noted at high frequencies is a very definite one. The divergence coincides with the drop of the frequency response of the source measured in the flow by the B&K sensor. Following the discussion of this effect in Appendix IV, we suspect that the B&K half-inch condenser microphone with nose cone has a frequency response which is dependent on airflow.

The nose cone of the B&K sensor introduces a cavity in front of the microphone cartridge; this cavity is covered by a fine metal screen of axial length h. The sampling correction due to the length of the cavity on the acoustic field, which is

$$\frac{\sin(k_s h/2)}{k_s h/2}$$

ORIGINAL PAGE IS
OF POOR QUALITY

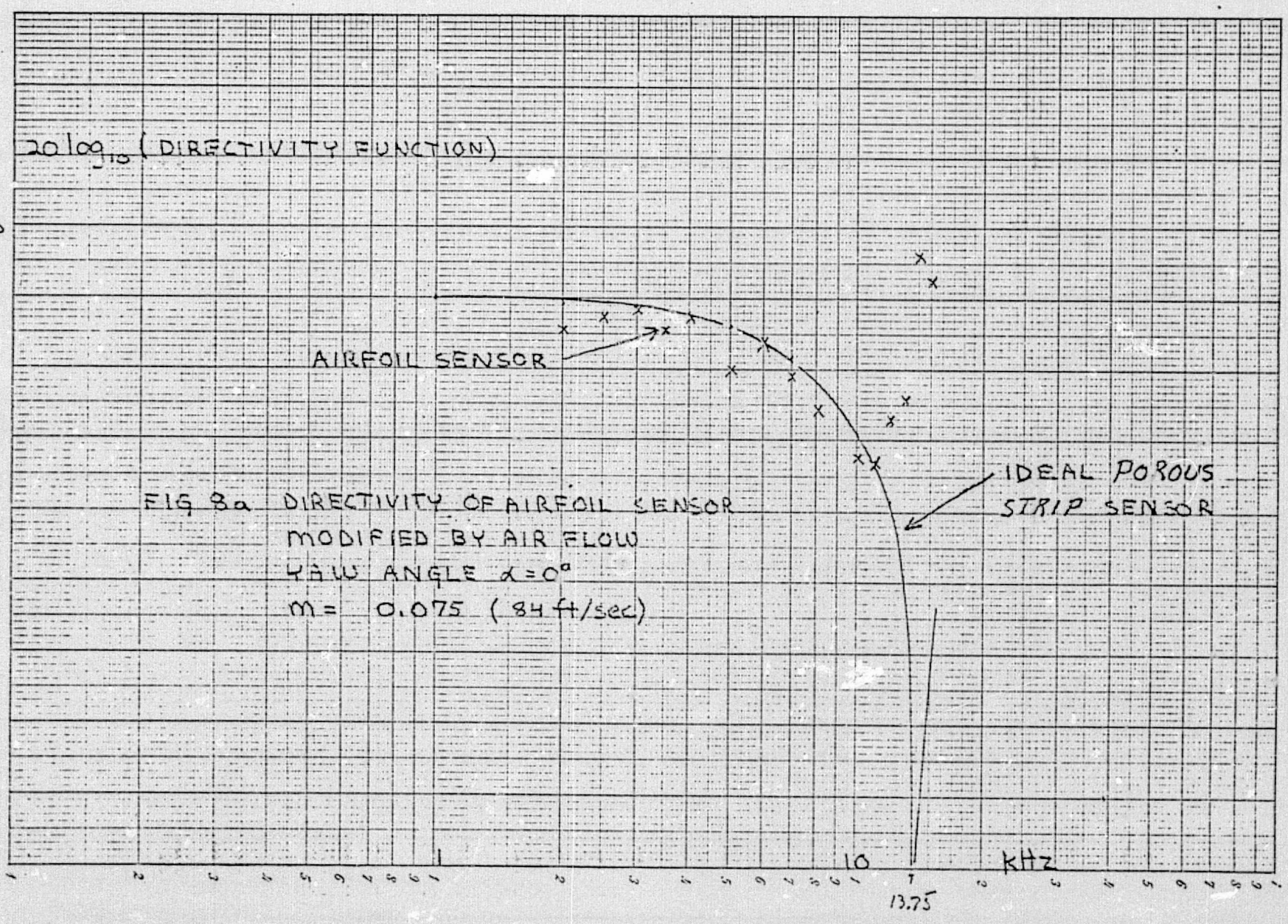

FIG 8a DIRECTIVITY OF AIRFOIL SENSOR
MODIFIED BY AIR FLOW
YAW ANGLE $\alpha = 0^\circ$
$m = 0.075$ (84 ft/sec)

ORIGINAL PAGE IS
OF POOR QUALITY

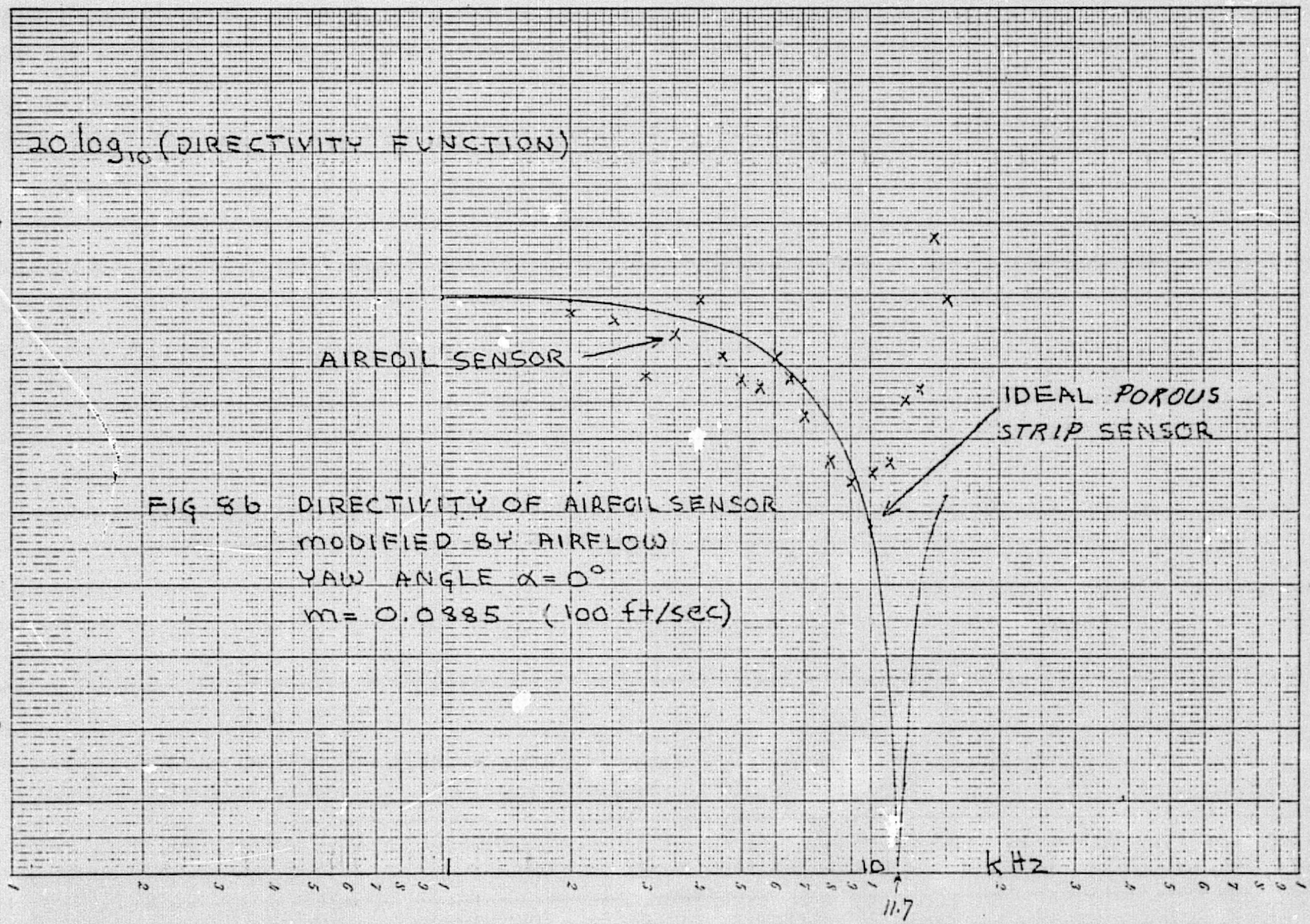

FIG 8b DIRECTIVITY OF AIRFOIL SENSOR
MODIFIED BY AIRFLOW
YAW ANGLE $\alpha = 0°$
$m = 0.0885$ (100 ft/sec)

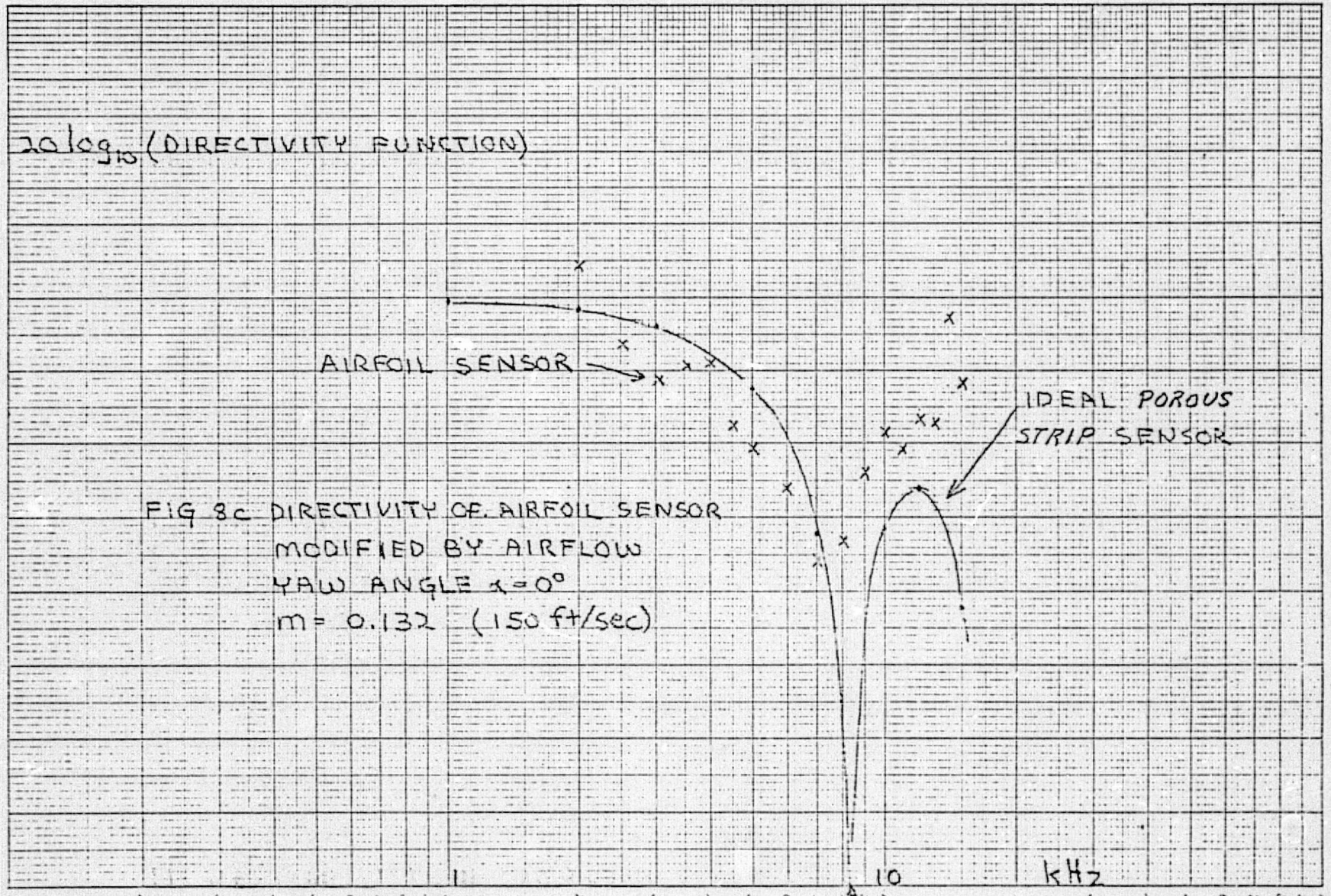

FIG 8c DIRECTIVITY OF AIRFOIL SENSOR MODIFIED BY AIRFLOW YAW ANGLE $\alpha = 0°$ $m = 0.132$ (150 ft/sec)

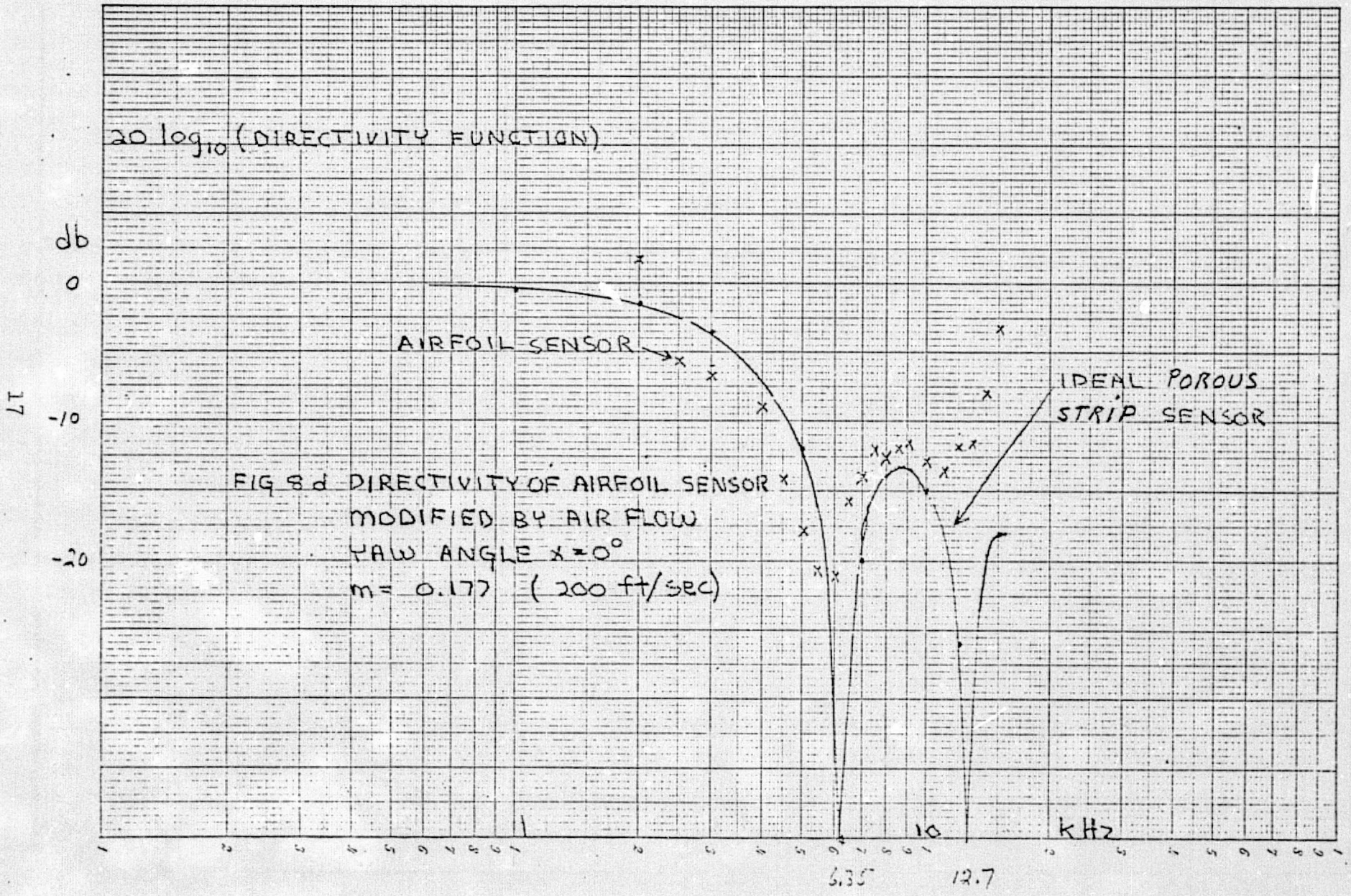
20 log10 (DIRECTIVITY FUNCTION)
db
0
-10
-20
AIRFOIL SENSOR
IDEAL POROUS STRIP SENSOR
FIG 8 d DIRECTIVITY OF AIRFOIL SENSOR MODIFIED BY AIR FLOW
YAW ANGLE x = 0°
m = 0.177 (200 ft/sec)
1
10
kHz
6.35
12.7

ORIGINAL PAGE IS
OF POOR QUALITY

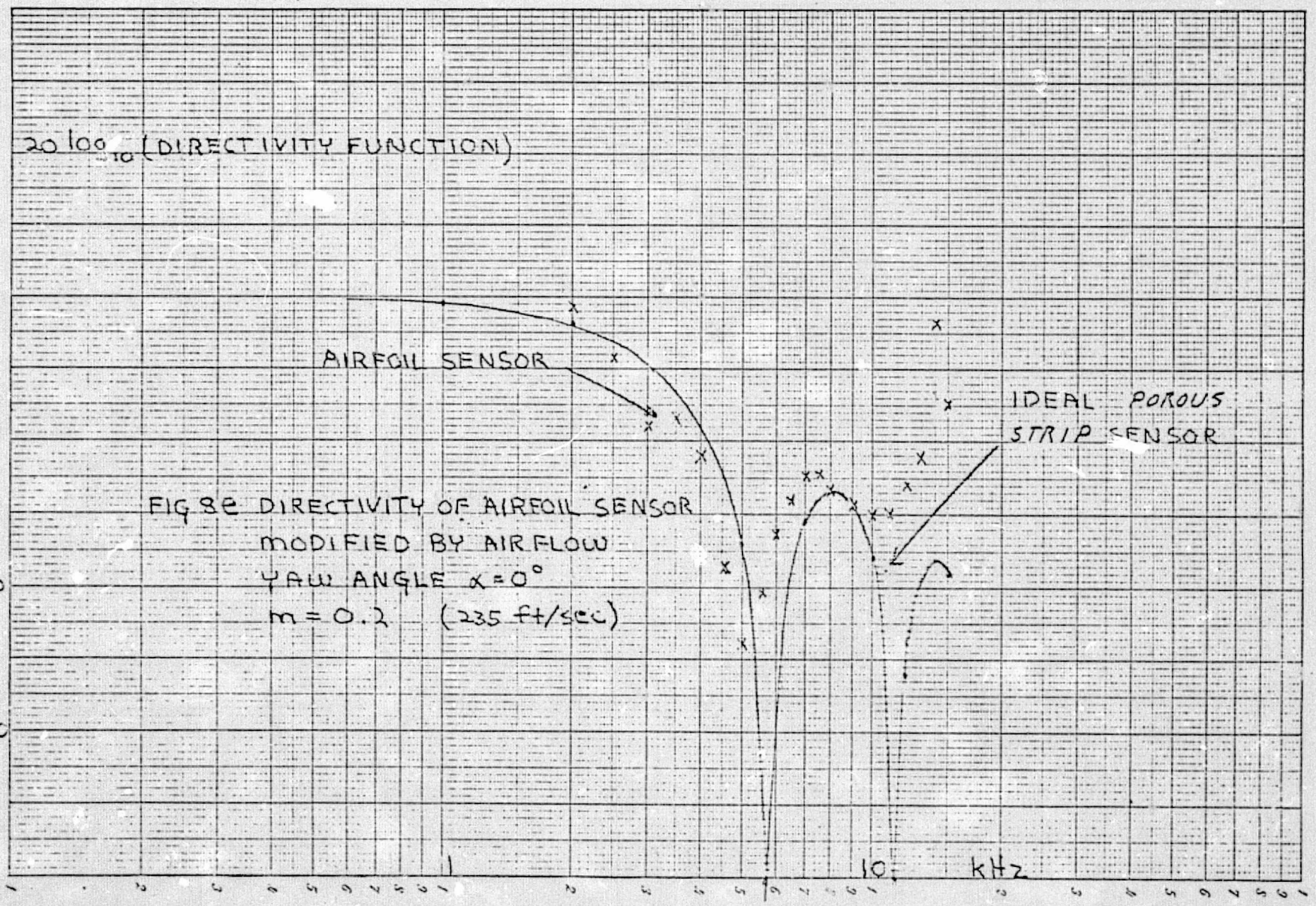

FIG 8e DIRECTIVITY OF AIRFOIL SENSOR MODIFIED BY AIRFLOW
YAW ANGLE $\alpha = 0°$
$m = 0.2$ (235 ft/sec)

is already included in the frequency response of the B&K sensor. This correction is in part compensated by the radial resonance of the cavity which occurs in the frequency region of 15 kHz. This compensation is also included in the frequency response of the B&K sensor at zero flow velocity. The resonance frequency of the radial mode will be shifted towards higher frequencies by the air flow and the modal damping of the resonance will be increased, producing a net and broad decrease of the frequency response in the region of 15 kHz. This decrease in sensitivity would explain the apparent decrease of the sound pressure of the Source in the same frequency region (see Fig. 8 of Appendix IV) and the divergence between the measured and calculated directivity functions above 10 kHz.

The preceeding comments are tentative. They suggest that the frequency response of the B&K sensor as a function of flow velocity should be investigated further.

The directivity functions of the ideal line sensor in Fig. 8 appear to be shifted towards higher frequencies (or lower flow velocities) than the experimental directivity functions. If the real directivity function of the Airfoil Sensor, measured in the anechoic room, had been used instead of the directivity function of a line sensor the agreement in Fig. 8 between the calculated and measured directivity functions would be somewhat better.

3.2 Yaw Angle $\alpha = 30°, 90°$

The acoustic data and Mach number correction for $\alpha = 30°$ and 90° are not presented for the following reasons.

At $\alpha = 30°$ the Airfoil Porous Sensor looks directly at the waves reflected from one side edge of the nozzle; hence, the interference pattern of this data is even sharper than at $\alpha=0°$.

Since the Mach number correction is also larger and starts at lower frequencies than for $\alpha=0°$, it follows that the accuracy of the results is very poor.

At $\alpha=90°$ there should be no Mach number correction. However, the directivity of the Sensor, which is now looking away from the acoustic source, is capturing mostly the residual reverberant field of the test room. Again, this result is not significant except that it shows that the Airfoil Sensor maintains its acoustic directivity in the air flow. This conclusion was already made from the case of $\alpha=0°$.

4. CONCLUSIONS

(1) The accuracy of the experiments with a Source in air flow is not very good for two main reasons: the interference at low frequencies of the waves reflected from the sides of the nozzle with the main beam of source; and at high frequencies the suspicion that the acoustic response of the B&K microphone with nose cone is sensitive to air flow.

(2) The effect of Mach number on the directivity function of the Airfoil Sensor follows the calculation based on an ideal end-fired line sensor for frequencies at least up to 10 kHz and in the range $M \leq 0.2$.

(3) Even when the Airfoil Sensor is pointing directly into the flow ($\theta=0$) and directly towards the Acoustic Source ($\alpha=0$) the directivity function modified by Mach number enters in the response of the Sensor; the net correction to the data becomes large at high flow velocities and high frequencies.

(4) The cause for the required corrections in air flow even for $\alpha = \theta = 0°$, is shown explicitly in the case of an equivalent line sensor; see Eq. 16 Appendix III: the wavenumber k_i of the gas inside the line sensor is not matched to the wavenumber component of the pressure field applied to the sensor:

$$k_i \neq \frac{k_s \cos\alpha}{1+M\cos\theta}$$

or, in terms of trace velocities,

$$c_i \neq \frac{c_o(1+M\cos\theta)}{\cos\alpha}$$

where c_i is the sound velocity of the gas inside the line sensor and c_o is the sound velocity of the gas outside the line sensor.

When the gas inside and outside the line sensor is the same, like air, the trace matching is never achieved except at M=0 and $\alpha=0°$. For M=0 the mismatch in trace velocities produces the usual directivity function which could take the form, for example, of directivity patterns in polar diagrams, α being the polar angle. The dependence on α is therefore desirable. The dependence on M $\cos\theta$ is not desirable.

The dependence of the directivity function on M $\cos\theta$ could be eliminated for each specific case if the gas inside the Airfoil Sensor were different from the gas outside such that

$$c_i = c_o (1 + M \cos\theta)$$

Then, for this case, the directivity function reduces to the usual one (directivity patterns) with dependence only on $\cos\alpha$. A different gas inside the sensor must be used for each product M $\cos\theta$. However, it appears possible to use a gas mixture inside the sensor, where the percentage of the gas components can be varied to satisfy the required value of c_i for a wide range of M $\cos\theta$. This is an enticing possibility which should be pursued: the effect of Mach number on the directivity functions, like those of Fig. 8, would be eliminated leaving only the usual dependence on the angle α.

APPENDIX VI*

FLOW NOISE TESTS OF THE AIRFOIL POROUS SURFACE SENSOR MODEL 342 AND OF THE B&K HALF-INCH CONDENSER MICROPHONE WITH NOSE CONE

*This appendix is identical to Appendix X of the following reference: The experiment has been supported jointly by NASA Ames and NASA Langley; Noiseux, D.U., *et al.*, "Development, Fabrication and Calibration of a Porous Surface Microphone in an Airfoil," NASA CR-_____, BBN Report No. 3014, March 1975.

1. INTRODUCTION

The Airfoil Porous Surface Sensor, Model 342, and the Bruel and Kjaer half-inch condenser microphone with nose cone have been tested in a quiet wind tunnel at flow velocities from 25 m/sec. (84 ft/sec) to 70 m/sec (235 ft/sec). Their flow noises are compared.

The B&K sensor is used as a reference to show the flow noise reduction achieved by the Airfoil Sensor. The B&K sensor is always pointed directly into the flow. The Airfoil Sensor is pointed at different yaw angles in the flow, in the range of 0° to 90°. Since the B&K sensor is essentially omnidirectional over its effective frequency range, up to 15 kHz, there is no reason to orient it differently than directly towards the flow; in fact, if it is pointed towards otherwise, its flow noise increases rapidly with the angle between its axis and the flow direction.

The relevant properties of the wind tunnel are given in Section 2, including its spectrum of turbulence. Section 3 describes the test setup. Section 4 presents the data of flow noise with discussion of the results. Section 5 offers some conclusions.

2. WIND TUNNEL

The flow noise tests were made in the new BBN quiet wind tunnel. Figure 1a and 1b show the elevation and plan views of the facility: it is a free jet in a semi-anechoic room.

A new nozzle was added to increase the flow velocities: it is a rectangular nozzle with dimensions of 28 inch high by 40 inch wide at the exit. The larger width is convenient for testing models, like the Airfoil Porous Surface Sensor which are long and thin in the horizontal plane. The maximum flow velocity attained 70 m/sec, (235 ft/sec). The minimum flow velocity, 24 m/sec, corresponds to the idling speed of the diesel.

The velocity profile at the exit face of the nozzle is very uniform over the full range of flow velocities with a rapid but smooth decrease of velocity at the sides of the nozzle: there is no flow separation on the sides of the nozzle.

The level of turbulence at the exit of the nozzle is very low. At the location of the microphone, one meter away from the exit plane, the turbulence spectrum on the axis of the nozzle is shown in Fig. 2, in third octave bands, for three different flow velocities: 100, 150 and 200 ft/sec. The low frequency part of the spectrum, below 100 Hz is attributed to the fan. The central part of the spectrum, from 100 Hz to 4 kHz at 100 ft/sec, to 8 kHz at 150 ft/sec and to 12.5 kHz at 200 ft/sec is the normal turbulence of the wind tunnel. The high frequency part above 12.5 kHz has a rising spectrum, with a slope of +9 dB per octave for third octave bands (or 6 dB/octave on a linear frequency scale): this part is not considered to represent free flow turbulence, but is believed to be caused by the hot wire probe. Nevertheless, the turbulence is very low over the whole frequency range of interest: 100 Hz to 10 kHz.

The wind tunnel is operated with open cycle air intake and exhaust.

ORIGINAL PAGE IS
OF POOR QUALITY

BBN HIGH SPEED FREE JET ACOUSTIC WIND TUNNEL
– ELEVATION –

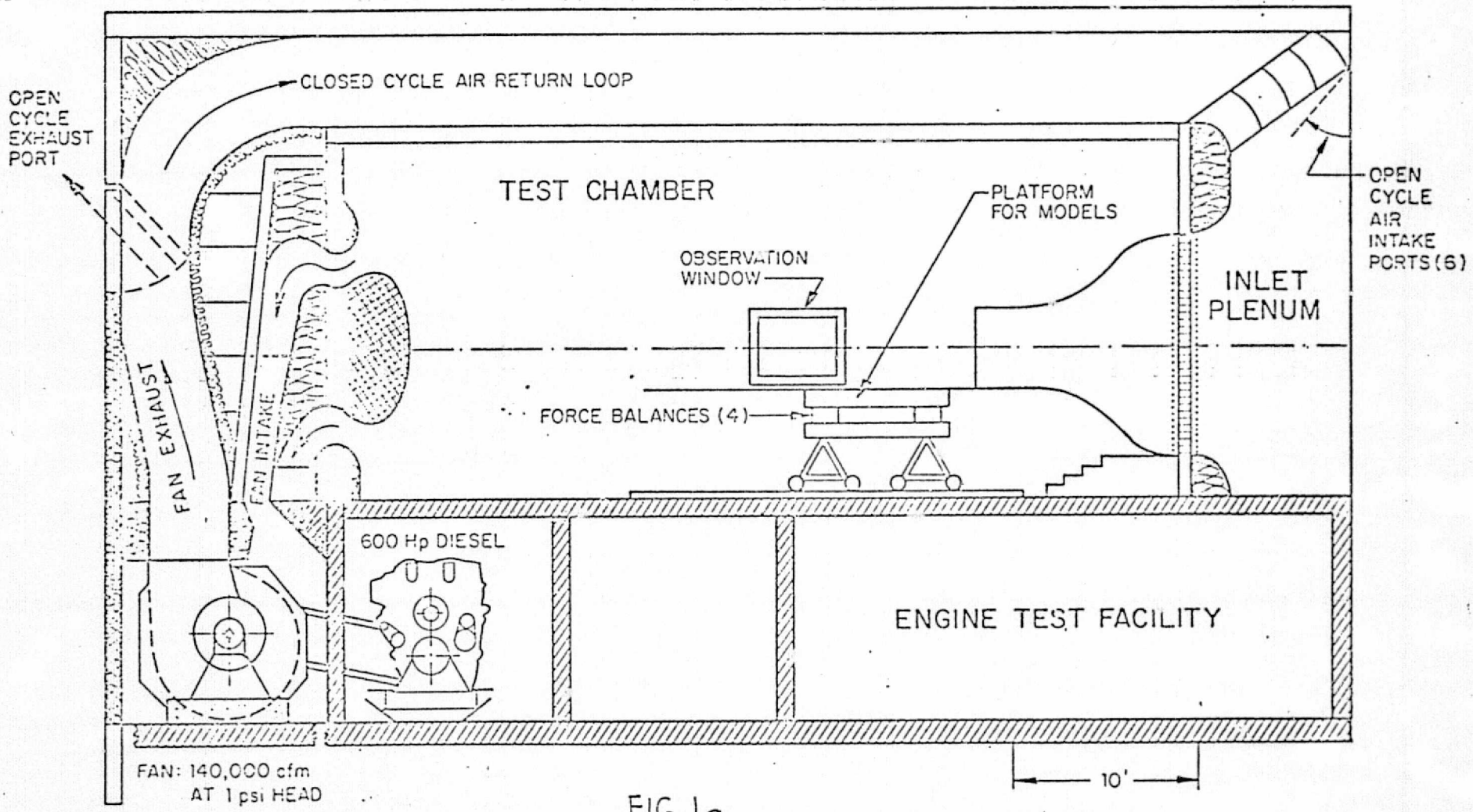

FIG. 1a

BBN HIGH SPEED FREE JET ACOUSTIC WIND TUNNEL
- PLAN VIEW -

ORIGINAL PAGE IS
OF POOR QUALITY

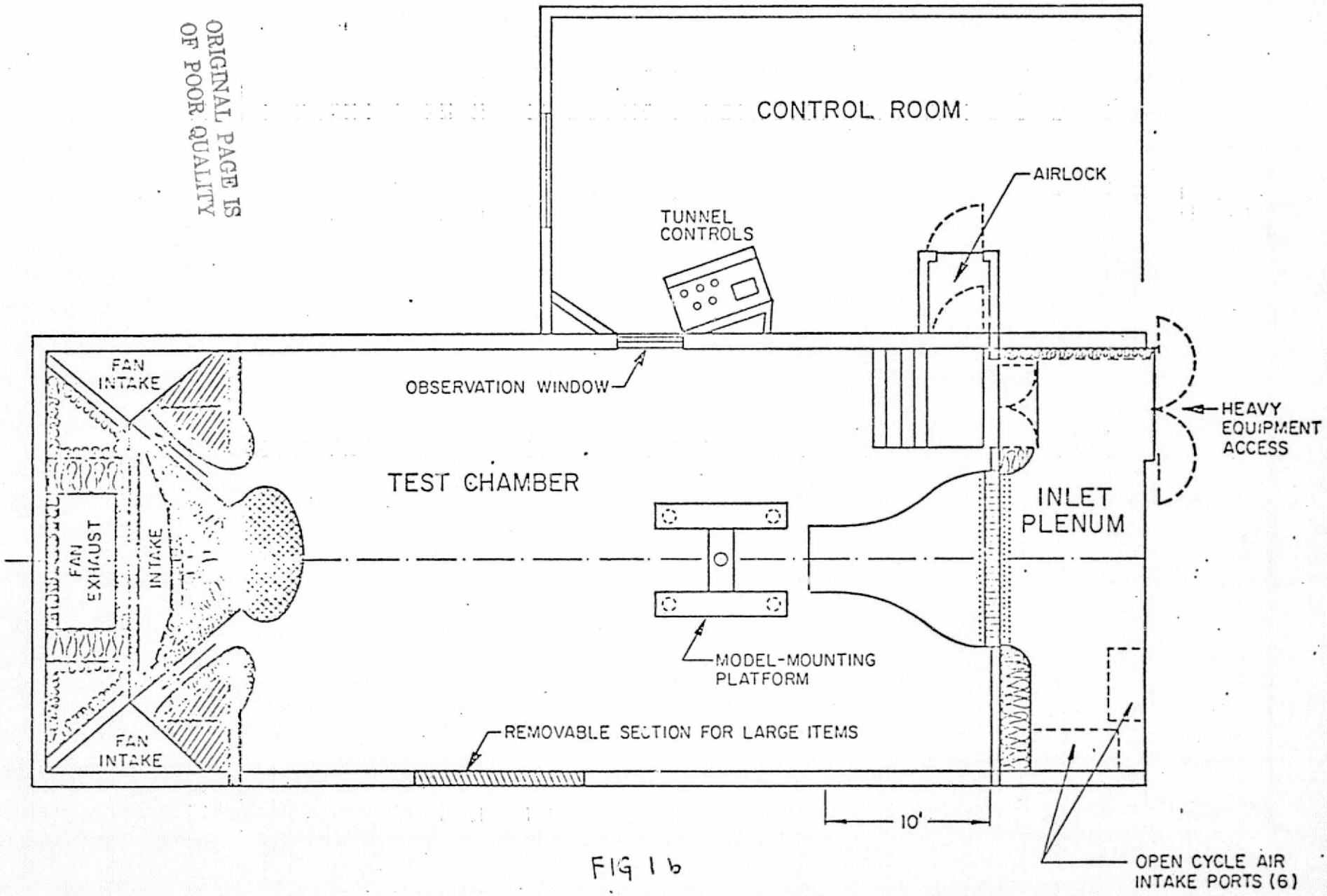

FIG 1 b

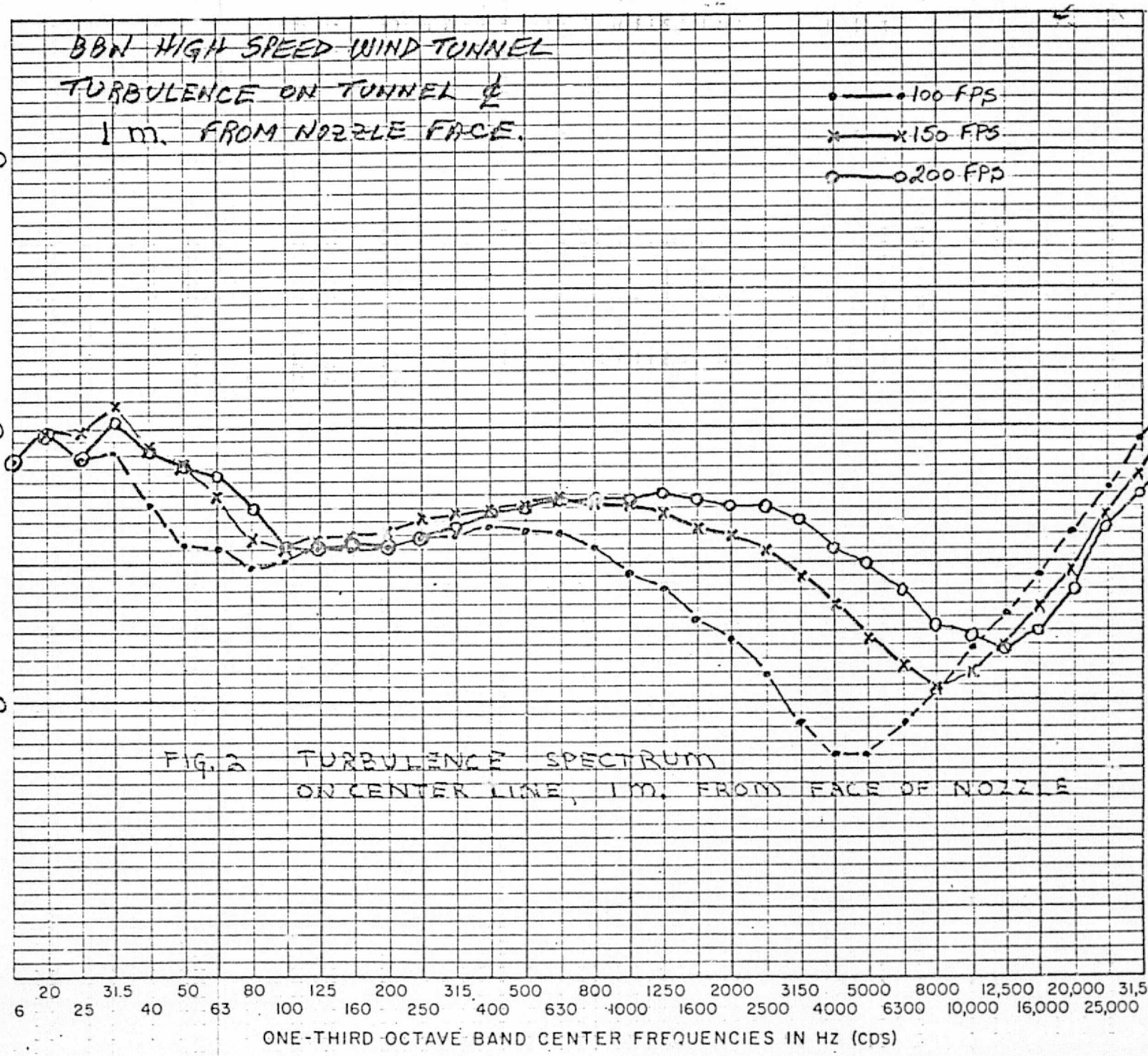

FIG. 2 TURBULENCE SPECTRUM ON CENTER LINE, 1 M. FROM FACE OF NOZZLE

BOLT BERANEK & NEWMAN INC

ORIGINAL PAGE IS
OF POOR QUALITY

3. TEST STAND

The Airfoil Sensor, its preamplifier base and tail end form an aerodynamic shape. The pipe cemented to the preamplifier base carries the electrical leads of the preamplifier; the pipe fits vertically inside the aerodynamic stand. The Airfoil sensor can be rotated horizontally with respect to the stand. The stand is bolted to a horizontal plate which is attached to the test platform. A protractor on the underside of the plate measures the yaw angle α, which is the rotation of the pipe and Airfoil Sensor with respect to the aerodynamic stand. Figure 3 shows the Airfoil sensor on the stand for zero yaw angle.

The Bruel and Kjaer half-inch condenser microphone uses the same stand as the Airfoil Sensor. An aerodynamic top is added to the stand as shown in Fig. 4. The preamplifier, which is a standard B&K preamplifier type 2615, is set inside an aerodynamic housing to which is soldered a vertical pipe which carries the electrical leads. The microphone and its preamplifier can be rotated in a horizontal plane, with respect to the stationary test stand. In all the tests, the nose cone used is the newer B&K type UA 0386, instead of the older type shown in the photograph.

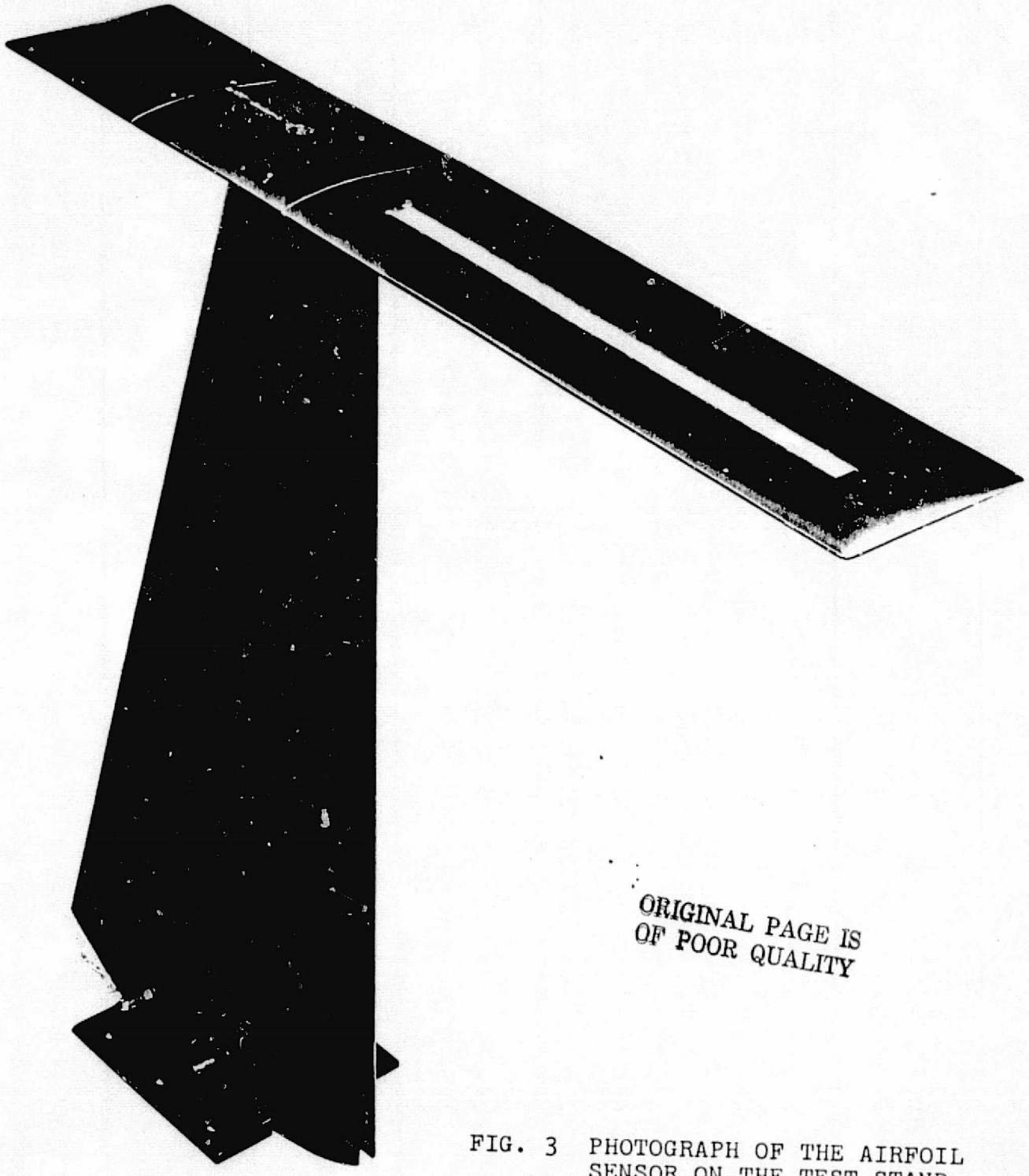

ORIGINAL PAGE IS
OF POOR QUALITY

FIG. 3 PHOTOGRAPH OF THE AIRFOIL SENSOR ON THE TEST STAND. YAW ANGLE $\alpha = 0$

ORIGINAL PAGE IS
OF POOR QUALITY

FIG. 4 PHOTOGRAPH OF THE B&K ½ INCH CONDENSER MICROPHONE WITH NOSE CONE, AND THE AERODYNAMIC HOUSING OF THE PREAMPLIFIER, ATTACHED TO THE TEST STAND.

4. FLOW NOISE TESTS

4.1 Test Conditions

All the results of flow noise are reduced to equivalent acoustic pressures of a plane wave incident along the axis of the sensors; i.e., the flow noise data are corrected for the frequency response of each sensor.

The frequency response of the Airfoil Sensor is shown in Fig. 5. The frequency response of the B&K half-inch microphone with nose cone is shown in Fig. 6: the microphone cartridge type 4133 and the nose cone type UA-0386 are used. The small scale variations in the frequency response of Fig. 6 are caused by the test setup in the anechoic room.

The centers of each sensor during the tests are located at approximately one meter from the face of the nozzle.

When the fan is off the background acoustic and electronic noise of the sensors are shown in Fig. 7. The low frequency part of the noise is mostly acoustic noise and 60 cycle hum pickup.

The aerodynamic stand on which sits the airfoil sensor or the B&K sensor generates a certain amount of noise which will contribute to the net flow noise measured by the sensors. The turbulent mixing region between the free jet and the free air strikes the stand in an area below the sensors; the fluctuating pressures generated in this area radiate as dipoles oriented perpendicular to the surface and the frequency spectrum of the noise radiated has a broad maximum at a low frequency given approximately by

$$f = \frac{0.2\ U_\infty}{h} \quad , \text{Hz}$$

P55

FIG 5 FREQUENCY RESPONSE OF POROUS SURFACE MICROPHONE TYPE 342 F1

ORIGINAL PAGE IS
OF POOR QUALITY

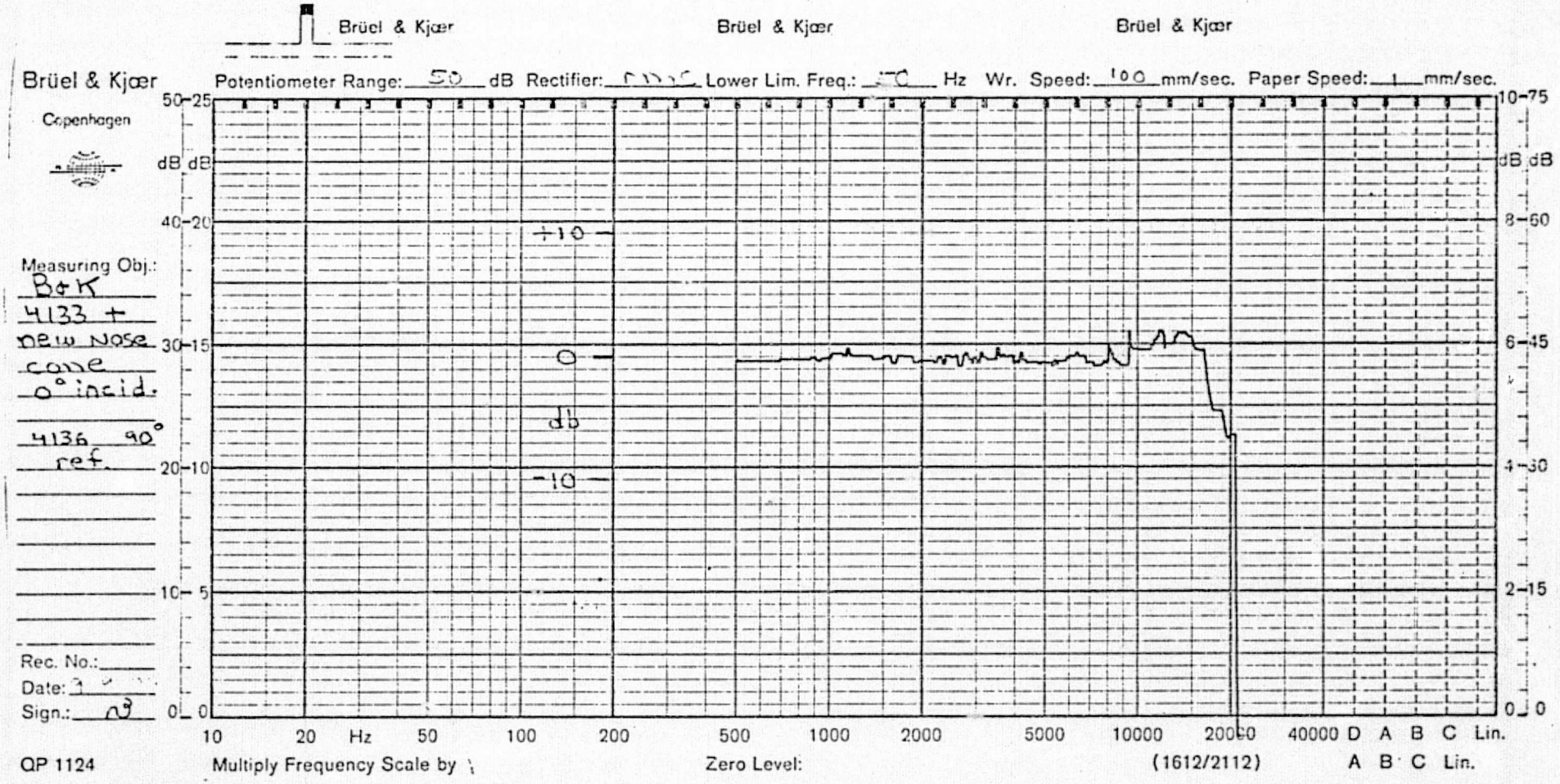

FIG 6 FREQUENCY RESPONSE OF B&K

½ INCH CONDENSER MICROPHONE

4133 WITH NOSE CONE UA-0386

ORIGINAL PAGE IS
OF POOR QUALITY

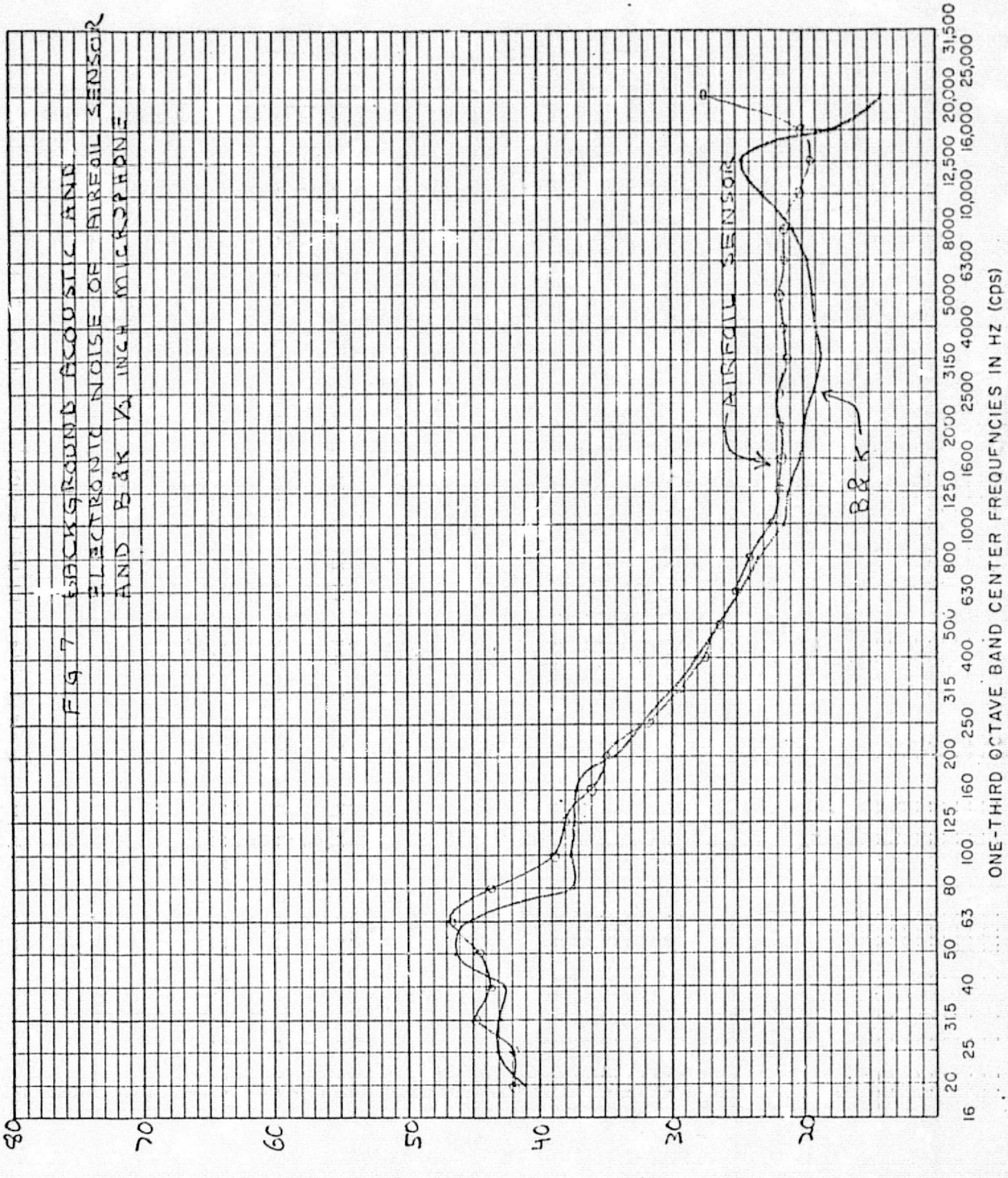

ORIGINAL PAGE IS
OF POOR QUALITY

where h is the thickness of the mixing region and U is the mean flow velocity; this frequency is roughly 100 to 200 Hz. It follows that the directivity pattern of this radiated noise has a minimum in the direction of flow (corresponding to yaw angle of 0° for the Airfoil Sensor) and increases gradually for directions perpenticular to the flow. The Airfoil Sensor at yaw angle near 0°, and the B&K sensor (which is always pointed into the flow) will be near a minimum of this radiated noise.

This low frequency noise generated by the stand could have been almost eliminated by extending the lower lip of the nozzle beyond the stand. But this extended surface would also create other noises, like radiation from its boundary layer and from the vibration of the surface, and would cause undesirable acoustic reflections. Hence, it was decided to accept the low frequency, low level, of the noise generated on the stand by the mixing region of the flow.

The trailing edge of the stand will create a similar but high frequency noise associated with the thickness of the boundary layer.

The noise radiated by the stand and the Airfoil Sensor were measured outside the free jet and mixing region at two locations which are specified in Fig. 8. At location 1, which is at the same elevation and axial distance from the nozzle as the sensor but immediately outside the mixing region, the pressure spectrum, measured with the B&K sensor, is shown in Fig. 9. At location 2, which is under the axis of the jet in front of the stand but outside of the jet and its mixing region we get the pressure spectrum of Fig. 10. The low frequency spectrum of the out-of-flow noise at location 2 is roughly 30 dB lower than at location 1: location 2 is in a null of the directivity of the noise

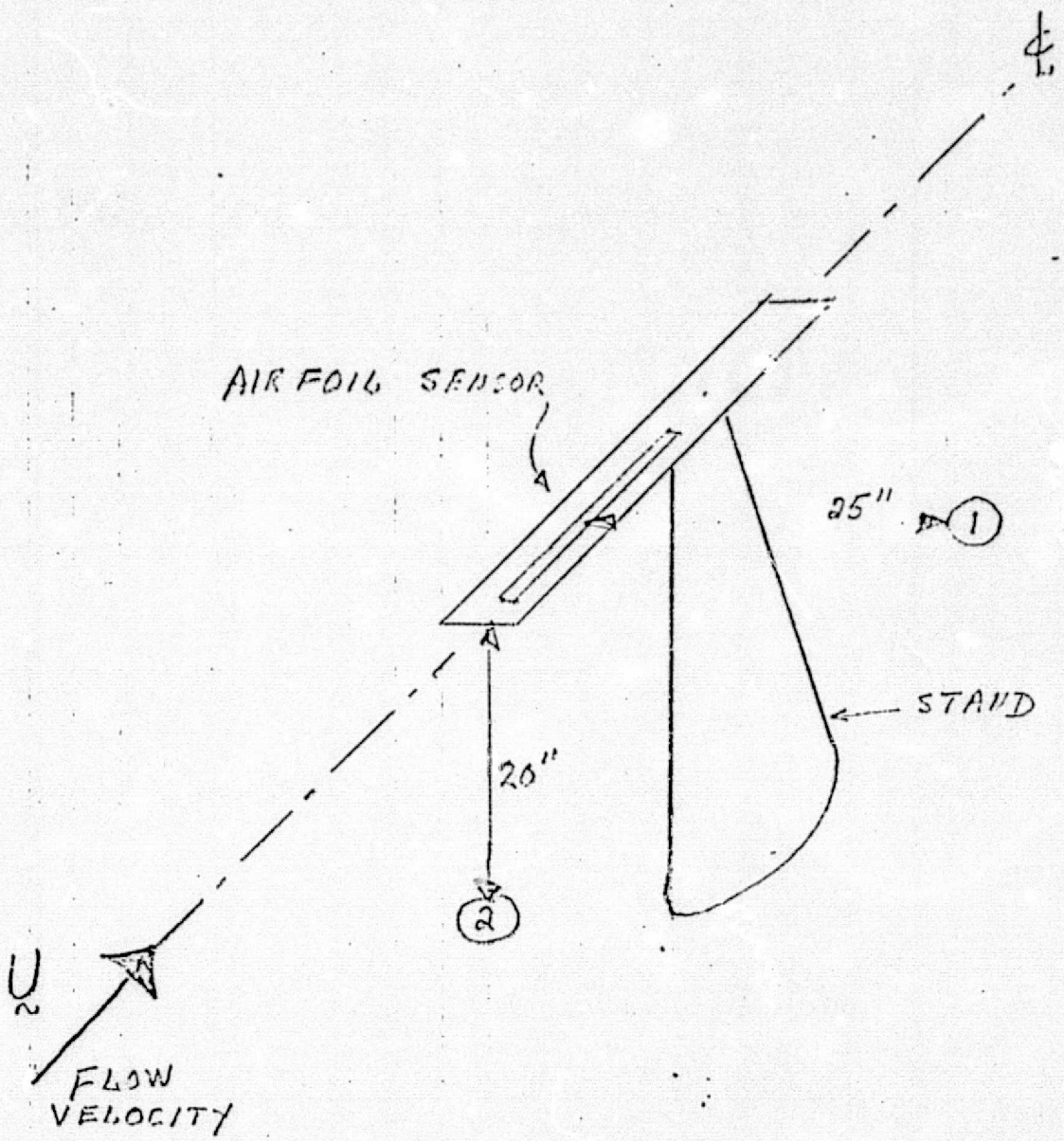

FIG. 8 : LOCATIONS 1 AND 2 OF MICROPHONES FOR THE MEASUREMENTS OF OUT-OF-FLOW NOISE

ORIGINAL PAGE IS
OF POOR QUALITY

ORIGINAL PAGE IS
OF POOR QUALITY

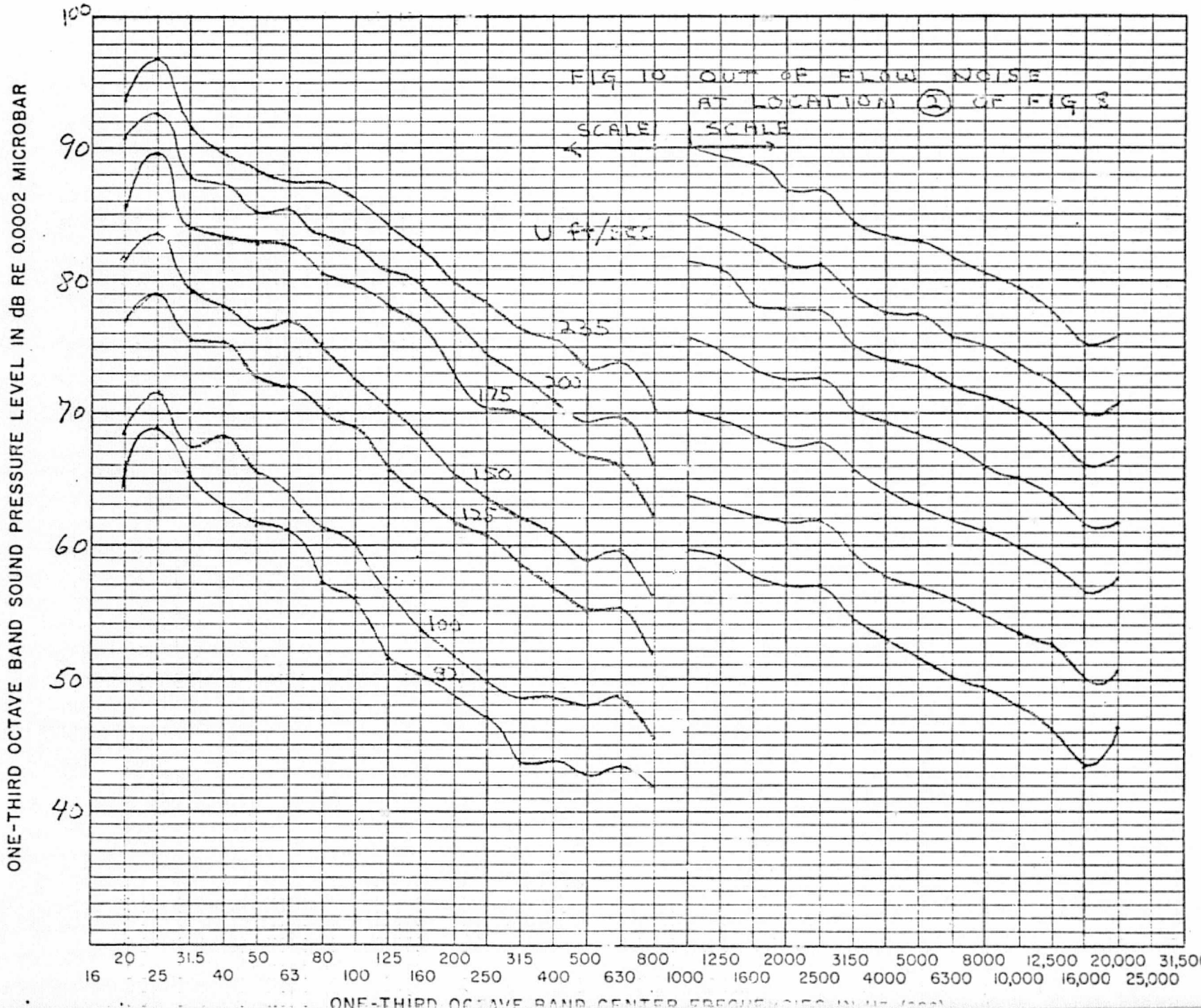

BOLT BERANEK & NEWMAN INC

generated by the mixing region hitting the stand; also the acoustic noise radiated through the nozzle is baffled by the nozzle itself. At high frequencies the noise at station 2 is also lower than at station 1 because station 2 is in a null of the pressure radiated by the trailing edge of the stand.

4.2 Flow Noise of the B&K Half-Inch Condenser Microphone With Nose Cone

The spectrum of the flow noise measured by a B&K half-inch condenser microphone with nose cone, pointing directly into the flow, is shown in Fig. 11, in third octave bands and for different flow velocities from 24 to 70 m/sec.

The levels of flow noise of Fig. 11 is lower than the out-of-flow noise measured at location 1 of Fig. 8, except towards high frequencies where they become roughly equal. The lower levels of Fig. 11 were anticipated because the B&K sensor is in a null of the directivity of the noise generated by the stand. When the levels of flow noise of Fig. 11 are compared with the out-of-flow noise measured at location 2 of Fig. 8, they are found to be higher; hence, the flow noise of the B&K sensor is dominated by the turbulence of the free jet reacting on the surface of the B&K sensor and its preamplifier base.

The flow noise of Fig. 11 will be the reference to which the flow noise of the Airfoil Sensor will be compared.

4.3 Flow Noise of the Airfoil Sensor

The frequency spectra, in third octave bands, of the flow noise of the Airfoil Porous Surface Sensor, are shown in Figs. 12 through 18, for yaw angles α from 0° to 90° in increments of 15° and for flow velocities of 25 to 70 m/sec in increments of 8 m/sec (25 ft/sec).

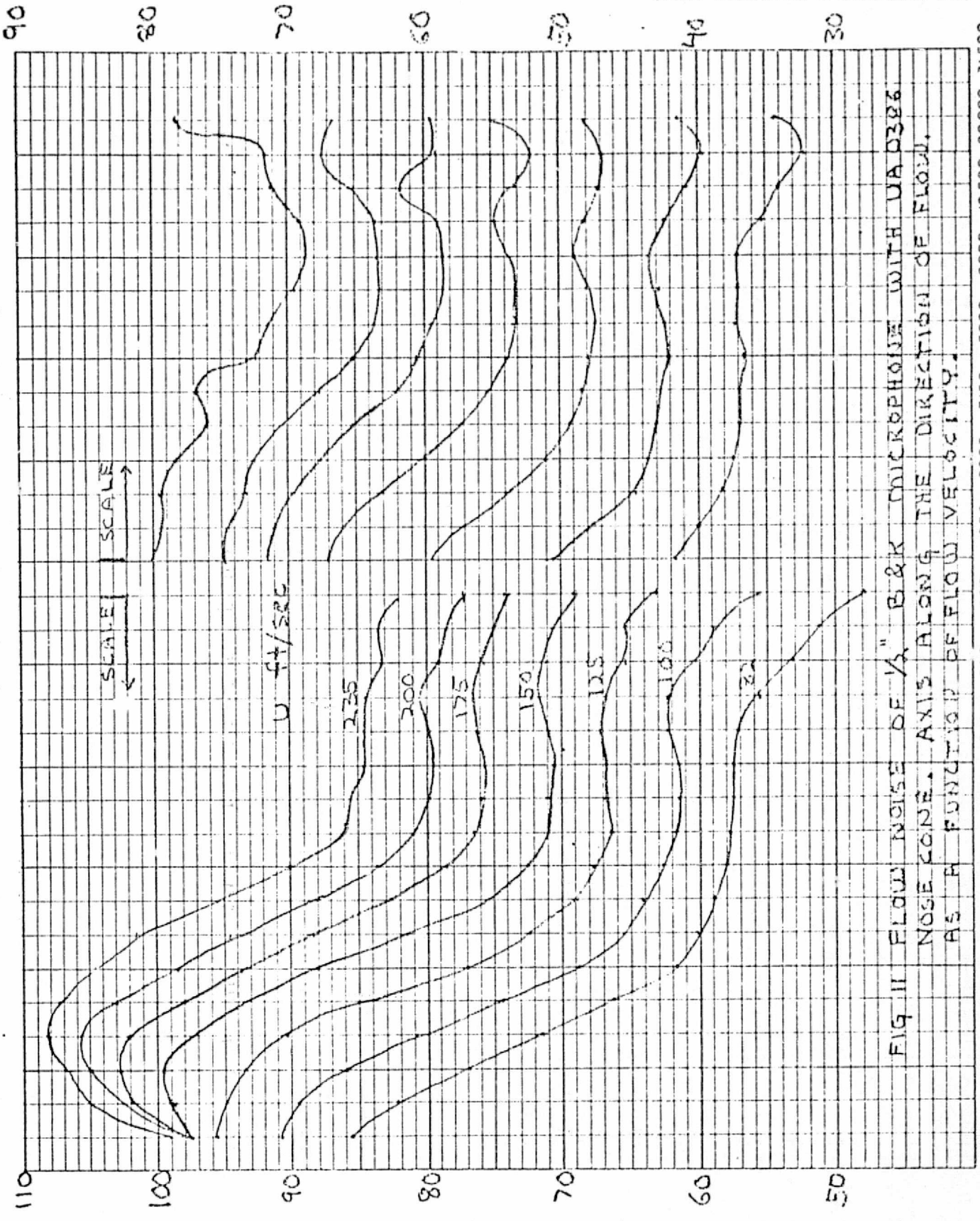

ORIGINAL PAGE IS
OF POOR QUALITY

ORIGINAL PAGE IS
OF POOR QUALITY

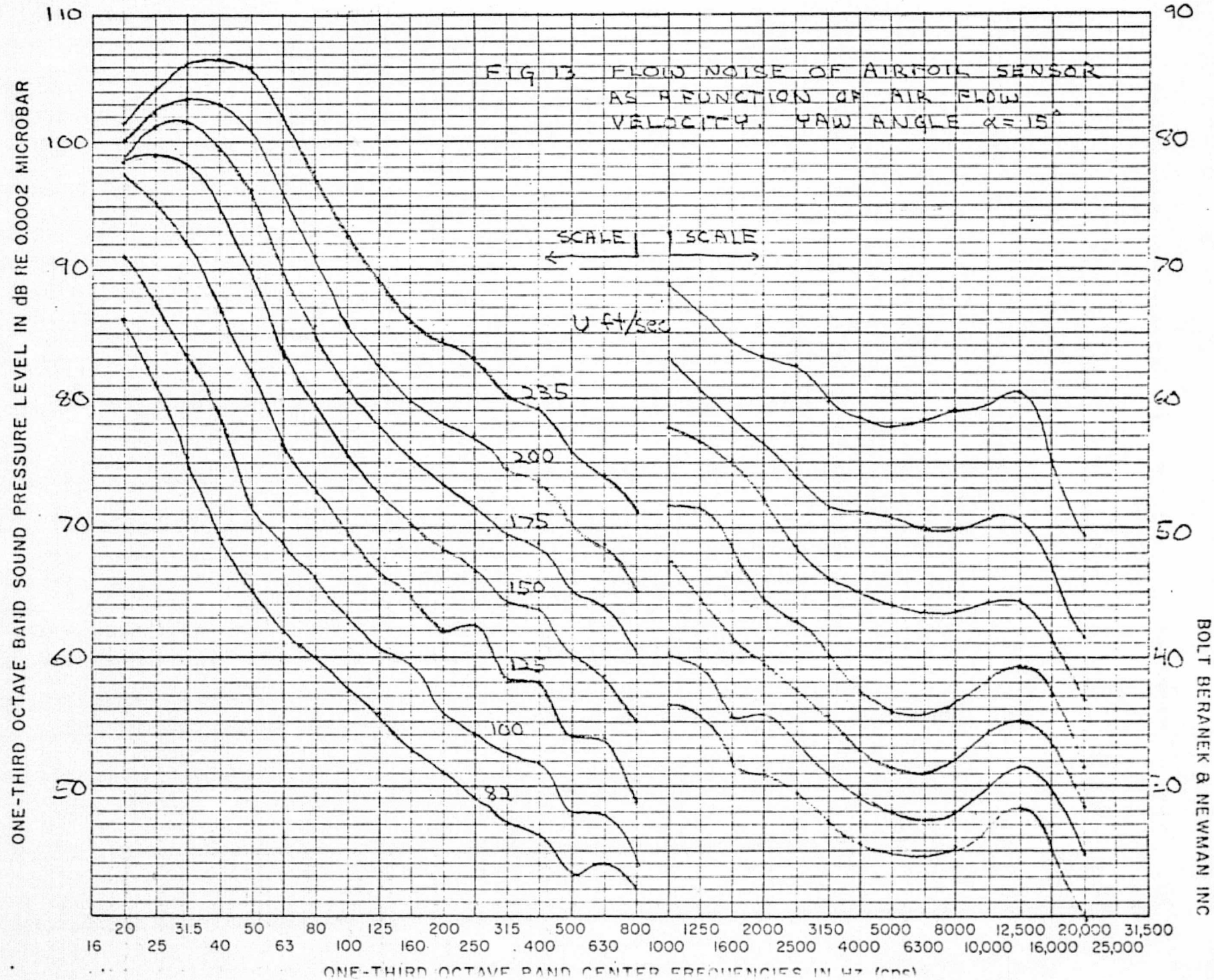
FIG 13 FLOW NOISE OF AIRFOIL SENSOR AS A FUNCTION OF AIR FLOW VELOCITY, YAW ANGLE α = 15°
SCALE
SCALE
U ft/sec
235
200
175
150
125
100
82
ONE-THIRD OCTAVE BAND SOUND PRESSURE LEVEL IN dB RE 0.0002 MICROBAR
110
100
90
80
70
60
50
90
80
70
60
50
40
30
20
10
20 31.5 50 80 125 200 315 500 800 1250 2000 3150 5000 8000 12,500 20,000 31,500
16 25 40 63 100 160 250 400 630 1000 1600 2500 4000 6300 10,000 16,000 25,000
ONE-THIRD OCTAVE BAND CENTER FREQUENCIES IN Hz (cps)
BOLT BERANEK & NEWMAN INC

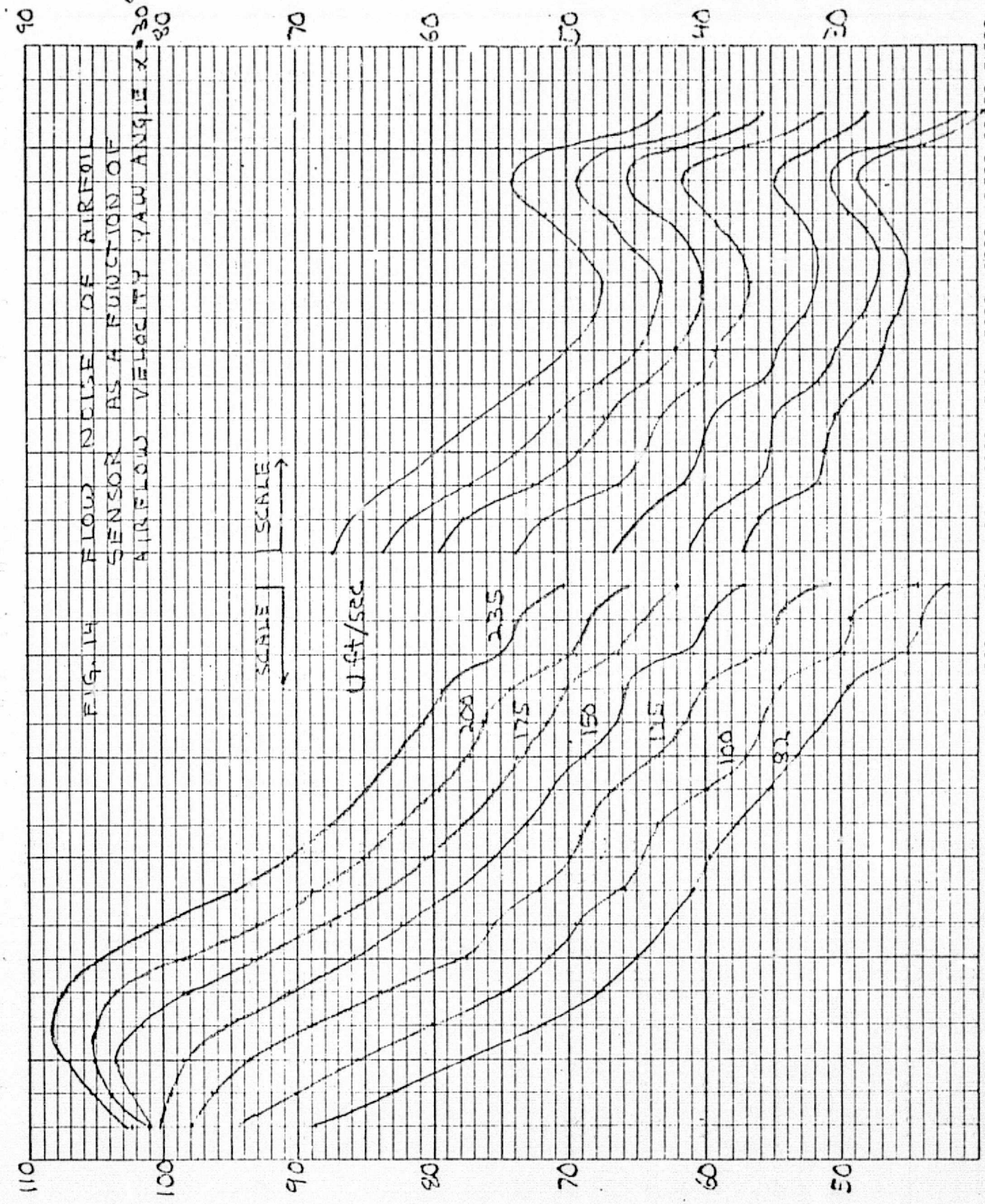

ORIGINAL PAGE IS
OF POOR QUALITY

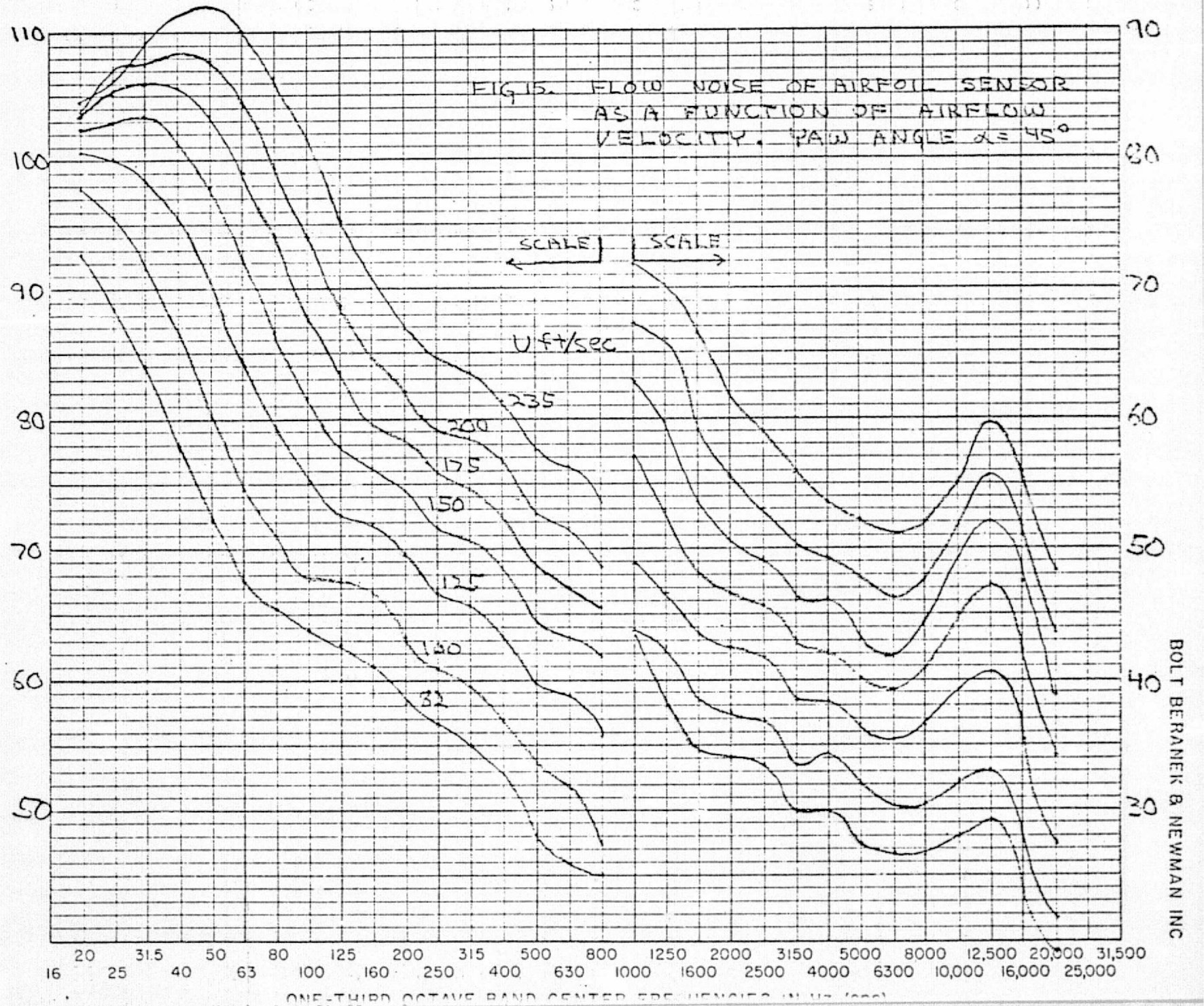

BOLT BERANEK & NEWMAN INC

ORIGINAL PAGE IS
OF POOR QUALITY

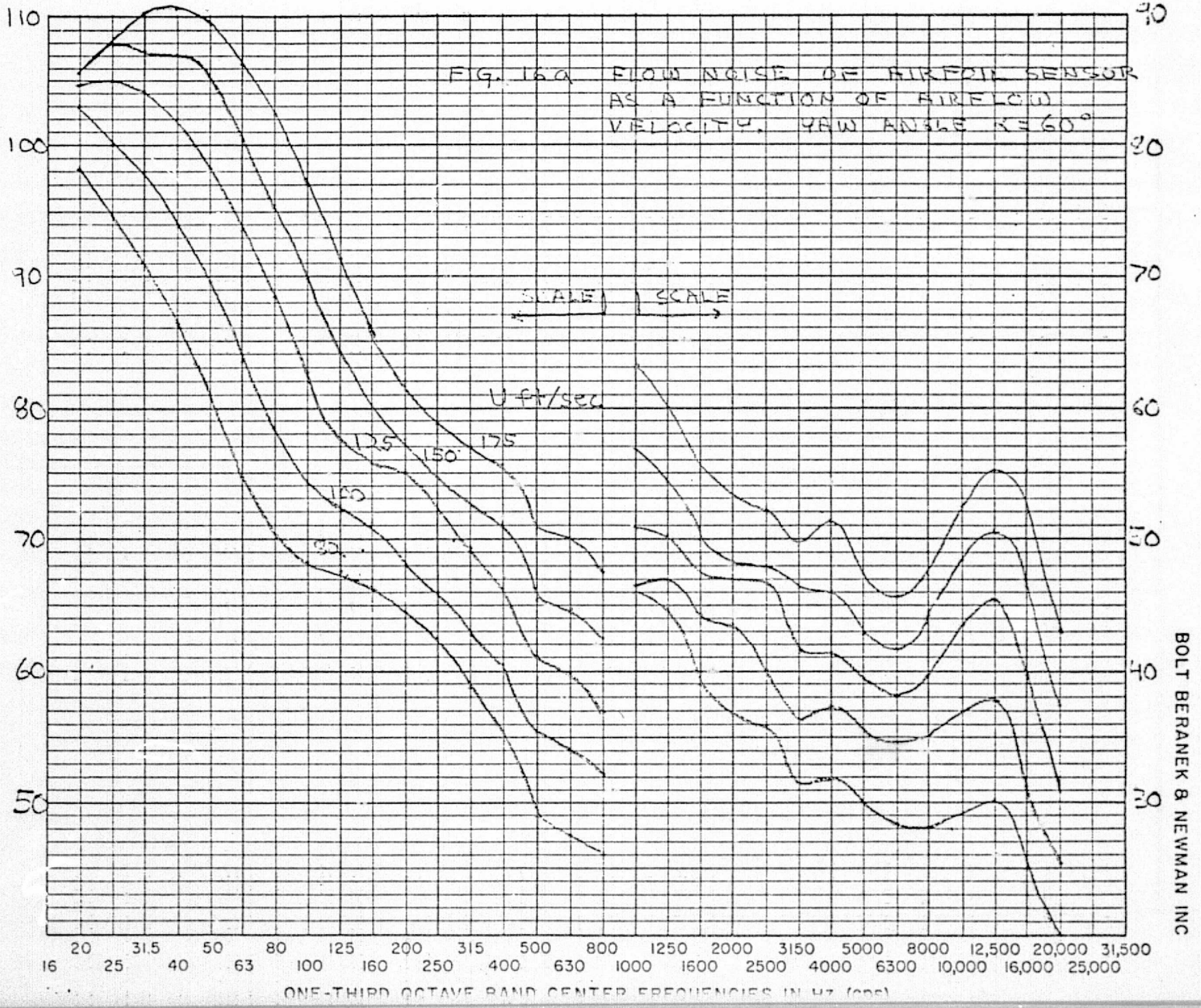

BOLT BERANEK & NEWMAN INC

ORIGINAL PAGE IS
OF POOR QUALITY

ORIGINAL PAGE IS
OF POOR QUALITY

ORIGINAL PAGE IS
OF POOR QUALITY

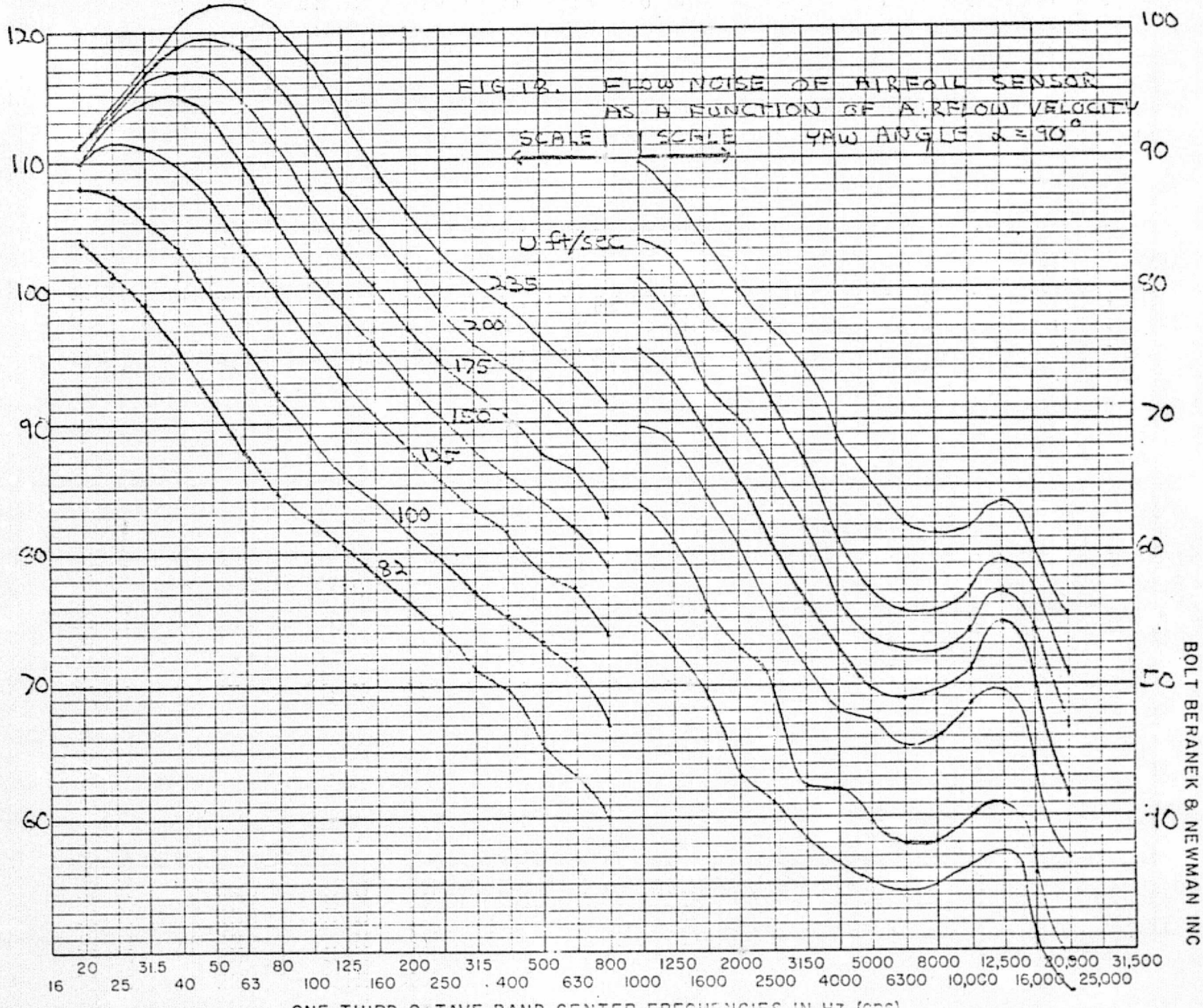

(1) In general, the spectrum of the flow noise at any flow velocity and yaw angle does not exhibit any conspicous local rise which could be associated with a coherent noise mechanism like a coherent vortex shedding. The accurate airfoil shape of the new design did not allow the generation of any significant noise of this type. However, there are indications that low levels of coherent noise are generated, which can be inferred from the small fluctuations in the noise spectra. These small fluctuations in the flow noise spectra could be separated and identified by using a narrow band analysis.

During the flow tests at different yaw angles and flow velocities, an observer near the airfoil but outside of the flow could, at times, detect the presence of some weak tones (≈400 Hz) emanating from the sensor (or the stand?); those weak tones, when they occur, would not be amplified nor shifted in frequency by an increase in flow velocity; they are like tones from cavity resonances rather than from vortex shedding. Their origin was not found.

(2) The general comment above about the low level of coherent noise of the new airfoil is further corroborated by comparing the flow noise of the older design and of the new design. Both can be compared only at low flow velocities because the older design was tested in a small wind tunnel only at 23 m/sec (74 ft/sec).

Comparing the flow noise of the new Airfoil Sensor at flow velocity of 25 m/sec (84 ft/sec) with the flow noise of the old design* at 22 m/sec (74 ft/sec), we find the following: at a yaw angle of 0°, the new design is quieter by about 5 dB. At a yaw

---

*NASA CR-114593, Appendix VI, Fig. 6.

angle of 30° the new design is quieter by roughly 10 dB. At a yaw angle of 60° the new design is quieter by roughly 15 dB; the rise in noise spectrum at 4 kHz, in the old design, and which was attributed to coherent flow noise of a turbulent boundary layer at the trailing edge, is not found in the new design.

The lower flow noise of the new design compared with the older design, is associated with the more accurate and the thinner airfoil (smaller thickness to chord ratio) of the new design and possibly to the more accurate directivity function of the new design at the small wavelengths of turbulence.

The turbulence spectrum of the new wind tunnel in which the new Airfoil Sensor is tested is in fact slightly higher, by a few dB, than the turbulence spectrum of the old wind tunnel in which the old design was tested. Although the scale of turbulence in the two wind tunnels have not been measured and compared, it is almost certain that in the *new* wind tunnel the old design would sense a higher flow noise than in the old wind tunnel.

(3) At 12.5 kHz the noise spectrum of the new Airfoil Sensor has a distinct "hump" which is not shifted in frequency by changes in flow velocity. The presence of this "hump" has not been explained. It would appear that this "hump" belongs to the frequency response of the Sensor. Perhaps it could be associated with a subsonic flexural wave of the porous strip; however, this possibility would contradict our earlier conclusion* that the first bending resonance of the porous strip occurs at 17 kHz and was identified in the frequency response of the sensor.

---

*See Appendix 9.

This "hump" of flow noise at 12.5 kHz, although not a very large one, merits further investigation.

(4) The flow noise at yaw angles of 15° and 30° is generally, lower than the flow noise at 0°.

As the yaw angle is increased towards 30° there are two competing effects: first, the wavenumber component of the flow noise projected along the axis of the porous strips decreases and therefore the filtering action of Airfoil Sensor decreases and the net flow noise should increase. In contrast, the path length on the porous strip, over which a pressure disturbance propagates is shortened as the yaw angle is increased. If the strength of this pressure disturbance is increasing with the path length over the surface of the airfoil, or is experiencing instability as in a transition from a laminar to a turbulent boundary layer, then the shorter path length with increasing yaw angle would produce a lower flow noise. In this competition a minimum flow is reached at yaw angle α of 30°; for larger yaw angles the noise filtering of the directivity function decreases rapidly.

A further source of noise, at large yaw angles is the noise radiated by the stand. This noise was discussed in Part 2 of Section 4.

(5) We cannot determine with the present test setup whether the boundary layer over the porous strips become turbulent.

Taking a Reynolds number R_x for the length x from the tip of the Airfoil Sensor to the far end of the porous strip and using the results obtained with a smooth flat plate with sharp leading edge, we would evoke a critical Reynolds number of 2×10^6 at which transition to turbulent flow can take place.

The numerical value of this critical Re is consistent with the relatively low intensity of turbulence of the free jet. For a yaw angle of 0° the path length x is 16.5 inches. Hence, the transition may start at flow velocities of 230 ft/sec.

Even if transition to a turbulent boundary layer would start to occur at the far end of one porous strip, the net increase in flow noise could not be large because only a small fraction of the strip is exposed to this transition.

4.4 Comparison Between the Flow Noises of the Airfoil Sensor and the B&K Half-Inch Condenser Microphone with Nose Cone

We recall that the B&K sensor is always pointed towards the airflow and that the Airfoil Sensor is oriented with different yaw angles α, 0° to 90° with respect to the flow. Also, the tests are made in very low turbulence.

(1) Low Frequency Noise Below 100 Hz

The low frequency noise below 100 Hz is primarily noise caused by the fan; since neither one of the two sensors has any directivity at low frequencies, they should sense equally well this noise. This is the case for yaw α of the Airfoil Sensor up to $\alpha = 45°$. At larger yaw angles, the Airfoil Sensor becomes somewhat noisier. This increase in noise is probably the low frequency noise generated by the stand; the directivity of this noise has a null at $\alpha = 0°$ such that the B&K sensor is not exposed to it. As the yaw angle of the Airfoil Sensor is increased, this sensor becomes progressively more exposed to the noise of the stand.

(2) Noise Spectrum Above 100 Hz and Low Flow Velocity

At low flow velocities and for zero yaw angle of the Airfoil Sensor, the flow noises are about the same. At larger yaw angles of 15° to 45° the Airfoil Sensor is quieter than the B&K sensor; at $\alpha = 60°$ they are about the same. At larger yaw angles of 75° and 90° the Airfoil Sensor is noisier by approximately 10 dB except above 3.1 kHz where they are about the same.

(3) Noise Spectrum Above 100 Hz; High Flow Velocities

For the different yaw angles α of the Airfoil Sensor we find the following:

$\alpha = 90°$: the Airfoil Sensor is quieter than the B&K sensor only above 3.1 kHz.

$\alpha = 60°$: the Airfoil Sensor is quieter than the B&K sensor above 400 Hz; the difference can be as much as 15 dB at 6.3 kHz.

$\alpha = 45°$: the Airfoil Sensor is quieter than the B&K sensor above 250 Hz; the difference can be as much as 20 dB at 5 kHz.

$\alpha = 30°$: this yaw angle yields the minimum flow noise of the Airfoil Sensor, especially at high frequencies; the airfoil sensor is quieter than the B&K sensor for frequencies above 200 Hz; the difference can be as much as 25 dB at 5 kHz.

$\alpha = 0°, 15°$: the flow noise of the Airfoil Sensor is everywhere lower than the flow noise of the B&K sensor; the difference is about 12 dB at 1 kHz and remains approximately 10 dB above 1 kHz.

5. CONCLUSIONS

The new Airfoil Porous Surface Sensor has shown significantly lower flow noise than the older design. This is due to the accurate airfoil section and to its small thickness to chord ratio.

Over the full range of flow velocities of the wind tunnel, 25 to 70 m/sec, and at any yaw angle of the Airfoil, the new design did not create in its flow noise any significant "tones".

The flow noise of the Airfoil Sensor is generally lower than the flow noise of the B&K half inch microphone with nose cone, for a wide range of yaw angles, 0° to 45°. At larger yaw angles, 60° to 90° the Airfoil Sensor is noisier, probably because it senses the noise generated by the stand on which it is mounted.

All these results of flow noise apply to very quiet flow. At higher turbulence than the turbulence of the present tests, the Airfoil Sensor is expected to be much quieter than the B&K sensor.